1-1-2012

Hdac3 is a Critical Regulator of Neural Crest Progenitor Cell Biology

Nikhil Singh
University of Pennsylvania, nikhil2@mail.med.upenn.edu

Hdac3 is a Critical Regulator of Neural Crest Progenitor Cell Biology

Abstract
Vertebrate embryogenesis relies on the coordinated development of multiple progenitor cell pools. Specific transcriptional programs regulate the specification, expansion, migration and eventual differentiation of these progenitor cell populations, and tight control of these programs is essential for normal development to occur. Class I histone deacetylases (Hdacs), including Hdac3, play critical roles in regulating gene transcription, through both epigenetic and non-epigenetic means. In this dissertation, I use mouse genetics to explore the previously undescribed role of Hdac3 in regulating neural crest progenitor cell behavior. By genetically deleting Hdac3 in premigratory neural crest cells, I use in vivo and ex vivo techniques to show that Hdac3 plays crucial roles in multiple facets of neural crest development, and that transcriptional programs involved in progenitor cell survival and differentiation are all under the control of this important enzyme.

Degree Type
Dissertation

Degree Name
Doctor of Philosophy (PhD)

Graduate Group
Cell & Molecular Biology

First Advisor
Jonathan A. Epstein

Keywords
Cardiac development, Craniofacial development, Differentiation, Epigenetics, Neural crest, Stem cell

Subject Categories
Cell Biology | Developmental Biology | Molecular Biology

HDAC3 IS A CRITICAL REGULATOR OF NEURAL CREST PROGENITOR CELL BIOLOGY

Nikhil Singh

A DISSERTATION

in

Cell and Molecular Biology

Presented to the Faculties of the University of Pennsylvania

in

Partial Fulfillment of the Requirements for the

Degree of Doctor of Philosophy

2012

Supervisor of Dissertation

_____

Jonathan A. Epstein, MD
Professor, Cell and Developmental Biology

Graduate Group Chairperson

_____

Daniel S. Kessler, PhD
Associate Professor, Cell and Developmental Biology

Dissertation Committee
Mitchell A. Lazar, MD, PhD, Professor, Departments of Medicine, Genetics
Edward E. Morrisey, PhD, Professor, Department of Medicine
Ben Z. Stanger, MD, PhD, Assistant Professor, Department of Medicine

Acknowledgements

Firstly I would like to thank Jon for his terrific mentorship and the wonderful learning environment that he creates in the lab. I would also like to thank all Epstein lab members and MCRC colleagues, including Chinmay Trivedi, Kurt Engleka, Arun Padmanabhan, Rajan Jain, Manvendra Singh, Ashley Cohen, MinMin Lu, Lan Chen and Li Li, for their contributions to this work. I would like to thank Mitch Lazar and Zheng Sun for the opportunity to collaborate with them on a very fun project. I would like to thank my thesis committee members, Mitch, Ed Morrisey and Ben Stanger for their input throughout this process. I would also like to acknowledge Tom Kadesch, who served on my thesis committee before his passing. I would like to thank the combined degree office and directors, including Skip Brass, Maggie Krall, and Maureen Osciak. Finally, I would like to thank my family for their support, as well as a fantastic group of friends/fellow combined degree students - Jarrod, Josiah, Marcus and Matt – who have helped to make this an absurdly fun experience.

ABSTRACT

HDAC3 IS A CRITICAL REGULATOR OF NEURAL CREST PROGENITOR CELL BIOLOGY

Nikhil Singh

Jonathan A. Epstein

Vertebrate embryogenesis relies on the coordinated development of multiple progenitor cell pools. Specific transcriptional programs regulate the specification, expansion, migration and eventual differentiation of these progenitor cell populations, and tight control of these programs is essential for normal development to occur. Class I histone deacetylases (Hdacs), including Hdac3, play critical roles in regulating gene transcription, through both epigenetic and non-epigenetic means. In this dissertation, I use mouse genetics to explore the previously undescribed role of Hdac3 in regulating neural crest progenitor cell behavior. By genetically deleting Hdac3 in premigratory neural crest cells, I use *in vivo* and *ex vivo* techniques to show that Hdac3 plays crucial roles in multiple facets of neural crest development, and that transcriptional programs involved in progenitor cell survival and differentiation are all under the control of this important enzyme.

Table of Contents

List of Tables

List of Figures

Chapter 1. Introduction

Summary

Developmental biology is among the oldest and most well established fields in the basic biological sciences. From their earliest incursions into this field, developmental biologists have been concerned with a single fundamental question:

How can a single cell give rise to the all of the cell types and structures that comprise a complex organism?

In much the same way that this single cell, the zygote, divides before giving rise to the rich diversity of cell types, the multitude of tissues, and the intertwined organ systems that comprise a multicellular organism, the field of developmental biology has itself divided before giving rise to new applications and entirely new areas of study, which are similarly intertwined. This field has been roughly subdivided into the studies of the growth and survival of cells, the specification and differentiation of cells, and morphogenesis of complex structures and organ systems. Indeed, the realization that development consists of these distinct but coordinated core processes was itself a critical advancement in the field.

Recent efforts in developmental biology have focused on understanding the molecular mechanisms underpinning these core developmental processes. Our burgeoning molecular understanding of these processes has not only helped us make inroads into answering developmental biology's most fundamental question, but it has profoundly influenced the study and categorization of congenital diseases in humans, as well as our understanding of the pathogenesis of certain adult disease states. Furthermore, elucidation of the molecular foundations of developmental biology has been a guiding force directing inroads into the nascent field of regenerative medicine.

At the heart of any molecular understanding of developmental processes lies the biology of the progenitor cell. It is impossible to understand how an organ develops and is remodeled *in utero* or how a tissue can be engineered and manipulated *ex vivo* without first understanding the factors directing the behavior of individual progenitor cells. This introductory chapter focuses on our increasing understanding of how progenitor cell behavior is regulated at the molecular level, and, in particular, at the level of the transcriptome. Transcriptional regulation in progenitor cells is discussed in the specific context of murine neural crest cell biology.

Extrinsic and intrinsic regulation of progenitor cell behavior

The central dogma of gene expression states that a cell's transcriptome is determined by the primary sequence of DNA that comprises its genome.

However, this dogma lies at odds with the basic premise of developmental biology, in which different progenitor cells, *each possessing the same genomic sequence*, diversify and exhibit vastly different transcriptional profiles.

As has become clear from molecular investigations into progenitor cell biology, external stimuli play an enormous role in influencing each progenitor cell's transcriptome, identity, and characteristics. For instance, the Notch signaling cascade, a direct cell-cell communication pathway, is a classical initiator of cellular differentiation in multiple developmental contexts (Andersson et al., 2011). Progenitor cells primed to receive Notch signals undergo transcriptional changes in response to Notch stimulation; these changes are mediated by the canonical downstream effector molecule of Notch signaling, the transcription factor NICD (Andersson et al., 2011). Similarly, the canonical Wnt signaling pathway, a paracrine signaling modality, has been shown in multiple settings to be critical for regulating the expansion of progenitor cell populations, again through a process mediated by nuclear translocation of a downstream effector molecule/transcription factor, ß-catenin (Klaus and Birchmeier, 2008). To be sure, numerous other signaling pathways and environmental stimuli have been shown to regulate countless aspects of progenitor cell behavior in many developmental processes. The influence of such external stimuli comprises a crucial, extrinsic level of regulation over the progenitor cell transcriptome, and offers insight into how cells with identical genomes can exhibit phenotypic differences.

However, despite their obvious importance, environmental triggers cannot account for all aspects of progenitor cell behavior. From the earliest transplantation studies, it has been appreciated that not all progenitor cells are equal; for instance, a neuronal progenitor cell will not differentiate into a cardiomyocyte if introduced into primary heart field, even if exposed to all of the environmental cues that normally drive cardiomyocyte differentiation. Clearly, there are additional levels of regulation at play – cell intrinsic processes that define a progenitor cell's competency to respond to specific external stimuli, as well as its ability to propagate information from such stimuli to its progeny, even after the stimulus is withdrawn. Many of these intrinsic processes fall into the realm of epigenetics.

Histone deacetylases and epigenetic regulation of gene expression

The field of epigenetics is comprised of the study of factors that stably affect transcription in a cell and its progeny without altering the sequence of DNA. Such factors can include long-lasting changes to the structure of chromatin that affect transcription at specific loci. In the operational definition of epigenetics proposed by Berger *et al.*, epigenetic processes begin with an *epigenator* – a signal, from either environmental or intracellular origin that results in activation of an *epigenetic initiator* (Berger et al., 2009). These *initiators* are responsible for translating a signal from the *epigenator* into an alteration to chromatin structure

or accessibility. Finally, this chromatin alteration must be maintained by an *epigenetic maintainer*. This *maintainer* confers longevity and heritability to chromatin alterations even in the absence of continued stimuli from the *epigenator*.

Classic *epigenetic maintainers* include covalent modifications to either DNA itself or to histone proteins. Histone modifications, including histone tail methylation or acetylation, affect the structure of chromatin, thereby affecting the ability of transcription factors and other nuclear proteins to bind to promoter or enhancer regions. These modifications persist through DNA replication, and thereby confer stability through multiple cell divisions.

Acetylation occurs on at least 12 different lysines in the H3 and H4 histone proteins (Wang et al., 2008). Histone tail acetylation is generally associated with transcriptionally active chromatin, as characterized by RNA Polymerase II binding (Wang et al., 2009). Negatively charged acetyl groups repel DNA from histone proteins, creating a 'relaxed,' euchromatic state, disrupting higher order chromatin structures, and permitting access to transcription factors and RNA Polymerase II (Wade et al., 1997). In a second mechanism by which histone acetylation status affects transcription, acetylated lysines serve as a binding substrate for bromodomain-containing transcription factors, resulting in RNA Polymerase II recruitment (LeRoy et al., 2008). Histone tail acetylation is tightly regulated by the antagonistic actions of histone acetyltransferases, such as p300, and histone deacetylases (Hdacs).

Mammals express 11 ‘classic’ Hdac proteins, characterized by a highly conserved deacetylase domain. The canonical role of the aptly named Hdacs is to deacetylate histone tails. As such, Hdacs are viewed primarily as transcriptional repressors (Haberland et al., 2009b). These 11 proteins are subdivided into four classes based on homology (Haberland et al., 2009b). The class I Hdacs - Hdac1, Hdac2, Hdac3 and Hdac8 - are important regulators of transcription, via chromatin-mediated transcriptional repression and, in some cases, via direct deacetylation of key transcriptional regulators (Haberland et al., 2009b, Haberland et al., 2009a, LeBoeuf et al., 2010). Hdac enzymatic activity is dependent on their association with large repressor complexes, such as the NuRD, CoREST or Sin3 complexes, which interact with Hdacs 1 and 2, and the NCoR and/or SMRT repressor complexes, which interact with Hdac3 (Yang and Seto, 2008). Hdacs do not possess intrinsic DNA binding ability, and are targeted to specific genomic loci through their interaction with corepressors, transcription factors and nuclear receptors (Yang and Seto, 2003).

Deletion studies of individual class I Hdacs have revealed highly specific, non-redundant roles in various mammalian cell lineages. For instance, despite widespread expression, global deletion of Hdac2 results predominantly in cardiac abnormalities, while global deletion of Hdac8 solely affects patterning of the anterior calvarium and viscerocranium (Trivedi et al., 2007, Haberland et al., 2009a). It was initially somewhat surprising that deletion of these global modulators of gene expression lead to dysregulation of specific pathways, rather

than to non-specific, ectopic upregulation of transcription. Perhaps equally surprisingly, tissue specific deletion studies have also revealed that an individual Hdac can mediate completely different processes either in different tissues or under different environmental conditions within the same tissue. The many roles played by class I Hdacs during development typify this tissue- and context-dependency of Hdac function.

Class I Hdacs in development

Many *epigenetic initiators*, including class I Hdacs, have been shown to modulate transcription during development by linking the external environment encountered by progenitor cells to heritable changes in gene expression. Class I Hdacs are widely expressed during mammalian development and play very specific roles in both early developmental processes as well as later stages of embryogenesis. Global deletion of Hdac1 or Hdac3 results in early embryonic lethality, and therefore many of the approaches used to study the role of class I Hdacs in development have made use of Cre recombinase, driven under the control of tissue-specific promoters, to excise floxed alleles of Hdac genes (Montgomery et al., 2007, Knutson et al., 2008).

Conditional deletion studies have revealed that Hdac1 and Hdac2 are functionally redundant in many tissues, and tissue-specific compound deletion of both results abnormalities in a variety of systems. For instance, deletion of Hdac1 and Hdac2 in embryonic epidermal progenitor cells results in impaired

specification of hair follicles and decreased epidermal stratification (LeBoeuf et al., 2010). Hdac1 and Hdac2 regulate epidermal development by working cooperatively with p63 and by directly deacetylating p53 in order to repress cell cycle inhibitors (LeBoeuf et al., 2010). Conditional deletion of Hdac1 and 2 in the developing nervous system has revealed critical, redundant roles in neuronal differentiation, oligodendrocyte differentiation, and myelination (Montgomery et al., 2009, Ye et al., 2009, Jacob et al., 2011). In the heart, Hdac1 and 2 act redundantly to regulate proliferation and contractility of developing cardiomyocytes. Additionally, Hdac2 is important in mediating the adult heart's hyertrophic response to pressure overload, in part by repressing the regulatory enzyme Inpp5f (Trivedi et al., 2007, Zhu et al., 2009).

Hdac3 as a unique class I Hdac

Hdac3 is a 49 kilodalton class I Hdac most similar in homology to Hdac8 (Haberland et al., 2009b). However, Hdac3 is unique among class I Hdacs in that it associates with NCoR or SMRT in a repressor complex, which is required for its catalytic activity (Guenther et al., 2001). Global deletion of Hdac3 in the mouse results in lethality at the gastrulation stage (Knutson et al., 2008). Hdac3 has been shown to regulate a variety of cellular processes, which are highly dependent on the type of tissue under investigation, as well as factors such as the nutritional state or developmental stage of the tissue. For instance, Hdac3 has been shown to mediate differentiation in osteoblast and myocyte precursors

in vitro (Schroeder et al., 2004, Zeng et al., 2006); Hdac3 has been shown to regulate cell cycle progression in cell lines and cardiomyocytes (Li et al., 2006, Bhaskara et al., 2008, Montgomery et al., 2008, Knutson et al., 2008, Trivedi et al., 2008); Hdac3 also plays important roles in metabolic regulation in multiple tissues, including the heart, through its action as a transcriptional repressor (Montgomery et al., 2008, Sun et al., 2011, Knutson et al., 2008, Alenghat et al., 2008).

As with other Hdacs, the functions of Hdac3 as a global agent of chromatin remodeling are determined by its genomic binding sites. Interestingly, ChIP-Seq studies have revealed that genomic localization of Hdac3 demonstrates very little overlap between different cell types, which is consistent with its broadly different functions in different tissues (Feng et al., 2011). Within each cell type, the Hdac3 repressor complex is targeted to different genomic loci by transcription factors or nuclear receptors expressed in that cell (Feng et al., 2011). Hdac3 has been shown to interact directly with transcription factors such as Zfp521 in osteoblast precursors and PPARα in cardiomyocytes, in order to mediate its functions as a chromatin-remodeling enzyme (Hesse et al., 2010, Montgomery et al., 2008). Recent evidence suggests that as little as one factor may influence the majority of Hdac3 binding sites within a given tissue. In the liver, where Hdac3 is an important regulator of the circadian expression of metabolic genes, Hdac3 binding specificity is predominantly determined by the nuclear receptor Rev-erbα (Feng et al., 2011). Rev-erbα directly associates with the Hdac3/NCoR complex

and is crucial for Hdac3-mediated transcriptional repression in hepatocytes. In fact, nearly all Hdac3 binding sites in hepatocytes, as determined by ChIP-Seq, overlap with Reverb-alpha binding sites. The abundance of Rev-erbα in hepatocytes is itself regulated by the metabolic state of the cell and circadian clock, resulting in a circadian oscillatory pattern to Rev-erbα nuclear localization. This periodicity results in a circadian pattern to Hdac3 genomic localization and function in the liver, offering an example of a contextual specificity to the function of Hdac3 within one cell type (Feng et al., 2011).

Clearly the functions of Hdac3 within a given tissue can be regulated by the expression and availability of its specific interacting partners within that tissue, as well as by related factors such as the nutritional state and zeitgeber time. However, little is known about how the functions of Hdac3 change within a specific tissue during other important biological transitions, including during organogenesis.

Hdac3 in cardiac development and homeostasis

The study of Hdac3 in the heart provides an example of the diverse, context-dependent functions of this important regulatory molecule from early development to adult homeostasis. Cardiac development is characterized by the gradual lineage restriction of multiple progenitor cell populations, a process tightly linked to the emergence of a three-dimensional organ of progressively increasing morphological complexity. In normal cardiac development, mesodermally-derived

bipotent myocardial progenitor cells in the cardiac crescent undergo progressive lineage restriction, ultimately giving rise to either vascular smooth muscle precursors or myocardial progenitor cells (Epstein, 2010). Myocardial progenitor cells further differentiate, giving rise to immature cardiomyotytes, as well as other specialized cardiac cell types. These immature cardiomyocytes form a spontaneously beating single-chambered tube, which begins to circulate blood into the developing vascular network of the embryo. As this primitive heart tube beats, it loops upon itself, forming a two-chambered organ with a single atrium and ventricle, populated by phenotypically distinct atrial and ventricular myocytes. These processes occur in parallel with development of the outflow tract, discussed in detail in Chapter 3. Emybronic ventricular myocytes lack the plasticity of myocardial progenitor cells but differ from adult cardiomyocytes in a number of regards. Embryonic cardiomyocytes express different contractile proteins than their adult counterparts, and exhibit high proliferative potential. As the two-chambered heart grows, driven by myocyte proliferation, the single ventricular chamber is septated, a process dependent on neural crest cells (further discussed in Chapter 3). In late gestation and early in the perinatal period, cardiomyocytes mature, a process characterized by alterations to their mechanical and electrophysiological properties and their decreased proliferative and regenerative potential (Porrello et al., 2011).

Hdac3 acts at multiple stages in the transition from bipotent myocardial progenitors to embryonic and, ultimately, adult cardiomyocytes. Unpublished data

generated by Trivedi et al. in the Epstein lab shows that deletion of Hdac3 at embryonic day 8.5 (E8.5) in biopotent myocardial progenitor cells results in severe myocardial thinning and lethality by E16.5. These cardiac abnormalities arise due to cell cycle arrest and decreased proliferation of embryonic cardiomyocytes. This cell cycle arrest is accompanied by upregulation of the cell cycle inhibitor p21 (encoded by the *Cdkn1a* gene). Preliminary results suggest that heterozygous deletion of *Cdkn1a* in mutant embryos partially rescues the early cardiac lethality, with a small number of mutants surviving until birth. Hdac3 has previously been shown to inhibit *Cdkn1a* transcription by directly binding to its promoter (Wilson et al., 2008); derepression of *Cdkn1a* in the absence of Hdac3 may therefore play a critical role in mediating the lethality following early cardiac deletion of Hdac3.

In addition to derepression of *Cdkn1a*, loss of Hdac3 in these mice leads to premature expression of markers of differentiated cardiomyocytes *in vivo*, and deletion of *Hdac3* in cultured E8.5 myocytes leads to precocious differentiation and spontaneous beating *in vitro*. Preliminary data from chromatin immunoprecipitation experiments has revealed that Hdac3 directly binds to the promoter regions of cardiac-specific genes in E8.5 hearts, suggesting that it may serve as a direct repressor of cardiomyocyte differentiation in bipotent myocardial progenitor cells. Overall, these results suggest that Hdac3 directly represses mediators of myocardial differentiation as well as the cell cycle inhibitor p21; following early deletion of Hdac3, the myocardial progenitor cells pool is therefore

depleted via a combination of premature differentiation and cell cycle arrest, leading to severe cardiac abnormalities later in gestation.

A study by Olson and colleagues has shown that deletion of Hdac3 slightly later in cardiac development, at E9.5 using *αMHC-Cre*, allows for the completion of embryogenesis. *αMHC-Cre* mediates recombination in differentiated cardiomyocytes, rather than bipotent precursors. *αMHC-Cre; Hdac3$^{f/f}$* mice are viable until two months of age; however, when fed a normal diet, these mice undergo cardiac hypertrophy at 4 weeks of age, which progresses to severe heart failure, culminating in lethality. This hypertrophy is characterized by myocardial lipid accumulation and fibrosis. The authors suggest that, following midgestational deletion of Hdac3, positive regulators of fatty acid uptake are derepressed, leading to progressive accumulation of lipid in the myocardium and eventual cardiac dysfunction and death.

In a collaborative effort with the Lazar lab, we have demonstrated that deletion of Hdac3 in perinatal myocytes - as opposed to bipotent progenitor cells or embryonic ventricular myocytes – results in dysregulation of a vastly different subset of genes than those dysregulated following mid-gestational deletion *(Sun et al., 2011)*. In this study, mice lacking cardiac expression of *Hdac3* show dysregulation of genes involved in the mitochondrial response to lipid overload. They exhibit no decrease in viability on a normal diet; however, when placed on a high fat diet, they exhibit severe cardiac defects leading to death. These data are summarized in the Appendix. These contrasting conditional deletion studies in

which Hdac3 has been deleted in the heart during midgestation versus in the perinatal period demonstrate that Hdac3 plays distinct roles in metabolic regulation at embryonic versus postnatal timepoints; furthermore, the time point at which Hdac3 is deleted in cardiomyocytes portends the long-term transcriptional perturbations that persist into adulthood.

Overall, these cardiac studies have revealed multiple roles for Hdac3 within a single cell lineage; Hdac3 inhibits differentiation down the cardiomyocyte lineage in bipotent myocardial precursors, represses genes involved in lipid metabolism in embryonic myocytes, and regulates different genes involved in the response to lipid overload in postnatal cardiomyocytes (Figure 1.1). Based on its roles in mediating developmental processes as well as cellular responses to environmental stimuli in the heart, Hdac3 is an attractive candidate *epigenetic initiator* that could integrate input from exogenous cues and regulate important developmental processes in a stage- and lineage-specific manner in other multipotent progenitor cells under complex regulation from external stimuli.

Neural crest development

Neural crest cells comprise a transient embryonic progenitor cell population, specific to vertebrates, that provides a useful model for studying progenitor cell specification, migration and differentiation in the context of the development of multiple tissues and organ systems. Neural crest cells are derived from ectoderm and are specified at the dorsal neural tube at E8.5 in the

mouse. They subsequently undergo epithelial to mesenchymal transformation (EMT), delaminate from the neural tube and migrate throughout the embryo. They ultimately give rise to transient embryonic structures including the mesenchyme of the pharyngeal arches, as well as structures that persist in the adult vertebrate, including much of the smooth muscle of the cardiac outflow tract, much of the bone, cartilage and connective tissue of the head and face, neurons and support cells of the peripheral nervous system, and the chromaffin cells of the adrenal medulla (Figure 1.2).

Neural crest cells develop in a dynamic milieu, under the influence of environmental cues that regulate many aspects of their behavior. Though little is known about the signals that direct the specification of murine neural crest cells, environmental cues that drive neural crest migration, survival and differentiation in the mouse are well understood (Sauka-Spengler and Bronner-Fraser, 2008). Changes to the extracellular matrix help to initiate EMT, while ephrin and semaphorin-neuropilin signaling from surrounding cells have been implicated in neural crest cell migration through the somitic mesoderm (Sauka-Spengler and Bronner-Fraser, 2008, Davy et al., 2004, Gammill et al., 2007). As well, numerous signals encountered by both migrating and postmigratory neural crest cells direct their survival and differentiation (discussed further in Chapter 2 and Chapter 3). While much is now known about the signaling modalities that influence murine neural crest cell behavior, we are only beginning to understand how neural crest cells are able to synthesize these signals into heritable changes

in gene expression, and how individual neural crest cells initially become competent to respond to these exogenous cues.

Epigenetic regulation of neural crest development

Neural crest cells are characterized by enormous developmental plasticity. However, it has long been appreciated that, from very early stages of neural crest development, there is in-equivalency between certain neural crest cells. Studies in which quail neural crest cells were transplanted into chick embryos have revealed the remarkable degree to which neural crest cells from one region along the rostro-caudal axis of the embryo can contribute to derivatives of another region - with some exceptions. Among the exceptions uncovered by Le Douarin and colleagues in a classic series of experiments; neural crest from the vagal region, which normally contributes to rostral elements of the enteric nervous system, was transplanted into the adrenomedullary trunk crest region, which normally gives rise to the adrenal medulla, sympathetic ganglia and the enteric plexi of the distal bowel. In this study, vagal neural crest cells were able to contribute to all derivatives of the adrenomedullary crest, with the exception of the distal enteric nervous system, to which they were unable to migrate (Le Douarin et al., 1975) . This limit on vagal trunk neural crest plasticity suggests that, in addition to being subject to external influences on their development, undifferentiated neural crest cells are subject to an intrinsic level of regulation.

Recent work has focused on understanding the nature of this intrinsic regulation of neural crest cell behavior.

Neural crest migration is regulated by the expression of transcription factors such as Sox10 and Ret in response to environmental cues. Mutations in these genes have been implicated in Hirschprung's disease in humans, in which failure of neural crest cells to migrate to the distal gut and differentiate into enteric ganglia leads to defects in colonic motility. Recently, Aebp2, a targeting protein for the Polycomb Repression Complex 2 (a regulatory complex involved in transcriptional regulation via histone methylation), was shown to regulate the expression of several transcription factors that mediate neural crest cell migration. Mice haploinsufficient for Aebp2 demonstrate aganglionic megacolon, due to failure of neural crest cells to migrate to the distal enteric nervous system (Kim et al., 2011). The migration of neural crest cells into the distal gut is a process that, as early as 1975, was hypothesized by LeDourain and colleagues to be under cell intrinsic regulation; this study of an important chromatin remodeling complex has now shown that it is indeed regulated at an epigenetic level.

Additional attempts to determine which factors underlie intrinsic regulation of neural crest first focused on genes such as Hox family members, which have been shown to restrict cranial neural crest cell plasticity during skull morphogenesis (Hunt et al., 1991). More recently, as the field has moved towards studies of chromatin remodeling enzymes that regulate neural crest

development, one of the first such studies in the mouse revealed a connection between epigenetic processes and expression of Hox genes in craniofacial development. Olson and colleagues showed that Hdac8 normally restricts the expression of Hox family members in the anterior cranium during development, and that deletion of Hdac8 leads to ectopic Hox gene activation (Haberland et al., 2009a). They further demonstrated that global deletion of Hdac8, as well as tissue specific deletion in neural crest, results in calvarial instability, leading to perinatal lethality (Haberland et al., 2009a).

Transcriptional regulation via chromatin remodeling complexes has thus far been implicated in a limited number of aspects of neural crest development. Identifying additional chromatin remodeling enzymes that control other aspects of neural crest development - and deciphering the transcriptional networks that they regulate - will be a fruitful and important area of research as we seek to understand how progenitor cells are regulated at the epigenetic level.

Conclusions

An emerging body of work has implicated chromatin-modifying enzymes in the regulation of important processes and transitions during the development of multiple progenitor cell populations, including neural crest. Class I Hdacs have been recognized as important regulatory enzymes in many developmental contexts; Hdac3 in particular has been shown to regulate developmental processes in a growing number of organ systems, and offers an appealing

candidate for further investigation into the intrinsic regulation of neural crest development.

Figure 1.1

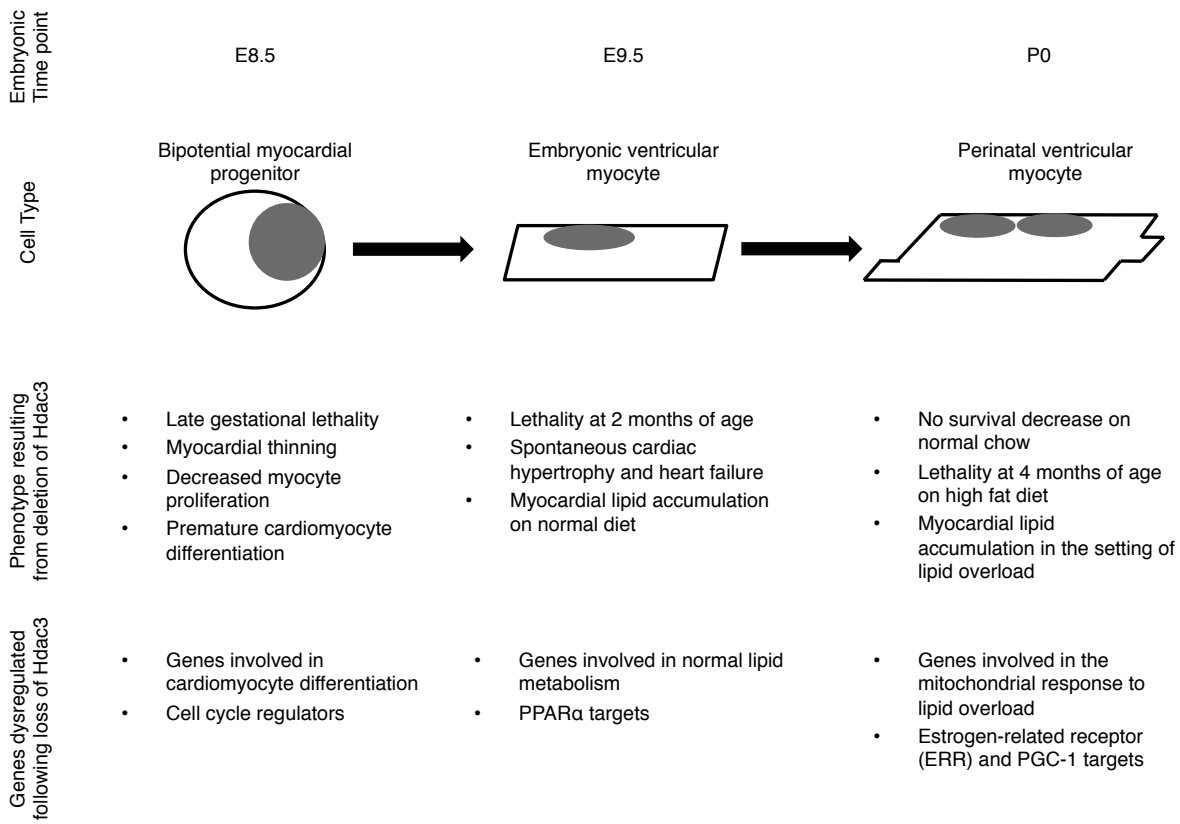
Embryonic Time point
E8.5
E9.5
P0
Cell Type
Bipotential myocardial progenitor
Embryonic ventricular myocyte
Perinatal ventricular myocyte
Phenotype resulting from deletion of Hdac3
• Late gestational lethality
• Myocardial thinning
• Decreased myocyte proliferation
• Premature cardiomyocyte differentiation
• Lethality at 2 months of age
• Spontaneous cardiac hypertrophy and heart failure
• Myocardial lipid accumulation on normal diet
• No survival decrease on normal chow
• Lethality at 4 months of age on high fat diet
• Myocardial lipid accumulation in the setting of lipid overload
Genes dysregulated following loss of Hdac3
• Genes involved in cardiomyocyte differentiation
• Cell cycle regulators
• Genes involved in normal lipid metabolism
• PPARα targets
• Genes involved in the mitochondrial response to lipid overload
• Estrogen-related receptor (ERR) and PGC-1 targets

Figure 1.1. Hdac3 functions in cardiomyocytes vary during cardiac development and postnatal homeostasis. A schematic diagram showing the different functions of Hdac3 in bipotential myogenic precursors, embryonic ventricular myocytes and perinatal cardiomyocytes, as well as the classes of genes that are dysregulated in a persistent manner following loss of Hdac3.

Figure 1.2

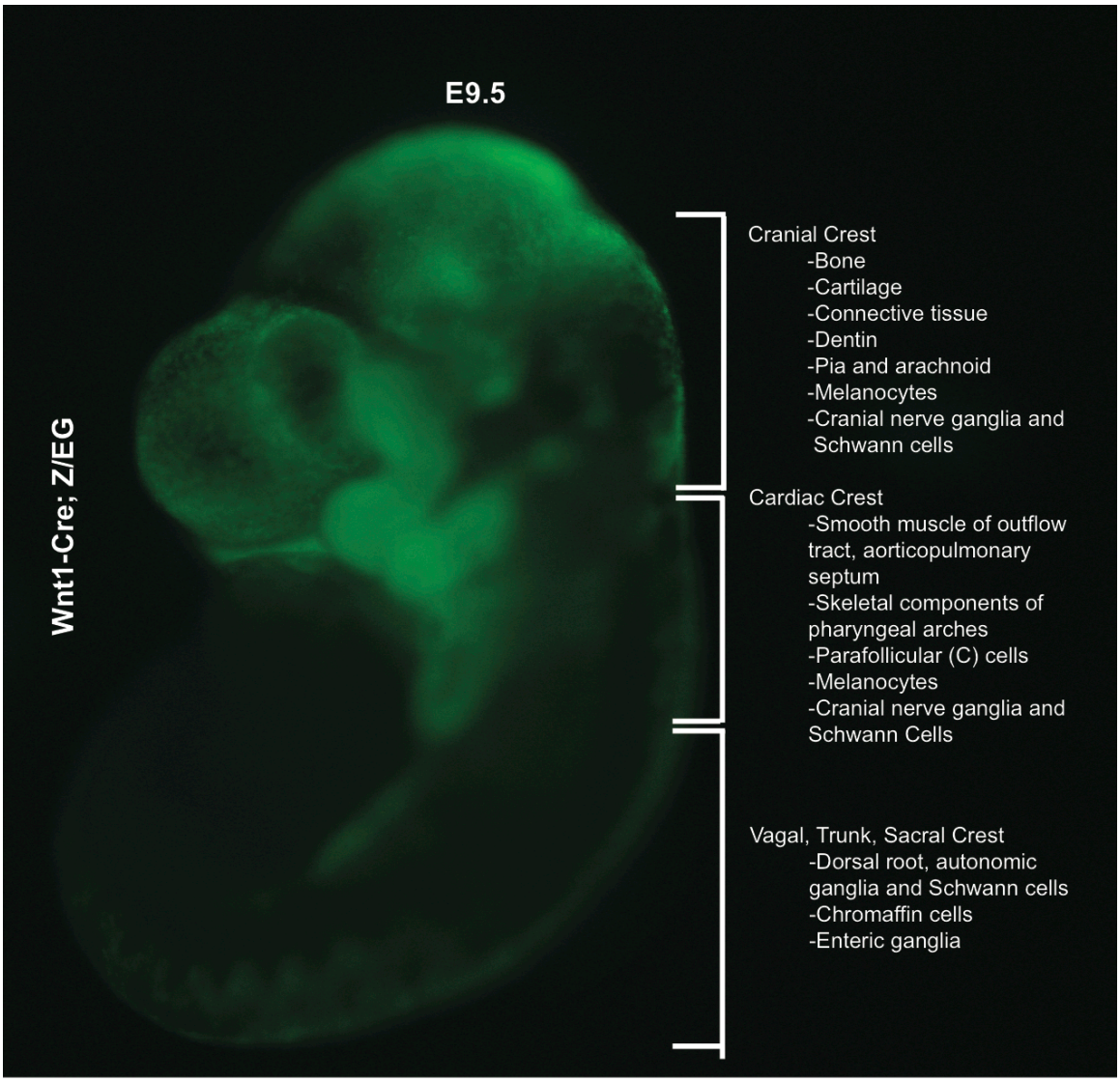
E9.5
Wnt1-Cre; Z/EG
Cranial Crest
-Bone
-Cartilage
-Connective tissue
-Dentin
-Pia and arachnoid
-Melanocytes
-Cranial nerve ganglia and Schwann cells
Cardiac Crest
-Smooth muscle of outflow tract, aorticopulmonary septum
-Skeletal components of pharyngeal arches
-Parafollicular (C) cells
-Melanocytes
-Cranial nerve ganglia and Schwann Cells
Vagal, Trunk, Sacral Crest
-Dorsal root, autonomic ganglia and Schwann cells
-Chromaffin cells
-Enteric ganglia

Figure 1.2. Neural crest cell developmental potential is organized along the rostro-caudal axis. A gross image of an E9.5 embryo under direct fluorescence in which neural crest cells and their derivatives have been genetically labeled using Wnt1-Cre and the Z/EG GFP reporter. Labels denote the derivatives of neural crest cells originating from each region of the dorsal neural tube.

Chapter 2. Hdac3-mediated repression of Bmp4 in neural crest cells regulates murine craniofacial development

Summary

Craniofacial development is characterized by reciprocal interactions between neural crest cells and neighboring cell populations of ectodermal, endodermal and mesodermal origin. Various modalities of cell-cell communication, such as Bmp signaling, play critical roles in coordinating the development of cranial structures, by modulating the growth, survival, and differentiation of neural crest cells. However, the regulation of these signaling pathways, particularly at the epigenetic level, remains poorly understood. In this chapter I describe the role of Hdac3 in regulating important signaling pathways and transcriptional networks in craniofacial development.

Introduction

Vertebrates are unique among metazoans in their reliance on neural crest cells to form a wide array of structures in the head. These neural crest-derived craniofacial structures are analogous to mesodermally- and ectodermally-derived structures in invertebrates (Gans and Northcutt, 1983). In midgestation in the mouse, neural crest cells populate the pharyngeal arches – a series of paired outpouchings that flank the developing pharynx, as well as the frontonasal prominence, an area that eventually gives rise to the nose and forehead. The first pharyngeal arch, which is the largest and most rostral of the arches, contains neural crest cells that will form structures in the face and neck (Alappat et al., 2003). Driven by the proliferation and continued influx of migrating neural crest cells, two distinct outgrowths from the first arch, known as the maxillary and mandibular prominences, grow dorso-ventrally and flank the developing oropharynx, eventually fusing at the ventral midline in what becomes the face. Failure of neural crest cells to migrate or proliferate appropriately can result in hypoplasia of these structures and the absence of fusion, which can manifest as abnormal facies and clefting (Ito et al., 2003, Vallejo-Illarramendi et al., 2009).

While initially dependent on the tightly-regulated growth of undifferentiated neural crest cells in the prominences, craniofacial development is also reliant on the ability of neural crest cells to differentiate into bone, cartilage, connective tissue, dental pulp and neurons that populate the mature face and skull. In the primordial environment of the growing pharyngeal arches, neural crest cells are

characterized by enormous developmental plasticity (Couly et al., 1993). In the setting of such plasticity, the ability of neural crest cells to contribute to such varied cell types is largely dependent on their exposure to environmental cues from surrounding cells of both neural crest and non-neural crest origin (Le Douarin et al., 2004). Indeed, as discussed in Chapter 1, both the survival and differentiation of neural crest cells are under tight regulation by multiple signaling modalities.

Murine genetics have proven invaluable in deciphering the exogenous signals that coordinate the growth and differentiation of cranial neural crest cells. For instance, models of conditional deletion and overexpression of Bmp4 have revealed roles for this signaling molecule in various aspects of craniofacial development. Bmp4 is primarily expressed by epithelial structures in the developing face, which signal to neural crest-derived mesenchyme to mediate processes such as palatogenesis and tooth development (Zhang et al., 2002, Mitsiadis et al., 2010). Interestingly, both abrogation and ectopic activation of BMP signaling lead to cell cycle dysregulation, cleft palate and tooth abnormalities, suggesting that this signaling pathway is subject to multiple levels of regulation in neural crest development (He et al., 2010).

While the correct spatial and temporal expression of signaling molecules is critical for normal craniofacial morphogenesis, little is known about how the signaling pathways involved in this process are regulated at the epigenetic level. Using *in vivo* and *in vitro* models, I show in this chapter that the class I histone

deacetylase Hdac3 regulates important genetic programs and signaling pathways involved in murine craniofacial development. Genetic deletion of Hdac3 in neural crest results in microcephaly, cleft palate, ossification defects and other craniofacial abnormalities in late gestation. Consistent with these observations, we observe dysregulation of mediators of craniofacial development in midgestation following loss of Hdac3, including transcription factors belonging to the Msx and Tbx families. We show that this aberrant gene expression is mediated, in part, by derepression of Bmp4 in neural crest. These results suggest that Hdac3-mediated repression of Bmp4 plays a critical role in craniofacial development.

Results

Hdac3 is expressed during embryogenesis and is efficiently deleted in premigratory neural crest cells by *Wnt1-Cre*

Immunohistochemistry of staged embryos demonstrates that Hdac3 is widely expressed at E10.5, including in the dorsal neural tube, where neural crest cells are specified before delaminating and migrating throughout the embryo (Figure 2.1 A). Hdac3 is also expressed by neural crest derivatives, including dorsal root ganglia (DRG) and cranial mesenchyme (Figure 2.1 A,B).

The *Wnt1-Cre* transgene is expressed by premigratory neural crest cells as early as E8.75 (Jiang et al., 2000). We used *Wnt1-Cre* and a floxed *Hdac3* allele (*Hdac3*^{f}) to delete *Hdac3* in premigratory neural crest cells and their derivatives, and we used the *Z/EG* reporter to lineage trace neural crest cells in both control and mutant embryos (Feng et al., 2011, Novak et al., 2000). In this lineage tracing strategy, Cre mediates a recombination event that results in the constitutive expression of GFP in all derivatives of *Wnt1-Cre*-expressing cells. Immunostaining for GFP reveales expression in the dorsal neural tube in both *Wnt1-Cre; Hdac3*$^{f/f}$ (termed *Hdac3*^{Wnt1NCKO}*); Z/EG* and *Wnt1-Cre; Z/EG* control embryos (Figure 2.1 A). In E10.5 *Hdac3*^{Wnt1NCKO} embryos, the GFP-positive cells in the dorsal neural tube show loss of Hdac3 protein, indicating efficient Cre-mediated recombination in neural crest (Figure 2.1 A). Lineage tracing analysis further demonstrates that neural crest cells populate the DRG, pharyngeal arches

and cranial mesenchyme in E9.5 and E10.5 *Hdac3*^{Wnt1NCKO}; *Z/EG* embryos, despite efficient deletion of Hdac3 in these tissues (Figure 2.1 A-C). Immunohistochemistry also reveals that Hdac3 deletion is specific to neural crest-derived mesenchyme, while expression is retained in ectoderm and endoderm (Figure 2.1 C). However, despite grossly intact neural crest cell specification and migration in the absence of Hdac3, marked hypoplasia of the neural crest-derived maxillary and mandibular prominences of the first pharyngeal arch is apparent by E10.5 in *Hdac3*^{Wnt1NCKO} embryos (Figure 2.1 C,D).

Hdac3^{Wnt1NCKO} embryos exhibit severe craniofacial abnormalities in late gestation, resulting in perinatal lethality

Hdac3^{Wnt1NCKO} embryos are found at expected Mendelian ratios in late gestation and are viable until birth (Table 2.1). However, these mice uniformly succumb at P0 (Table 2.1). *Hdac3*^{Wnt1NCKO} mice are born with microcephaly, micrognathia, a shortened snout and eyelid closure defects, with preservation of body morphology (Figure 2.2 A). Optical projection tomography and histology of *Hdac3*^{Wnt1NCKO} heads reveals cleft palate, which is also apparent in late gestation embryos (Figure 2.2 B,C). The palate defect is characterized by a large posterior cleft without additional facial clefting (Figure 2.2 B). Cleft palate is fatal in perinatal mice; afflicted pups are unable to generate suction and nurse, and subsequently die at P0 from dehydration and accumulation of air in the digestive

tract (Qiu et al., 1995, Condie et al., 1997). Consistent with these reports, *Hdac3*^{Wnt1NCKO} pups are unable to feed, as evidenced by the lack of a milk spot (Figure 2.2 A). The gross craniofacial defects observed in *Hdac3*^{Wnt1NCKO} mice are fully penetrant and are summarized in Table 2.2. We observed similar craniofacial abnormalties using a second neural crest driver, *Pax3*^{Cre} (Engleka et al., 2005); these abnormalities are also evident both at P0 and in late gestation (Figure 2.3).

Loss of Hdac3 leads to ossification defects in the calvarium and viscerocranium

In the adult vertebrate, osteoblasts are among the most abundant cell types generated by cranial neural crest. Neural crest-derived osteoblasts contribute to the bones of the face, the skull base and the entirety of the calvarium, with the exception of the parietal bone (Santagati and Rijli, 2003). Hdac3 has previously been implicated in multiple stages of osteoblast differentiation and maturation. In committed, undifferentiated osteoblasts that express the *Osx-Cre* transgene, deletion of Hdac3 leads to subtle abnormalities in calvarial osteoblast differentiation, and progressive abnormalities in trabecular bones that lead to perinatal runting, and death early in adulthood (Razidlo et al., 2010). While these findings demonstrate a role for Hdac3 in promoting bone formation, in both perinatal osteoblasts and in the MC3T3 cell line, Hdac3 inhibits the pro-osteogenic effects of Runx2, suggesting that Hdac3 is playing an anti-

osteogenic role in a slightly later stage of bone development (Schroeder et al., 2004, Hesse et al., 2010). In more mature osteoblasts, marked by RANKL expression, Hdac3 inhibits the anti-osteogenic effects of Runx2, resulting in a net pro-osteogenic role once again (Hesse et al., 2010).

Consistent with a pro-osteogenic role for Hdac3 in the earliest stages of bone development, *Hdac3*^{Wnt1NCKO} mice - in which Hdac3 is deleted well before osteoblasts are specified (before the onset of *Osx-Cre* expression) - exhibit severe bone defects in the calvarium and viscerocranium. Alcian blue/alizarin red staining of the late embryonic and perinatal heads reveales decreased ossification of the calvarium, particularly in the region of the frontal bone, where ossified bone is undetectable by alizarin red staining (Figure 2.4 A). The open frontal fontanel leads to hemorrhage in some newborn pups following parturition (Figure 2.2 B). The parietal bone develops normally in *Hdac3*^{Wnt1NCKO} mutants, consistent with its mesodermal origin (Figure 2.2B). In mutant embryos, ossification abnormalities of the viscerocranium were also identified in the mandible, skull base and tympanic ring (Figure 2.4 A).

Additional bone abnormalities in E17.5 mutant embryos are detected by Goldner's trichrome staining. Neural crest-derived calvarial bones, including the frontal bone, are thin and show minimal mineralization (Figure 2.4B). Additionally, at variable penetrance, absence of ossification in the cribiform plate results in encephalocoele, in which the brain herniates into the nasal sinuses (Figure 2.4

B). The ossification defects observed in *Hdac3*^{Wnt1NCKO} mice are summarized in Table 2.2.

We used an *ex vivo* approach to identify important regulators of ossification that are dysregulated following the loss of Hdac3. We grew cranial mesenchyme isolated from mutant and littermate controls in culture and found that Runx2, a critical regulator of ossification, and alkaline phosphatase, a marker of differentiating bone, are significantly downregulated in mutant cultures (Figure 2.4 C). We subsequently found that Runx2 expression in the developing calvarium and skull base is decreased *in vivo* at E12.5 (Figure 2.4 D). The Runx2 expression domain is diminished in spite of the presence of large numbers of neural crest cells in these regions in the mutant (Figure 2.4 D). These results suggest that downregulation of Runx2 in neural crest cells is an important mechanism by which ossification defects develop in *Hdac3*^{Wnt1NCKO} embryos.

Abnormal odontogenesis in the absence of Hdac3 leads to dental hypoplasia

In tooth development, signals from the epithelium initiate condensation of neighboring neural crest cells at E11.5 (Chen et al., 2000). As epithelial cells invaginate, they envelop neural crest cells, which will eventually form the pulp of the tooth (Figure 2.5 A). The early stages of odontogenesis proceed normally in *Hdac3*^{Wnt1NCKO} embryos, with tooth bud morphology at E15.5 appearing similar to littermate controls (Figure 2.5 A-D). However, expansion of the neural crest-

derived mesenchyme does not occur between E15.5-E17.5, resulting in hypolastic teeth with the absence of normal pitting (Figure 2.5 E,F). The tooth bud hypoplasia in mutant embryos parallels the hypoplasia observed in other neural crest-derived structures in late gestation (Figure 2.2).

Aberrant cell cycle regulation in Hdac3-deficient cranial mesenchyme leads to cleft palate and microcephaly

In order to determine the mechanism of cleft palate in *Hdac3*^{Wnt1NCKO} embryos, we performed a histological analysis of staged control versus mutant embryos. In normal palatogenesis, the anterior palate (referred to as the *primary palate*) is formed by the initial fusion of the maxillary prominences with the frontonasal prominence. *Hdac3*^{Wnt1NCKO} embryos exhibit posterior cleft palate, suggesting that secondary palatogenesis is disrupted (Figure 2.2 B). The posterior aspects of the hard palate (referred to as the *secondary palate*) are formed from two outgrowths of neural crest-derived mesenchyme that lie on either side of the stomodeum (primitive mouth). These outgrowths are referred to as the palatal shelves, and are detectable at E11.5 in the mouse (Figure 2.6 A). Between E11.5 and E13.5, the palatal shelves, driven by neural crest cell proliferation, expand towards the mandible (Figure 2.6 A,B). Between E13.5 and E14.5, the palatal shelves elevate relative to the tongue and fuse in the midline with the nasal septum (Figure 2.6 C). This newly formed structure subsequently ossifies, giving rise to the secondary palate.

Disruption of any of the stages of secondary palatogenesis - palatal shelf formation, expansion, elevation, fusion or ossification – can lead to cleft palate in mice, and similar mechanisms can contribute to secondary cleft palate in humans (Richarte et al., 2007, Ito et al., 2003, Vallejo-Illarramendi et al., 2009, He et al., 2011, Wu et al., 2008). Histological analysis of *Hdac3*^{Wnt1NCKO} embryos reveals that the palatal shelves form appropriately but are hypoplastic at E12.5 (Figure 2.6 E,F). Despite appropriate elevation of the medial aspect of the palatal shelves by E14.5, they do not meet at the midline (Figure 2.6 G). These results suggest that cleft palate results in *Hdac3*^{Wnt1NCKO} embryos due to a failure of palatal shelf expansion.

Expansion of the palatal shelves is dependent on proliferation and survival of the neural crest cells that make up the palatal shelf mesenchyme (Ito et al., 2003). In E12.5 control versus mutant palatal shelves that were matched for surrounding anatomical landmarks, we detected a significant increase in apoptosis and a trend towards decreased proliferation, as determined by Tunel and phospho-histone H3 staining, respectively (Figure 2.6 I). Increased Tunel staining is also visible throughout additional cranial neural crest-derived structures outside of the palatal shelf region, suggesting that hypoplasia of these structures is also mediated by increased apoptosis (Figure 2.6 I and data not shown).

To discern the nature of the cell cycle dysregulation in *Hdac3*^{Wnt1NCKO} cranial mesenchyme, we performed expression profiling by quantitative RT-PCR

in the anterior cranial region of mutant embryos and littermate controls (Figure 2.6 J). While *Hdac3* expression in mutant tissue is significantly downregulated, expression of additional class I Hdacs is unchanged (Figure 2.6 K). Strikingly, the expression of multiple cell cycle regulators was found to be altered in *Hdac3*^{Wnt1NCKO} cranial mesenchyme. *Cdkn1a* (p21), *Trp52* (p53), *Ccnd1c* (p57), *Ccnd1* (Cyclin D1), *Ccnd3* (Cyclin D3), *CcnG1* (Cyclin G1) and *Cdk2* are significantly upregulated in the absence of Hdac3, while *Cdkn2c* (p18) expression is downregulated (Figure 2.6 L).

Hdac3 has previously been shown to directly repress the cell cycle inhibitor p21 in multiple tissues (Wilson et al., 2008, Trivedi et al., 2008). In order to determine whether the substantial upregulation of p21 observed in *Hdac3*^{Wnt1NCKO} cranial mesenchyme could alone account for cleft palate and microcephaly in these embryos, we deleted Hdac3 in neural crest on a p21 null background (Deng et al., 1995). Homozygous p21$^{-/-}$ mice develop normally and are viable and fertile (Deng et al., 1995). We found that loss of p21 does not rescue the cleft palate and microcephaly observed in *Hdac3*^{Wnt1NCKO} embryos, suggesting that dysregulation of additional cell cycle modulators contributes to altered regulation of neural crest expansion in Hdac3-deficient cranial neural crest cells and, ultimately, to cleft palate and craniofacial hypoplasia (Figure 2.7).

The loss of Hdac3 results in dysregulation of core transcriptional networks that regulate craniofacial development

Multiple families of transcription factors have been implicated in neural crest cell cycle regulation in craniofacial development. We undertook a candidate approach to identify whether loss of Hdac3 results in misexpression of known regulators of cranial crest expansion and survival. *Msx1* and *Msx2* are expressed in the cranial mesenchyme, and are known to modulate the cell cycle during palatogenesis, viscerocranial morphogenesis, and tooth development (Alappat et al., 2003). We observed marked upregulation by quantitative RT-PCR of *Msx1*, *Msx2* and *Msx3*, in E12.5 mutant cranial mesenchyme (Figure 2.8 A). Msx family members promote apoptosis in neural crest cells, and their upregulation is consistent with the cell cycle dysregulation and increased apoptosis in $Hdac3^{Wnt1NCKO}$ mice (Alappat et al., 2003). Interestingly, transgenic overexpression of *Msx2* leads to cleft secondary palate, micrognathia, tooth hypoplasia and eyelid dysplasia due to increases in cell death, which phenocopies many aspects of the $Hdac3^{Wnt1NCKO}$ abnormalities (Winograd et al., 1997).

In addition to upregulation of Msx family members, we also observed significant upregulation of the Tbx family members *Tbx2* and *Tbx3* (Figure 2.8 A). *Tbx2* and *Tbx3*, like *Msx1* and *Msx2*, are normally expressed in neural crest-derived cranial mesenchyme and are similarly important in cell cycle regulation during palatogenesis (Zirzow et al., 2009). Loss of Tbx2 or Tbx3 in craniofacial development leads to cleft palate due to excessive proliferation, and both proteins have been identified as inhibitors of the cell cycle in palatogenesis

(Zirzow et al., 2009). Overall, upregulation of these Msx and Tbx family members – known inhibitors of neural crest survival - is consistent with the increased apoptosis and cell cycle dysregulation observed in *Hdac3*^{Wnt1NCKO} cranial mesenchyme, and the resultant craniofacial hypoplasia and cleft palate in mutant embryos.

Increased expression of *Bmp4*, a critical regulator of craniofacial development, in *Hdac3*^{Wnt1NCKO} cranial mesenchyme

Hdac3 is a global agent of gene repression and has previously been shown to directly regulate important transcriptional networks in multiple developmental contexts (Schroeder et al., 2004, Zeng et al., 2006). The upregulation of Msx and Tbx family members observed in *Hdac3*^{Wnt1NCKO} embryos could therefore plausibly occur as a result of their direct transcriptional derepression in the absence of Hdac3. However, Msx and Tbx family members have also been implicated in a genetic pathway involving Bmp4, and have been identified as direct targets of Bmp4 signaling in craniofacial development (Bei and Maas, 1998, Lee et al., 2007). Bmp4 is expressed predominantly by epithelial cells, which signal directly to neural crest to regulate palatogenesis and tooth development (Mukhopadhyay et al., 2006, He et al., 2010, Mitsiadis et al., 2010). Gain of BMP signaling results in craniofacial abnormalities that partially phenocopy the abnormalities identified in *Hdac3*^{Wnt1NCKO} embryos (He et al., 2010). However, loss of BMP signaling also phenocopies aspects of these

phenotypes, albeit through different mechanisms (Baek et al., 2011, Mitsiadis et al., 2010). We detected significant upregulation of *Bmp4* expression in the anterior cranial mesenchyme of E12.5 *Hdac3*^{Wnt1NCKO} embryos, which is consistent with the increased apoptosis and the pattern of transcriptional dysregulation observed in mutant craniofacial mesenchyme (Figure 2.8 A).

In craniofacial development, *Bmp4* expression is activated by Sonic Hedgehog signaling in an autoregulatory loop (Lan and Jiang, 2009, Zhang et al., 2002). However, little is known about how Bmp4 expression is restricted in the neural crest. We observed upregulation of *Bmp4* in conjunction with a small but statistically insignificant upregulation of *Shh* (Figure 2.8 A). These observations are consistent with a model in which Hdac3 directly represses transcription at the *Bmp4* locus, such that the loss of Hdac3 in neural crest leads to direct transcriptional derepression.

Based on these findings, we hypothesized that altered Bmp4 expression in Hdac3-deficient neural crest could account, in part, for the gene expression profile and phenotypic abnormalities observed in *Hdac3*^{Wnt1NCKO} embryos. We used an *ex vivo* approach to determine the importance of Bmp4 derepression in mediating the *Msx2* upregulation observed in Hdac3-deficient cranial neural crest. We found that total loss of Hdac3 in E12.5 cultured anterior mesenchymal cells results in massive cell death (data not shown). Therefore, we induced partial knockdown of *Hdac3* using shRNA, and examined the expression of *Bmp4* and *Msx2* in this tissue. We found that partial knockdown of *Hdac3* results in a trend

towards *Bmp4* upregulation, and statistically significant upregulation of *Msx2* (Figure 2.8 C). This upregulation of *Msx2* is abolished by siRNA-mediated knockdown of *Bmp4*. These results are consistent with a model in which Hdac3 regulates a Bmp4-Msx2 signaling pathway in cranial neural crest during craniofacial development.

Discussion

At multiple stages of neural crest development, the growth and survival of neural crest cells comes under positive and negative regulation from surrounding cell types (Sauka-Spengler and Bronner-Fraser, 2008). The signaling molecule Bmp4 is an important mediator of neural crest apoptosis in both early and late stages of craniofacial morphogenesis. Delamination of cranial neural crest cells from the dorsal neural tube requires the programmed death of neural crest cells at specific levels (rhombomeres) along the rostro-caudal axis. In the chick, Bmp4 is expressed specifically in these rhombomereic levels, both in neural crest cells themselves and in neighboring ectoderm (Graham et al., 1994). Bmp4 signaling upregulates *Msx2* in order to mediate apoptosis in these populations of neural crest cells, allowing suriving cells from other rhombomeres to appropriately populate the developing face (Graham et al., 1994). The mechanism by which *Bmp4* expression is restricted to particular rhombomeric levels is not known. Excessive Bmp4 signaling in the cranial neural crest in mouse has been shown to portend abnormal palatal shelf morphology, secondary cleft palate, and dental hypoplasia (He et al., 2010). These abnormalities are consistent with the phenotypes caused by *Msx2* transgenic overexpression as well as many of the phenotypes observed in $Hdac3^{Wnt1NCKO}$ embryos (Figure 2.1 C,D, Figure 2.2). It is therefore intriguing to speculate that Hdac3 could be required to restrict the expression of *Bmp4* in rhombocephalic neural crest. Loss of Hdac3 would

therefore result in persistent upregulation of *Bmp4* in cranial neural crest, leading to hypoplasia of craniofacial structures.

Both increased and decreased Bmp4 activity in neural crest development lead to dysregulation of downstream Msx and Tbx transcription factors and severe craniofacial abnormalities (He et al., 2010, Bei and Maas, 1998). That craniofacial morphogenesis is so exquisitely sensitive to Bmp4 activity speaks to the importance of fine regulation of *Bmp4* expression in neural crest development. Our study offers the first evidence of a chromatin remodeling enzyme playing a role in the regulation of *Bmp4* expression. While our data demonstrate that Hdac3 is required to repress *Bmp4* transcription, additional work is required to discern whether this transcriptional repression is mediated by direct Hdac3 binding at the *Bmp4* locus, or whether this repression is mediated through intermediates (further discussed in Chapter 4).

In this study we have also identified a distinct role for Hdac3 in promoting ossification of neural crest-derived bone. This finding is consistent with a pro-ossification role for Hdac3 previously identified in committed osteblast precursors, although we have found that deletion of *Hdac3* prior to commitment of osteoblasts results far more drastic deficiencies in bone development than deletion in committed precursors (Razidlo et al., 2010). The mechanism of a pro-ossification role of Hdac3 has not previously been described. In addition to regulating the Bmp4-Msx pathway, it is likely that Hdac3 regulates a wide range of other downstream targets in neural crest. While dysregulation of the Bmp4-

Msx pathway is sufficient to explain many of the craniofacial defects of Hdac3 mutant pups, it is unlikely to contribute to the ossification abnormalities. Paradoxically, deletion of *Msx1* and *Msx2* in neural crest leads to heterotopic bone formation, particulary in the frontal bone region, while *Msx2* transgenic overexpression also results in ectopic bone formation (Roybal et al., 2010, Liu et al., 1995). This suggests that additional targets of Hdac3 are likely to underlie the ossification abnormalities in $Hdac3^{Wnt1NCKO}$ mice.

Gene expression analysis of explanted tissue demonstrated that the critical regulator of ossification *Runx2* is significantly downregulated in Hdac3-deficient tissue. Hdac3 has not previously been shown to regulate Runx2 expression. However, Hdac3 antagonizes the pro-osteogenic activity of Runx2 in perinatal osteoblast precursors, while antagonizing the anti-osteogenic activity of Runx2 in more mature osteoblasts (Schroeder et al., 2004, Hesse et al., 2010). These diverse roles played by Hdac3 in the regulation of Runx2 in osteogenesis are reminiscent of the varied functions of Hdac3 in cardiac development and homeostasis (discussed in Chapter 1). In both organ systems, Hdac3 mediates vastly different - even antagonistic - processes in different developmental stages of the same tissue. Determining how the role of Hdac3 is altered during the course of each tissue's development will be an interesting area of future investigation.

Materials and Methods

Mice

Wnt1-Cre, *Pax3^{Cre}*, *Hdac3^{flox}* and *Z/EG* mice were maintained on mixed CD1/B6/129 genetic backgrounds, separated by 3-6 generations of incrossing from pure parental backgrounds (Jiang et al., 2000, Engleka et al., 2005, Feng et al., 2011, Novak et al., 2000). p21 null mice were on a pure 129 background (Deng et al., 1995). Mice were genotyped using previously described Cre-specific PCR primers (5'-TGC CAC GAC CAA GTG ACA GC-3', 5'-CCA GGT TAC GGA TAT AGT TCA TG-3') (Heidt and Black, 2005), and primers designed to distinguish between the control and floxed *Hdac3* allele (5'-GCA GTG GTG GTG AAT GGC TT-3', 5'-CCT GTG TAA CGG GAG CAG AAC TC-3'). Genotyping for the Z/EG transgene was performed by X-Gal staining tail samples. Littermate embryos were analyzed in all experiments unless otherwise noted. The University of Pennsylvania Institutional Animal Care and Use Committee approved all animal protocols.

Histology and immunohistochemistry

These techniques were performed on paraformaldehyde-fixed, paraffin imbedded slides as previously described (High et al., 2008). Mutant and littermate control embryos were generated from *Wnt1-Cre; Hdac3$^{f/+}$; Z/EG*, *Wnt1-Cre; Hdac3$^{f/+}$* or Pax3$^{Cre/+;}$ *Hdac3$^{f/+}$* animals crossed to *Hdac3$^{f/+}$*, *Hdac3$^{f/+}$*; *Z/EG*

or *Hdac3*$^{f/f}$ animals, respectively. Embryos were dissected in cold PBS, fixed overnight in 2% paraformaldehyde, dehydrated into 100% ethanol, embedded in paraffin and sectioned. H&E and Goldner's trichrome staining were performed using standard procedures. Primary antibodies used for immunohistochemistry were anti-GFP goat polyclonal (Abcam AB6673, 1:100), anti-GFP rabbit polyclonal (Invitrogen A-11122, 1:200) and rabbit polyclonal anti-Hdac3 (Santa Cruz sc-11417x, 1:10).

All control versus mutant histological and immunohistochemical images were taken at the same exposure and contrast settings, using NIS Elements software. ImageJ software was used to merge images and for quantification of neurofilament and tyrosine hydroxylase staining intensity. In some cases, ImageJ was used to decrease image brightness, and this was performed identically in control and mutant images.

Cell number, proliferation and apoptosis were quantified by manually counting nuclei, pHistone H3-, or Tunel-positive cells, respectively, in adjacent sections of the anatomically-defined palatal shelf region in a blinded manner.

Optical projection tomography

E10.5 embryos were fixed in 4% paraformaldehyde overnight. Embryos were bleached for 30 minutes in 5% H2O2 in PBST, digested in 10μg/mL proteinase K in PBST for 5 minutes and immunostained with mouse polyclonal Anti-2H3 (Iowa Hybridoma Bank, 1:100). An HRP Conjugated secondary

antibody and DAB substrate kit (Vector Laboratories) were used to visualize peripheral nerves.

For OPT scanning, embryos were dehydrated into 100% methanol, embedded in 1% low-melt agarose, cleared overnight in 1:2 (v/v) benzyl alcohol and benzyl benzoate, and scanned using the Bioptonics OPT scanner (3001M) (Sharpe et al., 2002). Image stacks were reconstructed using OsiriX software. Image contrast was optimized to reveal peripheral nerve patterning.

Alcian blue/alizarin red staining

Embryos and neonatal mice were fixed for 7 days in 90% ethanol for one week at 4°C. Samples were stained for 3-5 days at room temperature with Alcian blue solution (0.2mg/ml Alcian Blue, 80% ethanol, 3.5M acetic acid) to visualize cartilage, and then rehydrated with an ethanol/water gradient. Samples were then incubated with 1% KOH for 2, followed by incubation for 3 days with Alizarin Red solution (0.05mg/ml Alizarin Red S in 1% KOH) to visualize bone, followed by 3 washes (2-3 hours each) in 1% KOH solution.

Anterior cranial mesenchyme explant cultures

The anterior cranial mesenchyme of wild type CD1 embryos was dissected in sterile PBS supplemented with 1% penicillin/streptomycin (Gibco). Tissue was triturated in cold 0.25% trypsin (Gibco), incubated on ice for 5 minutes, and then at 37°C for 10 mins on a nutator. 10% v/v FBS was used to

stop trypsination, cells were further triturated to a single cell suspension, spun at 300x g for 5 minutes, resuspended in αMEM (Invitrogen A10490-01), filtered through a 40μm filter, and played in 6-well plates. After two hours, cells were transfected with 5nmol of total siRNA using 4 μL of Lipofectamine 2000 (Invitrogen) per well in 600μL total volume of serum free αMEM and Optimem (Gibco). Control siRNA (D-001810), Hdac3 siRNA (L-043553), and Bmp4 siRNA (L-043095) were obtained from Thermo Scientific. After overnight transfection, media was replaced with serum-free αMEM and cells were grown for an additional 24 hours before being harvested for RNA isolation.

RNA isolation, complementary DNA synthesis and quantitative RT-PCR

From explanted cranial mesenchyme, RNA was harvested in 1mL of Trizol (Invitrogen). Cells were sheared with trituration and by being passed twice through a 26 gauge needle.

For E12.5 cranial mesenchyme expression profiling, *Wnt1-Cre; Hdac3*$^{f/f}$ and litermate Cre-negative control embryos were microdissected with tungsten needles in cold PBS. Samples were immediately immersed in 1mL Trizol and homogenized with a handheld homogenizer. Samples were passed twice through a 26 gauge needle to shear genomic DNA and incubated at room temperature for 10 minutes. 100μL of BCP reagent (Molecular Research Center) was added to samples, which were mixed for 15s and spun in a microcentrifuge at 11.5k rmp for 15mins at 4°C. The aqueous phase was then combined with 600μL of 70%

ethanol. The sample was applied to a Qiagen RNeasy spin column, and subsequent kit steps, including on column DNAse I digestion, were followed. Total RNA was eluted in 50µL of RNAse free water (Qiagen), and evaporated down to a total volume of 15µL. Complementary DNA (cDNA) was synthesized according to kit instructions with the Superscript III system (Invitrogen).

Quantitative RT-PCR was performed in triplicate using Sybr Green (Applied Biosystems). *Gapdh* was used as a reference control gene. Primer sequences (Table 2.3) were designed using IDT software, unless otherwise indicated. All primer pairs were designed to flank exon-exon junctions. Primer pairs were validated with a four point standard curve, and only primers offering r^2 values >0.97 were used.

Statistics

The chi-squared test and student's two-tailed t test were used to ascertain differences between groups. A x^2 or p-value of less than 0.05 was considered significant.

Table 2.1. *Hdac3*^{Wnt1NCKO} mice exhibit perinatal lethality.

***Wnt1-Cre; Hdac3*$^{f/+}$ x *Hdac3*$^{f/+}$**				
E16.5-E18.5	**# Observed**	**Observed**	**#Expected**	**Expected**
Hdac3$^{+/+}$	9	0.12	9	0.13
Hdac3$^{f/+}$	17	0.23	19	0.25
Hdac3$^{f//f}$	8	0.11	9	0.13
Wnt1-Cre; Hdac3$^{+/+}$	7	0.09	9	0.13
Wnt1-Cre; Hdac3$^{f/+}$	23	0.31	19	0.25
***Wnt1-Cre; Hdac3*$^{f/f}$**	**11**	**0.15**	**9**	**0.13**
Total	75			
Chi Sq	**0.82**			
P1	**# Observed**	**Observed**	**# Expected**	**Expected**
Hdac3$^{+/+}$	10	0.14	9	0.13
Hdac3$^{f/+}$	26	0.36	18	0.25
Hdac3$^{f//f}$	10	0.14	9	0.13
Wnt1-Cre; Hdac3$^{+/+}$	9	0.12	9	0.13
Wnt1-Cre; Hdac3$^{f/+}$	18	0.25	18	0.25
***Wnt1-Cre; Hdac3*$^{f/f}$**	**0**	**0**	**9**	**0.13**
Total	73			
Chi Sq	**0.03**			

Table 2.2. Late gestation and perinatal craniofacial abnormalities in *Hdac3*^{Wnt1NCKO} mice.

E16.5-P0	***Wnt1-Cre***	***Wnt1-Cre; Hdac3***$^{f/f}$
Microcephaly	0% (0/14)	100% (19/19)
Cleft palate	0% (0/14)	100% (19/19)
Eyelid closure defects	0% (0/14)	100% (19/19)
Ossification defects of:		
Calvarium	0% (0/5)	100% (3/3)
Mandible	0% (0/5)	100% (3/3)
Base of skull	0% (0/5)	100% (3/3)
Tympanic rings	0% (0/5)	33% (1/3)

Table 2.3. Quantitative RT-PCR primer sequences

Gene name	Protein	Sequence (5' – 3')	Product size	Genomic size
Alpl	Alkaline phosphatase	TGCAAGGACATCGCATATCAG TCCAGTTCGTATTCCACATCAG	116	2975
Bmp2	Bmp2	CGCAGCTTCCATCACGAA TGCAGATGTGAGAAACTCGTC	117	6222
Bmp4	Bmp4	GAGCAGAGCCAGGGAAC GAAGAGGAAACGAAAAGCAGAG	138	1140
Ccnd1	Cyclin D1	GCCCTCCGTATCTTACTTCAAG GCGGTCCAGGTAGTTCATG	145	1538
Ccnd3	Cyclin D3	GCGTGCAAAAGGAGATCAAG GATCCAGGTAGTTCATAGCCAG	120	1001
Ccng1	Cyclin G1	CAGTTCTTTGGCTTTGACACG TTCCTCTTCAGTCGCTTTCAC	147	1597
Cdk2	Cdk2	GCATTCCTCTTCCCCTCATC GGACCCCTCTGCATTGATAAG	128	1251
Cdk4	Cdk4	TACATACGCAACACCCGTGGACAT AGTCGTCTTCTGGAGGCAATCCAA	155	931
Cdkn1a	p21	CTTGCACTCTGGTGTCTGAG GCACTTCAGGGTTTTCTCTTG	145	651
Cdkn1b	p27	TGGACCAAATGCCTGACTC GGGAACCGTCTGAAACATTTTC	144	705
Cdkn1c	p57	CAGGACGAGAATCAAGAGCAG CGACGCCTTGTTCTCCTG	150	694
Cdkn2a	p16 Ink4a (Trivedi et al., 2008)	ATCTGGAGCAGCATGGAGTC CGAATCTGCACCGTAGTTGA	198	5198
Cdkn2c	p18	AAACGTCAACGCTCAAAATGG GACAGCAAAACCAGTTCCATC	133	3524
Cdkn2d	p19 Ink4d	CTTCATCGGGAGCTGGTG AGGCATCTTGGACATTGGG	138	1140
Dmp1	Dmp1	CCCAGTTGCCAGATACCAC	140	4503

		CACTATTTGCCTGTCCCTCTG		
Gapdh	Gapdh	CGTCCCGTAGACAAAATGGT GAATTTGCCGTGAGTGGAGT	177	2011
Hdac1	Hdac1	GAGATGACCAAGTACCACAGTG AAACAAGCCATCAAACACCG	135	4741
Hdac2	Hdac2	AGAAGGAGACAGAGGACAAGA CGAGGTTCCTAAAGTTGGAGAG	144	3045
Hdac3	Hdac3	CCATTCTGAGGACTACATCGAC TGTGTAACGGGAGCAGAAC	142	6837
Hdac8	Hdac8	ACCGAATCCAGCAAATCCTC CAGTCACAAATTCCACAAACCG	149	22619
Msx1	Msx1	AAGATGCTCTGGTGAAGGC TGGTCTTGTGCTTGCGTAG	132	2296
Msx2	Msx2	CTCGGTCAAGTCGGAAAATTC GTTGGTCTTGTGTTTCCTCAG	121	3859
Msx3	Msx3	AGTCGCGCACTCTTGTC TATTGCTTCTGGTGAAACTTGC	141	786
Nog	Noggin	ATCTGGAGCAGCATGGAGTC CGAATCTGCACCGTAGTTGA	116	116
Opg	Osteoprogerin (Hesse et al., 2010)	AAGAGCAAACCTTCCAGCTGC CACGCTGCTTTCACAGAGGTC	104	1762
Osr1	Osr1	GATGAGCGACCTTACACCTG ATCCTTTCCCACACTCTTGAC	124	820
Osr2	Osr2	TTGCTCATTCACGAGAGGAC TCCCACACTCCTGACATTTG	145	1101
Osx	Osterix (Hesse et al., 2010)	TCTGCTTGAGGAAGAAGCTCACTAT GGC AGGCAGTCAGACGAGCTGTGC	345	None
Rankl	RANK ligand	AGGCTCATGGTTGGATGTG GAGGACAGAGTGACTTTATGGG	114	5355
Runx2	Runx2	GCTATTAAAGTGACAGTGGACGG GGCGATCAGAGAACAAACTAGG	91	58590

Scx	Scleraxis	ACACCCAGCCCAAACAG TCCTTCTAACTTCGAATCGCC	97	992
Shh	Sonic hedgehog	TCCAAAGCTCACATCCACTG CGTAAGTCCTTCACCAGCTTG	128	2846
Smo	Smoothened	AGCTGCCACTTCTATGACTTC GATCTCACAGTCAGGAATGGG	126	1096
Spry2	Sprouty 2	AGAGGATTCAAGGGAGAGGG ATCAGGTCTTGGCAGTGTG	96	2882
Tbx1	Tbx1	TGGGACGAGTTCAATCAGC TGTCATCTACGGGCACAAAG	145	1544
Tbx2	Tbx2	CACAAACTGAAGCTGACCAAC GAAGACATAGGTGCGGAAGG	147	1054
Tbx3	Tbx3	AGCCAACGATATCCTGAAACTG GTGTCTCGAAAACCCTTTGC	150	1946
Trp53	p53	AGTTCATTGGGACCATCCTG GCTGATATCCGACTGTGACTC	149	6524
Zfp521	Zfp521	ACAAGATCCATCAGTGCCAG CTCTCCGAAATCACACCCTTC	134	9196

Figure 2.1

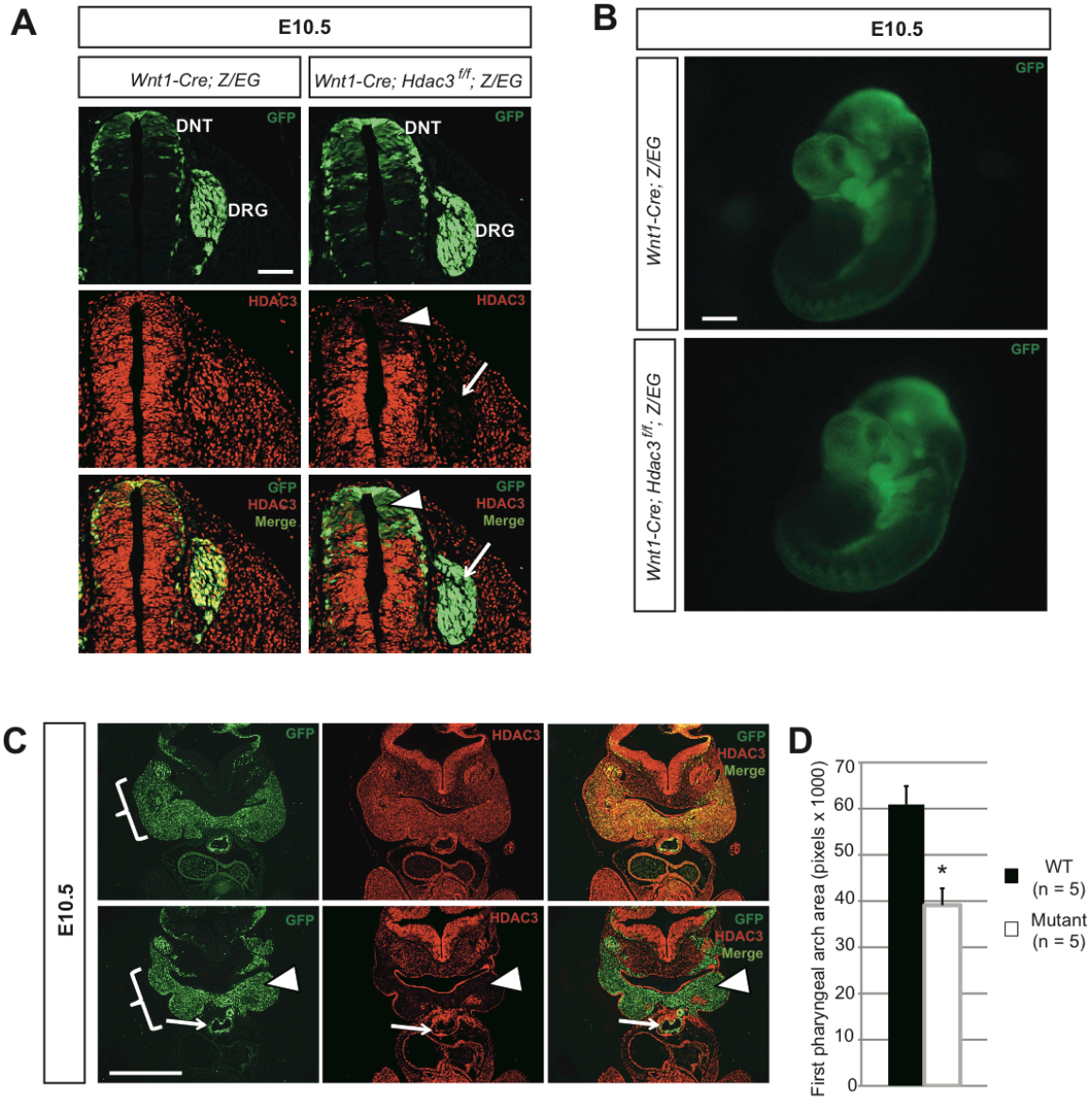
A
E10.5
Wnt1-Cre; Z/EG
Wnt1-Cre; Hdac3 f/f; Z/EG
DNT
GFP
DRG
HDAC3
GFP
HDAC3
Merge
B
E10.5
Wnt1-Cre; Z/EG
Wnt1-Cre; Hdac3 f/f; Z/EG
GFP
C
E10.5
GFP
HDAC3
GFP
HDAC3
Merge
D
First pharyngeal arch area (pixels x 1000)
70
60
50
40
30
20
10
0
*
WT
(n = 5)
Mutant
(n = 5)

Figure 2.1. Deletion of Hdac3 in neural crest results in cranial hypoplasia at E10.5. A. Immunohistochemistry for GFP and Hdac3 in frontal sections of the dorsal neural tube (DNT) and dorsal root ganglia (DRG) at E10.5. *Wnt1-Cre* derivatives marked by GFP expression are found in the control (left) and mutant DNT and DRG. Mutants exhibit efficient deletion of Hdac3 in premigratory neural crest cells in the DNT (arrowhead) and in postmigratory cells in the DRG (arrow), while control embryos show Hdac3 expression in both regions. **B.** Gross fluorescent images of E9.5 embryos. Neural crest cells populate the developing face and pharyngeal arches in control and mutant embryos. **C.** Immunohistochemistry for GFP and Hdac3 in frontal sections of the rostral pharyngeal arches in E10.5 embryos. While the first pharyngeal arch (open bracket) is populated by *Wnt1-Cre* derivates in both control and mutant embryos, Hdac3 is efficiently deleted, specifically in neural crest-derived cells (arrowhead). **D.** Quantification of first pharyngeal arch size in three serial sections from control and mutant embryos. Error bars indicate standard error of the mean. Asterisk denotes $p < 0.05$. Scale bars: **A:** 100μm. **B**: 300μm. **C**. 400μm.

Figure 2.2

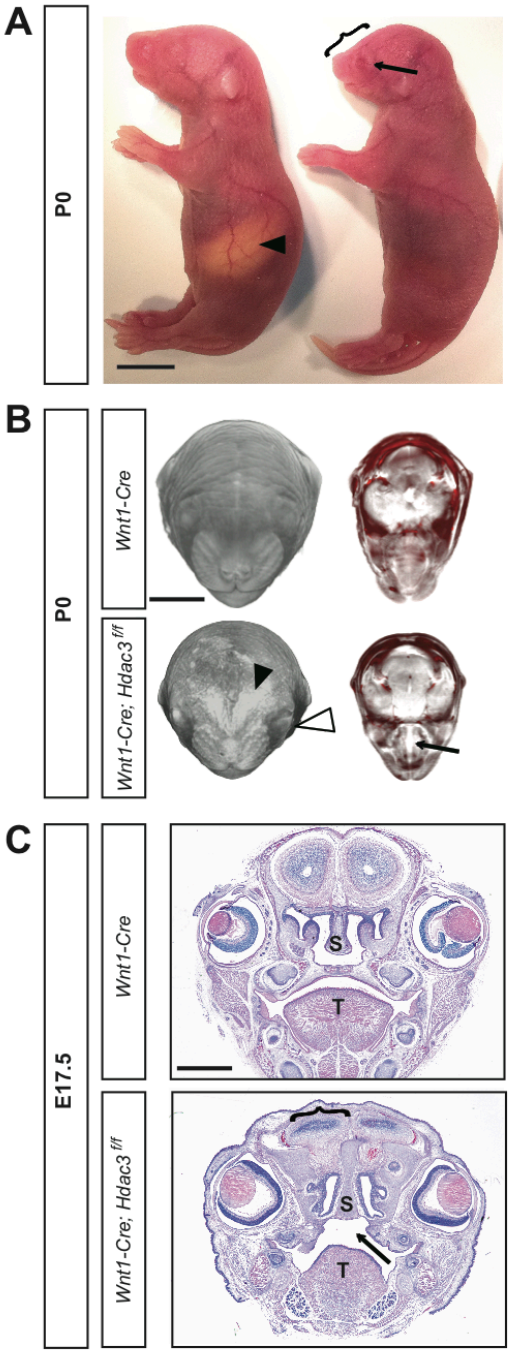
A
P0
B
P0
Wnt1-Cre
Wnt1-Cre; Hdac3 f/f
C
E17.5
Wnt1-Cre
Wnt1-Cre; Hdac3 f/f
S
T
S
T

Figure 2.2. Craniofacial abnormalities in *Hdac3*^{Wnt1NCKO} mice. A. Gross image of a control (left) and mutant P0 pup. Mutants have severe cranial hypoplasia, characterized by a shortened snout (bracket) and micrognathia, and are unable to feed, as indicated by the lack of a milk spot (arrowhead). Mutants also exhibit eyelid dysplasia (arrow). **B.** Optical projection tomography renderings of P0 heads. (Left panels) Viewed *en face*, an area of hemorrhage (black arrowhead) and eyelid closure defects (white arrowhead) are visible in the mutant. (Right panels) Virtual transverse sections cut through the level of the eyes demonstrates a cleft palate (arrow) in the mutant. **C.** H&E stained coronal sections of E17.5 heads. Cleft palate is indicated by the arrow. S: Nasal septum. T: Tongue. Scale bars: **A:** 500μm. **B:** 2mm. **C:** 1.4mm.

Figure 2.3

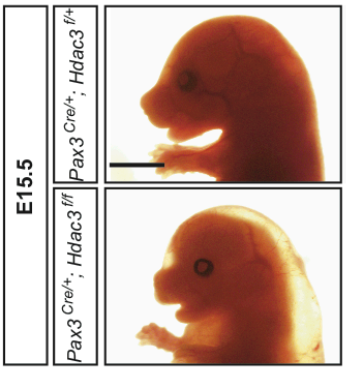

Figure 2.3. Deletion of Hdac3 with *Pax3^{Cre}* recapitulates the craniofacial abnormalities observed using *Wnt1-Cre*. Gross images of E15.5 embryos. The mutant exhibits pronounced microcephaly and shortened snout. Scale bar: 800μm.

Figure 2.4

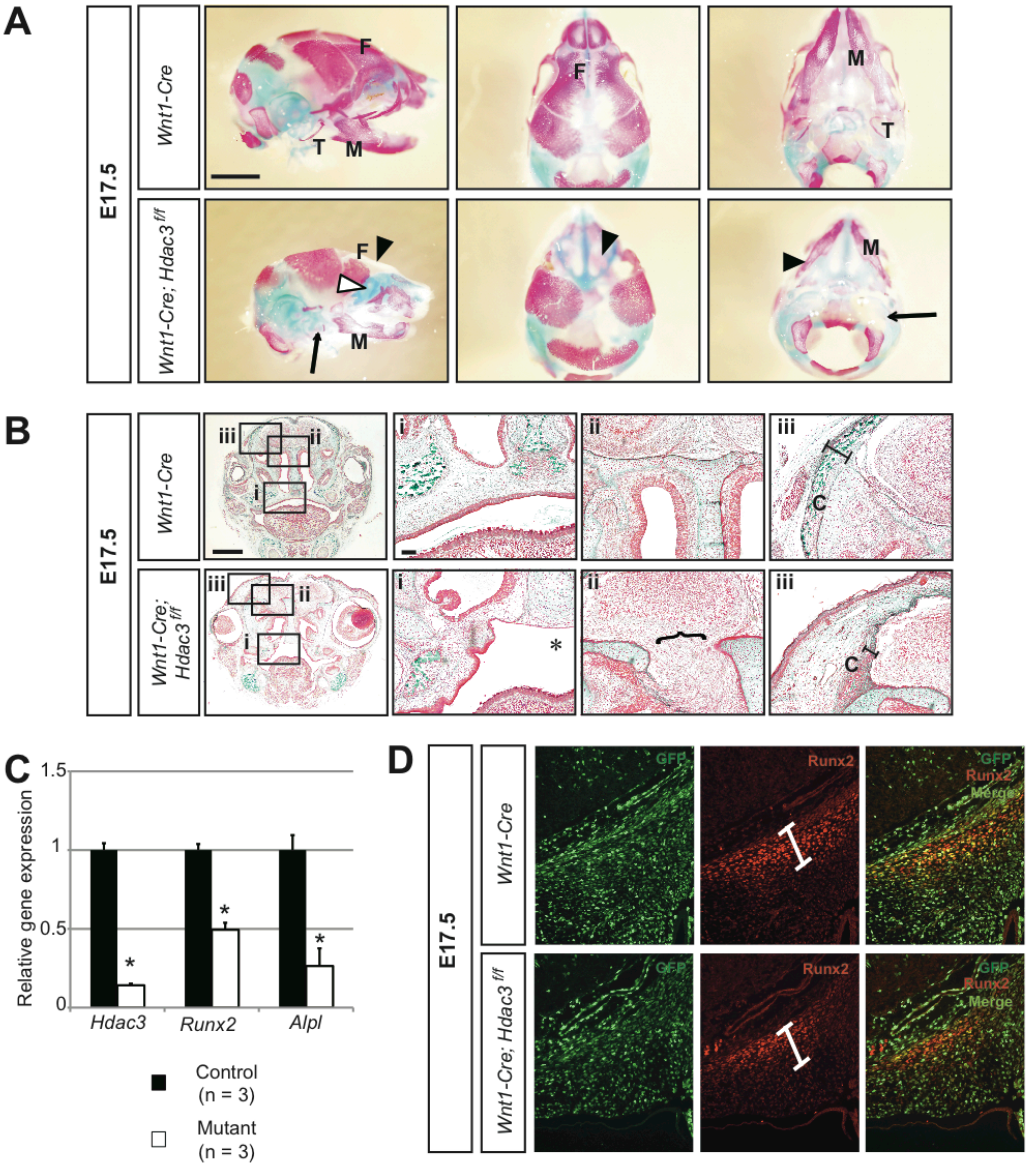
A
E17.5
Wnt1-Cre
Wnt1-Cre; Hdac3 f/f
F
T
M
B
C
Relative gene expression
1.5
1
0.5
0
Hdac3
Runx2
Alpl
Control (n = 3)
Mutant (n = 3)
D
GFP
Runx2
Merge

Figure 2.4. *Hdac3*^{Wnt1NCKO} embryos exhibit defects in craniofacial bone due to dysregulation of important regulators of ossification. A. Alcian blue and alizarin red staining of E17.5 heads. Purple staining indicates ossified bone, blue staining indicates cartilage. Mutants exhibit incomplete ossification of the sphenoid bone (white arrowhead), complete absence of ossification of the frontal bone (F) (black arrowhead), and decreased ossification of viscerocranial structures such as the tympanic ring (T) (arrow). M: Mandible. **B.** Goldner's trichrome staining of E17.5 heads. Green staining represents bone, red staining represents connective tissues. (Inset i) Asterisk (*) indicates cleft palate in the mutant. (Inset ii) Open bracket indicates an area of brain herniating through the base of the skull in the mutant. (Inset iii): Decreased ossification of the calvarium (C) in the mutant. **C.** Quantitative RT-PCR analysis for regulators of ossification, performed on E14.5 microdessected anterior cranial mesenchyme. Gross fluorescent images on the left show representations of the area that was microdissected to obtain RNA. **D.** Representative mmunohistochemistry for Runx2 and GFP in frontal sections of E14.5 heads. Neural-crest derived cells, marked by GFP expression, show decreased expression of Runx2 in regions corresponding to the base of the skull and calvarium.

Figure 2.5

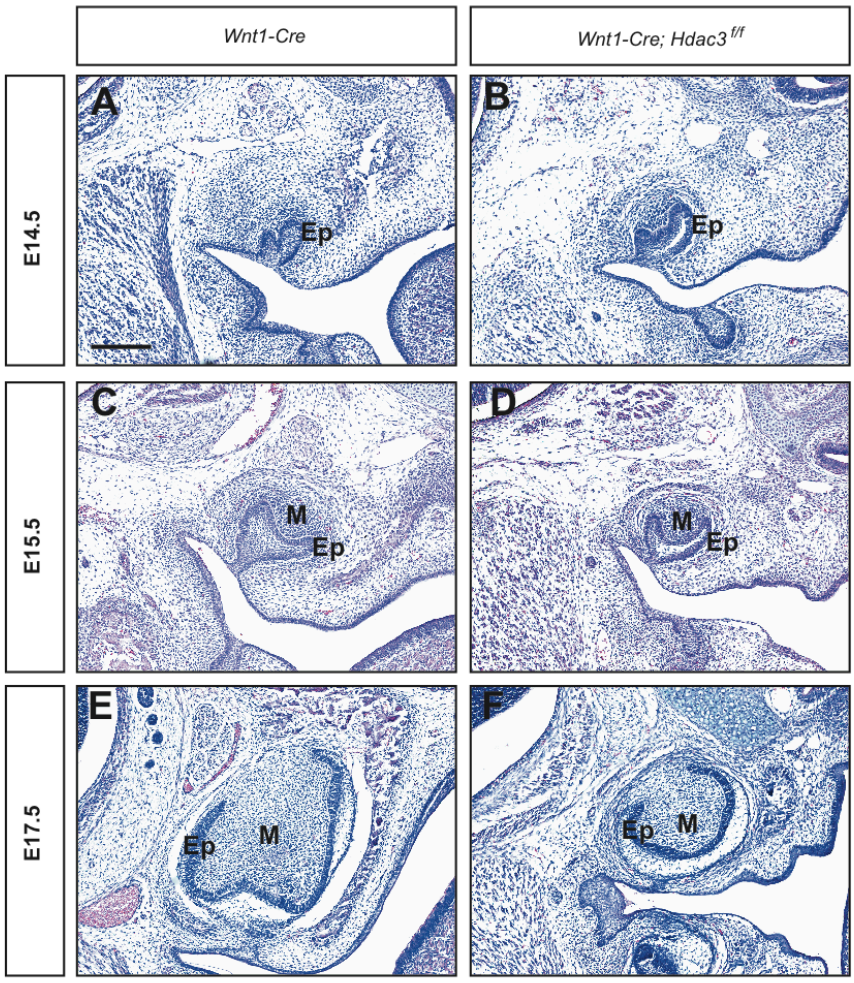

Figure 2.5. The loss of Hdac3 causes hypoplasia of neural crest-derived dental mesenchyme. A-F. H & E stained frontal sections of control and mutant heads at E17.5. Early stages of tooth morphogenesis, including epithelial invagination (**A & B**), and mesenchymal specification (**C & D**) occur normally in the absence of Hdac3. **E&F.** However, at E17.5, the dental pulp shows decreased bulk in mutants. Ep: Epithelium. M: mesenchyme. Scale bar 200μm.

Figure 2.6

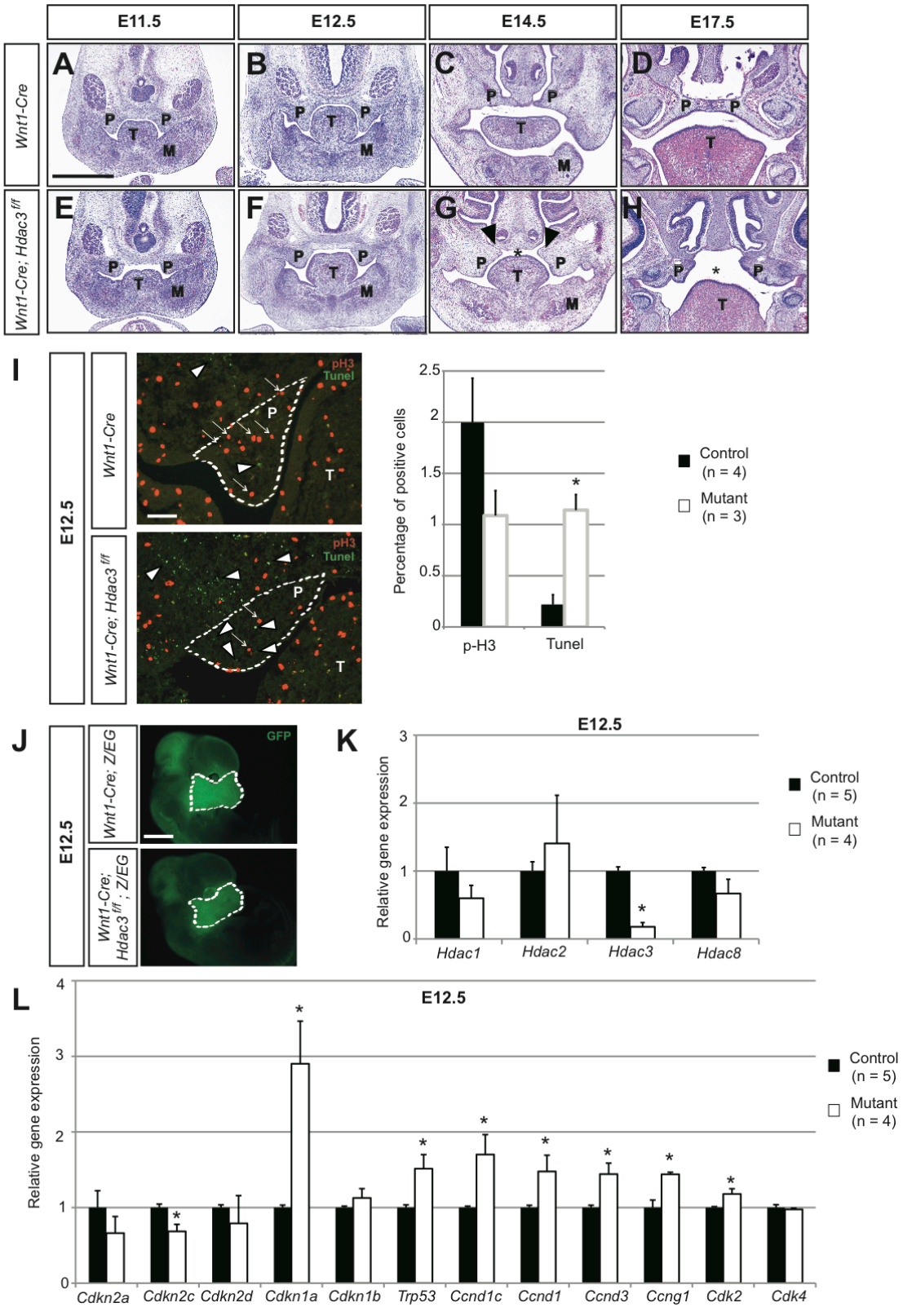
E11.5
E12.5
E14.5
E17.5
Wnt1-Cre
Wnt1-Cre; Hdac3 f/f
A
B
C
D
E
F
G
H
P
T
M
*
I
E12.5
Wnt1-Cre
Wnt1-Cre; Hdac3 f/f
pH3
Tunel
Percentage of positive cells
2.5
2
1.5
1
0.5
0
p-H3
Tunel
Control (n = 4)
Mutant (n = 3)
J
E12.5
Wnt1-Cre; Z/EG
Wnt1-Cre; Hdac3 f/f ; Z/EG
GFP
K
E12.5
Relative gene expression
3
2
1
0
Hdac1
Hdac2
Hdac3
Hdac8
Control (n = 5)
Mutant (n = 4)
L
E12.5
Relative gene expression
4
3
2
1
0
Cdkn2a
Cdkn2c
Cdkn2d
Cdkn1a
Cdkn1b
Trp53
Ccnd1c
Ccnd1
Ccnd3
Ccng1
Cdk2
Cdk4
Control (n = 5)
Mutant (n = 4)

Figure 2.6. Cell cycle dysregulation and increased apoptosis underlie cleft palate in *Hdac3*^{Wnt1NCKO} mice. A-H. H&E stained frontal sections of control and mutant embryos at the level of the palatal shelves. **A-D.** In control embryos, the palatal shelves (P) expand towards the mandible (M) before elevating above the tongue (T), meeting in the midline at E14.5 and ossifying by E17.5. **E-H.** In mutant embryos, the palatal shelves are severely hypoplastic at E12.5 and do not meet in the midline at E14.5 (*), although the medial aspects of the palatal shelves do elevate above the tongue (arrowheads). **I.** Images on the left show the areas defined as palatal shelves in control and mutant embryos at E12.5. Phospho-histone H3 (pH3)- (arrows) and Tunel- (arrowheads) positive nuclei were counted relative to total nuclei in serial sections of the pharyngeal arch mesenchyme. **C.** Representative gross fluorescent images showing the area of cranial mesenchyme microdissected for expression profiling. **D&E.** Quantitative RT-PCR results for class I Hdacs (**D**) and cell cycle regulators (**E**) in E12.5 cranial mesenchyme. Scale bars: **A**: 400µm. **B**: 50µm. **C**: 150µm.

Figure 2.7

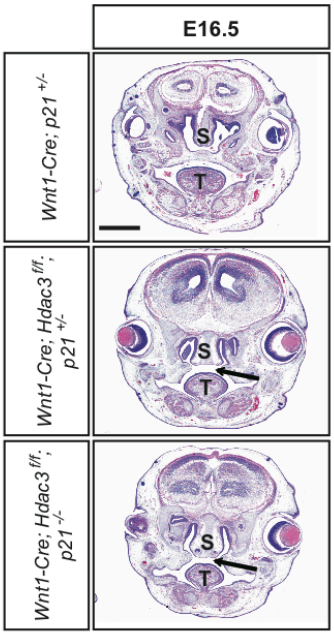
E16.5
Wnt1-Cre; p21 +/-
Wnt1-Cre; Hdac3 f/f; p21 +/-
Wnt1-Cre; Hdac3 f/f; p21 -/-
S
T
S
T
S
T

Figure 2.7. Loss of p21 does not rescue craniofacial abnormalities in *Hdac3*^{Wnt1NCKO} mutants. H&E stained frontal sections of E16.5 heads. Neural crest deletion of Hdac3 on a p21+/- or p21-/- background results in cleft palate (arrow). Scale bar: 400μm.

Figure 2.8

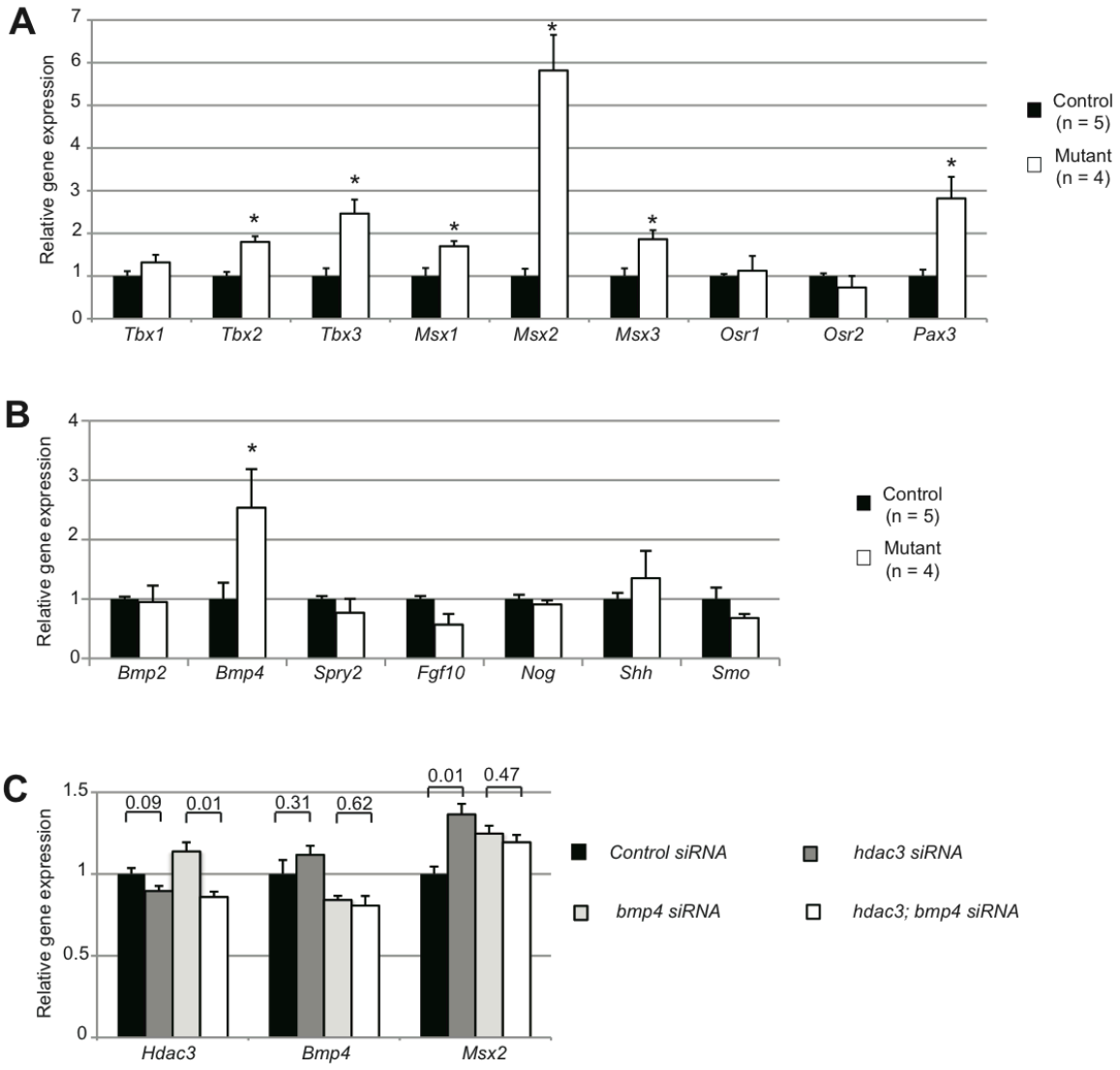
A
Relative gene expression
0
1
2
3
4
5
6
7
Tbx1
Tbx2
Tbx3
Msx1
Msx2
Msx3
Osr1
Osr2
Pax3
Control (n = 5)
Mutant (n = 4)
B
Relative gene expression
0
1
2
3
4
Bmp2
Bmp4
Spry2
Fgf10
Nog
Shh
Smo
Control (n = 5)
Mutant (n = 4)
C
Relative gene expression
0
0.5
1
1.5
0.09
0.01
0.31
0.62
0.01
0.47
Hdac3
Bmp4
Msx2
Control siRNA
hdac3 siRNA
bmp4 siRNA
hdac3; bmp4 siRNA

Figure 2.8. Bmp4 and downstream targets are dysregulated in *Hdac3*^{Wnt1NCKO} cranial mesenchyme. A-B. Quantitative RT-PCR from E12.5 cranial mesenchyme for **(A)** transcription factors known to regulate the cell cycle in cranial neural crest and palatogenesis and **(B)** Important signaling molecules involved in these processes. **C.** Quantitative RT-PCR from explanted cranial crest cells treated with control, *Hdac3* or *Bmp4* siRNA. The critical downstream Bmp4 target *Msx2* is upregulated in the absence of Hdac3, and dysregulation is rescued by *Bmp4* knockdown. Numbers above brackets denote p values in student's two-sided t test.

Chapter 3. Hdac3 regulates smooth muscle differentiation in neural crest cells and development of the cardiac outflow tract

This chapter contains data and text that has been published in Circulation Research *(Singh et al., 2011).*

Summary

Chapter 2 discusses craniofacial abnormalities resulting from neural crest deletion of Hdac3. Neural crest cells in more caudal regions of the embryo make important contributions to the smooth muscle of the cardiac outflow tract (OFT) and great vessels, the neurons and support cells of the peripheral nervous system, and the chromaffin cells of the adrenal medulla. In this chapter, I describe the role of Hdac3 in cardiac OFT development, and contrast it to the role of Hdac3 in neural crest-mediated craniofacial and nervous system development.

Introduction

Like craniofacial development, mammalian cardiac outflow tract and aortic arch morphogenesis is characterized by the tightly coupled development of multiple cell types. The complexity of this process is underscored by the prevalence of congenital anomalies of great vessel patterning in humans (Jain et al., 2010). As discussed in Chapter 1, the heart, OFT and aortic arch are formed by several developmentally distinct cell populations, including cardiomyocytes (derived from the first and second heart fields), vascular smooth muscle cells (derived from the second heart field and neural crest), and endothelial cells (Vincent and Buckingham, 2010). These populations of cells interact within the maturing pharyngeal arches - a dynamic milieu in which cross-regulation between these cell types, as well as the pharyngeal endoderm and ectoderm, results in the coordinated development of the OFT, great vessels and neighboring structures (Park et al., 2008, Guo et al., 2011). Many of the processes that regulate cell fate decisions and patterning during OFT development are also active in vascular remodeling in adult disease states in humans (Yoshida and Owens, 2005).

The OFT initially develops as a single vessel, the truncus arteriosus, comprised of myocardium and smooth muscle cells emerging from a single, unseptated ventricle. Neural crest cells, which make up the bulk of the pharyngeal arch mesenchyme, contribute to the smooth muscle of the OFT and also condense to form much of the smooth muscle of the aortic arch arteries - a

series of paired vessels that connect the developing truncus arteriosus to the dorsal aortae (Stoller and Epstein, 2005). The aortic arch arteries are then extensively remodeled, eventually giving rise to the mature aortic arch and several great vessels. Neural crest cells also contribute to septation and rotation of the OFT, with secondary effects on septation of the ventricles. These processes are highly dependent on the migration, expansion and differentiation of cardiac neural crest in response to cues from neighboring cells (Jain et al., 2010).

Murine models of congenital cardiovascular abnormalities have shed new light on the interplay between cell populations in the pharyngeal arches, as well as on the pathogenesis of human congenital cardiac disease. For instance, human mutations in components of the Notch signaling pathway can result in Alagille syndrome, a heterogeneous disorder that can include cardiac OFT defects. It has been demonstrated in mice that active Notch signaling in both neural crest cells and the second heart field is critical for OFT morphogenesis (High et al., 2007, High et al., 2009). Notch signaling from endothelial cells to neural crest in the pharyngeal mesenchyme via the Notch ligand Jagged1 is required to initiate smooth muscle differentiation in the aortic arch arteries; in the absence of such signaling, mice develop cardiac abnormalities reminiscent of those found in Alagille patients (High et al., 2007).

Normal development of the OFT relies on intact migration of neural crest cells into the pharyngeal arches, survival and proliferation of post-migratory

neural crest, differentiation of neural crest cells into smooth muscle, and rotation of the developing vasculature, which creates the stereotyped, three-dimensional structure of the mature OFT. While Notch signaling drives smooth muscle differentiation, other signaling modalities including the WNT, FGF and TGFß pathways, as well as activation of the MAPK pathway by integrin signaling mediate these additional stages of OFT formation and remodeling (Huh and Ornitz, 2010, Guo et al., 2011, Zhang et al., 2010b, Newbern et al., 2008, Vallejo-Illarramendi et al., 2009).

In addition to numerous signaling pathways, epigenetic processes and chromatin remodeling agents have also been shown to regulate aspects of OFT development (Chang and Bruneau, 2011). Human mutations in the chromatin remodeling enzyme Chd7 have been associated with neurocristopathy and OFT abnormalities (Lalani et al., 2006). In the mouse, Chd7 expression in pharyngeal ectoderm regulates the growth of the fourth and sixth pharyngeal arteries and formation of the aortic arch (Randall et al., 2009). Chd7 is also required cell-autonomously by human embryonic stem cell-derived neural crest cells, in order to regulate neural crest specification and migration (Bajpai et al., 2010). Chd7 directly interacts with the PBAF (polybromo- and Brg1-associated factor-containing complex) chromatin remodeling complex in order to regulate the expression of Sox9 and Twist1, both of which play crucial roles in neural crest (Bajpai et al., 2010). Brg1-containing nucleosome remodeling complexes also regulate the expression of smooth muscle contractile proteins, and smooth

muscle-specific deletion of the *Brg1* gene in mice results in partially penetrant patent ductus arteriosus (Zhang et al., 2011). In the second heart field, Brg1 expression is required to mediate proliferation and OFT patency (Hang et al., 2010).

Histone methylation is an important *epigenetic maintainer* in many developmental processes, including in OFT formation. The polycomb repressor complex protein Rae28 regulates cardiac expression of the transcription factor Nkx2.5, and *Rae28*$^{-/-}$ mutant mice demonstrate abnormalities such as double outlet right ventricle (DORV) (Shirai et al., 2002). Similarly, endothelial deletion of the histone demethylase Jarid2 results in cardiac abnormalities and OFT abnormalities including DORV. Loss of Jarid2 results in upregulation of Notch1, which drives smooth muscle differentiation in neural crest cells; this provides an example of epigenetic control of an important signaling pathway in OFT formation (Mysliwiec et al., 2011).

As discussed in Chapter 1, it is unsurprising that a process as intricate as OFT development requires tight regulation of transcription factors and signaling molecules by many chromatin remodeling complexes. However, while many such complexes have been implicated in OFT development, Class I Hdacs have not previously been shown to modulate any aspects of this process. In fact, genetic deletion of either *Hdac1*, *Hdac2* or *Hdac8* in neural crest does not affect OFT development (Haberland et al., 2009a). In this chapter, I use *in vivo* and *ex vivo* approaches to determine the role of Hdac3 in cardiac outflow tract development

and show that there is a specific requirement for Hdac3 in cardiac neural crest cells undergoing smooth muscle differentiation. Furthermore, I show evidence of a genetic interaction between Hdac3 and the Notch signaling pathway in regulating this process.

Results

Hdac3 is efficiently deleted in cardiac and trunk neural crest derivatives by *Wnt1-Cre*

Immunohistochemical analysis reveals that Hdac3 is normally expressed in the neural crest-derived pharyngeal arch mesenchyme (Figure 3.1 A), conotruncal cushions of the developing outflow tract (Figure 3.1B) and chromaffin cells of the adrenal medulla (Figure 3.1 C) embryos at E10.5. In *Hdac3*^{Wnt1NCKO} mutant embryos, Hdac3 protein is absent in each region (Figure 3.1 A-C). Co-staining for GFP in embryos expressing the Z/EG reporter confirms that Hdac3 deletion is specific to neural crest derivatives.

Quantification of the total number of GFP-positive cells populating the caudal pharyngeal arches reveals no significant difference between control and mutant embryos at E11.5 (Figure 3.1 D. Therefore the specification and migration of cardiac neural crest cells remains intact despite efficient deletion of Hdac3. This lies in contrast to the situation in the rostral pharyngeal arches, in which loss of Hdac3 leads to pronounced hypoplasia at E10.5 (discussed in Chapter 2).

Loss of Hdac3 in neural crest results in severe cardiovascular and thymus abnormalities

In neurocristopathy in humans, and in multiple mouse models in which neural crest developmental processes have been disrupted, craniofacial

abnormalities often also portend cardiovascular abnormalities. As neural crest cells make important contributions to the development of the cardiac OFT, we sought to analyze OFT morphology in *Hdac3*^{Wnt1NCKO} embryos. Neural crest gives rise to the smooth muscle of the aortic arch from its origin to the ductus arteriosus and large proportions of the smooth muscle in the great arteries. This smooth muscle is critical for vascular integrity during development. In several mutant embryos, we observed complete absence of the preductal aortic arch (Figure 3.2 A versus 3.2 B), a condition known as interrupted aortic arch (IAA) type B in humans. Other mutants demonstrated aortic arch hypoplasia (Figure 3.2 C). Both IAA type B and aortic arch hypoplasia are rare cardiac abnormalities in humans, although both are commonly found in patients with DiGeorge syndrome and other neurocristopathies (Morini et al., 2001).

In addition to contributing directly to the aortic arch and great arteries, neural crest cells are involved in septation and rotation of the OFT, and directly give rise to the smooth muscle of the aorticopulmonary septum. Failure of septation can result in persistent truncus arteriosus (PTA), while a combination of incomplete septation and deficient outflow tract rotation can result in DORV. We observed examples of PTA and DORV in *Hdac3*^{Wnt1NCKO} embryos (Figure 3.2 D and data not shown). It is thought that neural crest cells in the developing aorticopulmonary septum signal to adjacent myocardium during the formation of the intraventricular septum. Consistent with the role of neural crest-derived smooth muscle in ventricular septation, we have observed severe ventricular

septal defects (VSDs) in many *Hdac3*^{Wnt1NCKO} embryos (Figure 3.2 E). Table 3.1 summarizes the cardiovascular abnormalities observed in late gestation *Hdac3*^{Wnt1NCKO} embryos.

In order to provide further support for our findings, we used a distinct neural crest Cre driver, *Pax3*^{Cre}, to delete *Hdac3*. *Hdac3*^{Pax3NCKO} also die by P1 and exhibit a similar array of cardiovascular defects as *Hdac3*^{Wnt1NCKO} embryos (Figure 3.3, Table 3.2, Table 3.3). These findings support the conclusion that Hdac3 is required in cardiac neural crest.

The thymus is derived primarily from endoderm but develops in close association with the pharyngeal arches and neural crest. The thymic primordia migrate caudally through the pharyngeal mesenchyme during midgestation to final destinations in the anterior mediastinum. The thymuses of *Hdac3*^{Wnt1NCKO} embryos fail to descend appropriately and are dysplastic (Figure 3.4). The abnormal thymic development in *Hdac3*^{Wnt1NCKO} embryos is consistent with prior studies that have documented the vital role of neural crest during thymus development, including in thymic migration, intrathymic smooth muscle formation, pericyte formation, and egress of thymocytes (Foster et al., 2008, Foster et al., 2010, Zachariah and Cyster, 2010).

Peripheral neurogenesis and development of the adrenal medulla occur normally in *Hdac3*^{Wnt1NCKO} embryos

In addition to smooth muscle of the OFT, neural crest cells in the cardiac and trunk region form the neurons that populate the dorsal root, sympathetic and enteric ganglia, and the chromaffin cells of the adrenal medulla. In order to determine the requirements for Hdac3 in the formation of these derivatives, we first analyzed the peripheral nervous system of *Hdac3*^{Wnt1NCKO} embryos. The neurofilament 2H3 is a marker of differentiated neurons. Immunostaining for 2H3 and GFP reveals that differentiated neurons populate the dorsal root ganglia and enteric ganglia of E10.5 *Hdac3*^{Wnt1NCKO}*; Z/EG* embryos, and that these cells are neural crest-derived (Figure 3.5 A and data not shown). Quantification of peripheral neuron staining intensity in the dorsal root ganglia reveals no significant difference between mutant and control embryos (Figure 3.5B). Optical projection tomography reconstructions of whole mount 2H3-stained embryos revealed normal patterning of the peripheral nervous system, including cranial nerves, dorsal root and sympathetic ganglia, in *Hdac3*^{Wnt1NCKO} embryos compared to controls (Figure 3.5 C).

The adrenal medullae of E14.5 *Hdac3*^{Wnt1NCKO}*; Z/EG* embryos also develop normally when compared to control littermates, as determined by immunohistochemistry for the neuroendocrine marker tyrosine hydroxylase (TH) and for GFP (Figure 3.6). Quantification of TH staining intensity reveals no significant abnormalities in chromaffin cell development in the absence of Hdac3 (Figure 3.6).

The aortic arch arteries of E11.5 *Hdac3*^{Wnt1NCKO} embryos show decreased expression of smooth muscle markers

In midgestation, neural crest cells make up the bulk of the mesenchyme in the third, fourth, and sixth pharyngeal arches (Figure 3.1 A,D, Figure 3.7 A,B). A subset of these cells directly apposes the endothelium of the developing aortic arch arteries (Figure 3.7 B). Between E10.5 and E11.5, these neural crest derivatives condense in response to signals from the endothelium and differentiate into the smooth muscle of the aortic arch arteries, eventually giving rise to a layer of smooth muscle actin (SMA)-positive tissue that is normally several cells thick by E11.5 (Figure 3.7 A, C, D) (High et al., 2008). In mutant embryos, as in littermate controls, neural crest cells appropriately populate the mesenchyme surrounding the arch arteries (Figure 3.1 D, 3.4 E, F). However, in three of four E11.5 mutant embryos, we observed profound deficiencies in smooth muscle populating the nascent arch arteries, as assessed by immunohistochemistry for SMA and the additional smooth muscle marker SM22*α* (Figure 3.7 E, G, H, Figure 3.8). These defects are particularly pronounced in the left fourth and sixth arteries (Figure 3.7 E, I), which give rise to the preductal aortic arch and ductus arteriosus, respectively – areas that are affected in late gestation *Hdac3*^{Wnt1NCKO} mutants (Table 3.1). Of note, parts of the second arch arteries that are largely populated by non-neural crest-derived smooth muscle cells develop normally in mutants (Figure 3.7 A, E, I). The 75% penetrance of gross smooth muscle deficiencies in the caudal arch arteries at E11.5 parallels

the penetrance of aortic arch abnormalities observed at E17.5 in *Hdac3*^{Wnt1NCKO} embryos (Table 3.1). Mid-gestational decreases in aortic arch artery smooth muscle have previously been shown to portend OFT defects (High et al., 2007), and we therefore hypothesized that these smooth muscle deficiencies observed at E11.5 account for the late gestational cardiovascular phenotype observed in *Hdac3*^{Wnt1NCKO} embryos.

Hdac3-deficient neural crest cells exhibit a cell autonomous defect in smooth muscle differentiation

In order to determine the mechanism underlying smooth muscle abnormalities in E11.5 *Hdac3*^{Wnt1NCKO} embryos, we first determined rates of proliferation and apoptosis in third, fourth and sixth pharyngeal arch mesenchyme at E11.5 using phospho-histone H3 and Tunel staining, respectively. In contrast to the abnormal cell cycle regulation observed in the first pharyngeal arch (Chapter 1), neither proliferation nor apoptosis rates are significantly altered in the caudal *Hdac3*^{Wnt1NCKO} arches when compared to littermate controls (Figure 3.7 J). This suggests that neither increases in cell death in arch artery smooth muscle, nor decreased smooth muscle proliferation contribute to the defects observed.

Based upon our *in vivo* observations, we hypothesized that neural crest expression of Hdac3 is required for smooth muscle differentiation. We used an *ex vivo* approach to test this hypothesis. We performed neural tube explant

assays using E9.5 *Hdac3^{Wnt1NCKO}; Z/EG* and *Wnt1-Cre; Z/EG* control embryos. Genetically labeled neural crest cells were allowed to migrate from the dorsal neural tube onto a surrounding layer of fibronectin under conditions that allow for spontaneous differentiation into smooth muscle. Both control and Hdac3-deficient neural crest cells are able to migrate from the dorsal neural tube onto the fibronectin layer (Figure 3.9 A, B). However, while control cells assume a large, flat conformation after two days in culture, mutant cells maintain a rounder phenotype (Figure 3.9 A, B). Co-staining for GFP and SMA revealed that control cells are able to efficiently form smooth muscle in culture, while the proportion of GFP-positive cells costaining for SMA is significantly lower in mutant explant cultures (Figure 3.9 C-G). These results suggest that Hdac3-deficient neural crest cells exhibit a primary defect in smooth muscle differentiation, consistent with the decreased smooth muscle observed in E11.5 mutant aortic arch arteries.

The Notch ligand Jagged1 is downregulated in *Hdac3^{Wnt1NCKO}* aortic arch arteries

Notch signaling via the Jagged1 ligand is critical for smooth muscle formation in neural crest cells, and loss of Notch signaling in the neural crest results in a similar array of OFT defects as observed in this study, with similar decreases in aortic arch artery smooth muscle at E11.5 (High et al., 2007). Jagged1 is initially expressed in the endothelial cells of the nascent aortic arch arteries at E10.5, and in a positive feedback loop, Jagged1 expression is

upregulated in surrounding neural crest cells in response to Jagged1-mediated Notch activation (High et al., 2008, Feng et al., 2010). OFT development is exquisitely dependent on endothelial and neural crest expression of Jagged1; indeed, even heterozygous deletion of *Jagged1* in neural crest portends OFT defects (L. Manderfield, 2011 *Circulation*, accepted for publication).

Immunohistochemistry in *Hdac3*^{Wnt1NCKO} embryos demonstrates that Jagged1 expression in the aortic arch arteries is significantly decreased at E11.5 when compared to *Wnt1-Cre* littermate controls (Figure 3.10A). Quantification of Jagged1 staining intensity in the region surrounding each aortic arch artery indicates that deficient Jagged1 expression is most prominent in the mesenchyme surrounding the left fourth aortic arch artery (Figure 3.10B). This finding is consistent with our observations of decreased smooth muscle formation in this artery, and abnormal development of the left fourth arch artery derivatives in late gestation.

In order to determine the importance of Notch signaling in mediating the cardiovascular phenotype of *Hdac3*^{Wnt1NCKO} embryos, we crossed a conditional, constitutively active form of the Notch effector molecule, NICD, into the *Hdac3*^{Wnt1NCKO} background (Stanger et al., 2005). We found that *Wnt1-Cre; R26*$^{NICD/+}$ embryos die between E12.5-E14.5 of neural tube closure defects (data not shown). These embryos also demonstrate gross abnormalities in the morphology of the pharyngeal arches, with complete ablation of the left fourth and sixth arches at E11.5 (data not shown). These abnormalities preclude direct

comparison of the morphology at these regions between control and *Hdac3*^{Wnt1NCKO} embryos in the presence versus the absence of NICD expression. However, the area of confluence of the right fourth and sixth arteries remains in embryos overexpressing NICD in neural crest. Therefore we have evaluated both Jagged1 and SMA staining in this region of the arch arteries.

Wnt1-Cre; R26$^{NICD/+}$ embryos demonstrate increased SMA staining as well as increased expression of Jagged1 compared to *Wnt1-Cre* embryos (Figure 3.11A-F). These observations are consistent with the role of Notch signaling in promoting both cell autonomous smooth muscle differentiation as well as Jagged1 expression in surrounding cells. In the setting of Hdac3 conditional mutants, we have observed increased SMA staining in *Wnt1-Cre; Hdac3*$^{f/f;}$ *R26*$^{NICD/+}$ embryos compared to *Wnt1-Cre; Hdac3*$^{f/f}$ litermates; this SMA staining is comparable to that observed in *Wnt1-Cre; R26*$^{NICD/+}$ embryos (Figure 3.11G-L. However, we do not observe ectopic Jagged1 expression in *Wnt1-Cre; Hdac3*$^{f/f}$*;* *R26*$^{NICD/+}$ embryos, as in *Wnt1-Cre; R26*$^{NICD/+}$ arches (Figure 3.11G-L).

Constitutive Notch activation in neural crest therefore results in cell autonomous rescue of smooth muscle expression, without ectopic expression of Jagged1. These observations are consistent with a model in which Hdac3 is important in mediating Notch-mediated Jagged1 expression.

Discussion

In this study, we have elucidated a specific role for Hdac3 in smooth muscle differentiation of cardiac neural crest cells during OFT and aortic arch artery morphogenesis. The specificity of this role is underscored by the lack of peripheral nervous system or adrenal abnormalities in *Hdac3*^{Wnt1NCKO} mutants. The smooth muscle deficiencies observed in *Hdac3*^{Wnt1NCKO} embryos lead to OFT and aortic arch artery abnormalities, such as DORV, PTA and type B IAA – abnormalities that are attributable to a failure of cardiac neural crest-derived structures to form properly (Stoller and Epstein, 2005). It is interesting to note that while these abnormalities are commonly found in human patients with neurocristopathy, additional OFT malformations often found in such patients, including retroesophageal right subclavian artery and vascular rings, were not observed in this study; this is likely because these latter two lesions are generally associated with abnormal persistence of structures which normally regress during development, rather than with the failure of such structures to form appropriately (Stoller and Epstein, 2005).

In the pharyngeal arches, populations of neural crest cells, pharyngeal endoderm, epithelial cells and cardiomyocytes exist in close association with one another, and exert important regulatory roles mediating cell-cell communication. The signals between these cells exist in a delicate balance, and are instrumental for coordinating their migration, proliferation and differentiation. Cardiac OFT

malformations have been described as a common endpoint for disruptions to these processes in the pharyngeal arches; indeed, numerous mouse models in which crosstalk between progenitor cell populations is disrupted result in a wide array of OFT defects (Jain et al., 2010, Huh and Ornitz, 2010, Guo et al., 2011, Zhang et al., 2010b, Newbern et al., 2008, Vallejo-Illarramendi et al., 2009, High et al., 2008). Notch signaling via the Jagged1 ligand has previously been shown to initiate a cascade of smooth muscle differentiation in the aortic arch arteries, as well as to upregulate the expression of Jagged1 itself, in a positive feedback loop (High et al., 2008, Feng et al., 2010). The decreased expression of Jagged1 in the aortic arch arteries of *Hdac3*^{Wnt1NCKO} embryos suggests that Hdac3 may be required for Notch-mediated upregulation of Jagged1 and subsequent propagation of smooth muscle differentiation in the aortic arch arteries. Future work will elucidate the direct targets of Hdac3 that are responsible for its regulation of smooth muscle differentiation and Jagged1 be it through direct deacetylation of transcription factor targets, or via epigenetic silencing of target loci.

In addition to its relevance to congenital heart disease, smooth muscle formation is clinically important in the setting of coronary arterial stent restenosis, where proliferation of smooth muscle cells results in neointimal hyperplasia. Agents such as sirolimus, and rapamycin have been shown to be clinically useful in preventing restenosis at least in part by shifting the balance of smooth muscle cells from a proliferating, less differentiated phenotype towards a more quiescent

and contractile cell type (Martin et al., 2004, Hegner et al., 2009). Many of the pathways involved in smooth muscle formation in embryogenesis are thought to be similarly involved in smooth muscle differentiation and vascular remodeling in the adult (Owens et al., 2004). While we have demonstrated a requirement for Hdac3 in smooth muscle differentiation during embryonic cardiac development, additional work is needed to determine whether Hdac3 plays an analogous role in smooth muscle formation and phenotypic modulation in the adult vasculature. Hdac inhibitors are widely used therapeutic agents and have previously been proposed as useful agents in the treatment of heart failure (Trivedi et al., 2007). Given a potential role of Hdac3 in modulation of vascular smooth muscle behavior, vascular effects of Hdac inhibitors in various patient populations, including those with coronary disease and vascular stents, will be interesting topics for future study.

Materials and Methods

Mice

To evaluate the role of Notch signaling in mediating the cardiovascular phenotype in *Hdac3*^{Wnt1NCKO} mice, *Wnt1-Cre; Hdac3*$^{f/+}$ mice were crossed to *Hdac3*$^{f/+}$*; R26*$^{NICD/+}$ mice (Stanger et al., 2005). Additional crosses and techniques are described in Chapter 2. All animal protocols were approved by the University of Pennsylvania Institutional Animal Care and Use Committee.

Micrographs, Histology and immunohistochemistry

These techniques are described in Chapter 2. For gross pictures of OFTs, image brightness and contrast were adjusted in Adobe Photoshop to enhance OFT detail. OFT morphological diagrams were obtained by tracing and false-coloring H&E images in Adobe Illustrator

Primary antibodies used for immunohistochemistry were anti-GFP goat polyclonal (Abcam AB6673, 1:100), anti-GFP rabbit polyclonal (Invitrogen A-11122, 1:200), rabbit polyclonal anti-HDAC3 (Santa Cruz sc-11417x, 1:10), mouse monoclonal anti-SMA (Sigma A2547, 1:200), mouse polyclonal Anti-2H3 (Iowa Hybridoma Bank, 1:25), rabbit polyclonal anti-tyrosine hydroxylase (Chimicon AB152, 1:500), rabbit polyclonal anti-Jagged-1 (Santa Cruz SC-8303, 1:10).

All control versus mutant histological and immunohistochemical images were taken at the same exposure and contrast settings, using NIS Elements software. ImageJ software was used to merge images and for quantification of neurofilament and tyrosine hydroxylase staining intensity. In some cases, ImageJ was used to decrease image brightness, and this was performed identically in control and mutant images. Quantification of dorsal root ganglion and adrenal medulla size was performed using multiple serial sections from multiple control and mutant samples that were matched for anatomical landmarks.

Cell number, proliferation and apoptosis in pharyngeal arches III-VI were quantified by manually counting nuclei, pHistone H3-, or Tunel-positive cells, respectively, in adjacent sections of the anatomically-defined pharyngeal arch region in a blinded manner. For quantification of SMA and Jagged1 staining intensity, serial sections from three severely affected E11.5 *Wnt1-Cre; Hdac3*$^{f/f}$ embryos were compared to littermate *Wnt1-Cre* and *Wnt1-Cre; Hdac3*$^{f/+}$ control embryos. Quantification was performed using ImageJ in a blinded manner.

Whole mount immunostaining and optical projection tomography. E10.5 embryos were fixed in 4% paraformaldehyde overnight. Embryos were bleached for 30 minutes in 5% H2O2 in PBST, digested in 10μg/mL proteinase K in PBST for 5 minutes and immunostained with mouse polyclonal Anti-2H3 (Iowa Hybridoma Bank, 1:100). An HRP Conjugated secondary antibody and DAB substrate kit (Vector Laboratories) were used to visualize peripheral nerves.

For OPT scanning, immunostained embryos were dehydrated into 100% methanol, embedded in 1% low-melt agarose, cleared overnight in 1:2 (v/v) benzyl alcohol and benzyl benzoate, and scanned using the Bioptonics OPT scanner (3001M) (Sharpe et al., 2002). Image stacks were reconstructed using OsiriX software. Image contrast was optimized to reveal peripheral nerve patterning.

Neural Tube Explant Assays

Mutant embryos were obtained from crosses in which *Wnt1-Cre; Hdac3*$^{f/+}$*; Z/EG* males were crossed to *Hdac3*$^{f/f}$ females, and age-matched control embryos were generated from *Wnt1-Cre*; *Z/EG* males crossed to WT females. Control and mutant embryos were dissected in parallel in a blinded manner. E9.5 embryos were dissected in sterile Hank's balanced salt solution (HBSS) supplemented with 1% penicillin/streptomycin. The neural tube from the otic placode to first dorsal root ganglion was dissected and incubated in 0.75mg/mL type I collagenase (Worthington biochemical) in HBSS for 20 minutes at 37°C. Using tungsten needles, the neural tube was then microdissected from the surrounding mesenchyme, split in half longitudinally, and plated on glass chamber slides pre-coated with 200μg/mL fibronectin (Roche). Explants were incubated for 48 hours at 37°C and 5% CO_2 in DMEM supplemented with 2% horse serum and 1% penicillin/streptomycin. Following fixation and immunostaining, each GFP+ cell

that had delaminated from the neural tube was scored as SMA-positive or SMA-negative.

Statistics

The chi-square test and student's 2-tailed t test were used to ascertain differences between groups. A x^2 or p-value of less than 0.05 was considered significant.

Table 3.1. Late gestation cardiovascular and thymic abnormalities in *Hdac3*^{Wnt1NCKO} embryos.

E16.5-18.5	***Wnt1-Cre***	***Wnt1-Cre; Hdac3***$^{f/f}$
IAA type B	0% (0/6)	32% (6/19)
Aortic arch hypoplasia	0% (0/6)	16% (3/19)
PTA	0% (0/6)	5% (1/19)
DORV	0% (0/6)	26% (5/19)
VSD	0% (0/6)	69% (11/16)
Thymic Dysplasia	0% (0/6)	100% (19/19)

Table 3.2. *Hdac3*^{Pax3NCKO} die by P1.

Pax3$^{Cre/+;}$ Hdac3$^{f/+}$ x **Hdac3$^{f/+}$**

P1	# Observed	Observed	# Expected	Expected
Hdac3$^{+/+}$	6	0.08	9	0.13
Hdac3$^{f/+}$	25	0.35	17	0.25
Hdac3$^{f//f}$	13	0.18	9	0.13
Pax3$^{Cre/+;}$*; Hdac3$^{+/+}$*	9	0.13	9	0.13
Pax3$^{Cre/+;}$*; Hdac3$^{f/+}$*	18	0.25	17	0.25
Pax3$^{Cre/+;}$*; Hdac3$^{f/f}$*	**0**	**0**	**9**	**0.13**
Total	71			
Chi Sq	**0.01**			

Table 3.3. Late gestation cardiovascular and thymic abnormalities observed in *Hdac3*^{Pax3NCKO} embryos recapitulate those observed using *Wnt1-Cre.*

E16.5-18.5	***Pax3*^{Cre}*; Hdac3*$^{f/+}$	***Pax3*^{Cre}*; Hdac3*$^{f/f}$
IAA type B	0% (0/6)	50% (6/12)
Aortic arch hypoplasia	0% (0/6)	0% (0/12)
PTA	0% (0/6)	17% (1/12)
DORV	0% (0/6)	17% (2/12)
Dorsal edema	0% (0/6)	100% (12/12)
Thymic Dysplasia	0% (0/6)	100% (12/12)

Figure 3.1

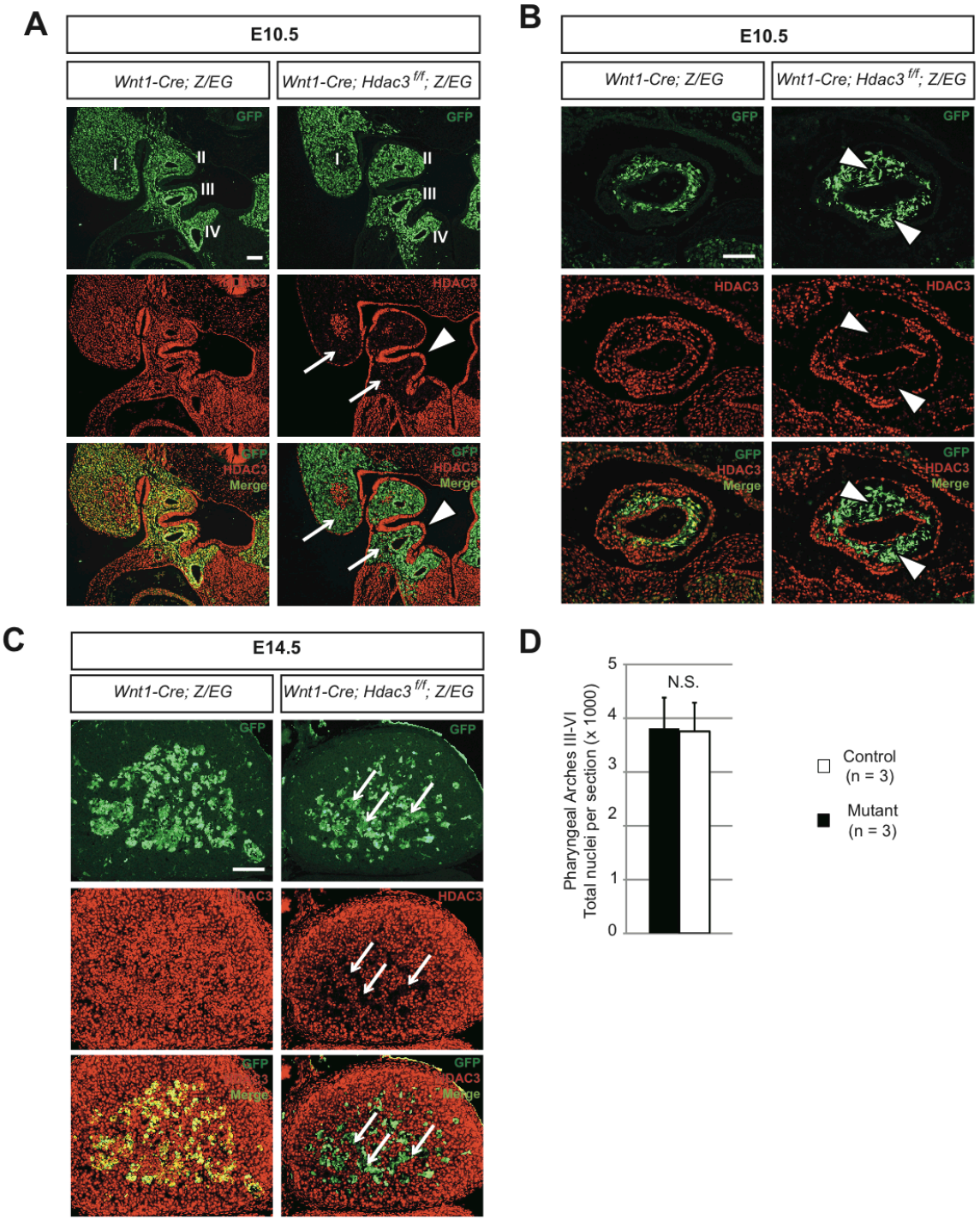
A
E10.5
Wnt1-Cre; Z/EG
Wnt1-Cre; Hdac3 f/f; Z/EG
GFP
HDAC3
Merge
I
II
III
IV
B
E10.5
Wnt1-Cre; Z/EG
Wnt1-Cre; Hdac3 f/f; Z/EG
C
E14.5
Wnt1-Cre; Z/EG
Wnt1-Cre; Hdac3 f/f; Z/EG
D
Pharyngeal Arches III-VI
Total nuclei per section (x 1000)
N.S.
Control
(n = 3)
Mutant
(n = 3)

Figure 3.1. *Wnt1-Cre* efficiently deletes Hdac3 in the pharyngeal arch mesenchyme, conotruncal cushions and adrenal medulla. A-C, Immunohistochemistry for GFP and Hdac3 **A,** Frontal sections of the pharyngeal arches at E10.5. Neural crest derivatives expressing GFP populate the pharyngeal arches of control (left) and mutant embryos. In control embryos, Hdac3 is expressed throughout the pharyngeal arch region. Mutant embryos show deletion of Hdac3 in the neural crest-derived pharyngeal mesenchyme (arrows), with retention of Hdac3 expression in ectoderm and pharyngeal endoderm (arrowheads). Roman numerals denote pharyngeal arch number. **B.** Frontal sections of the conotruncal cushions at E10.5. Neural crest derivatives, marked by GFP expression, are found in the conotruncal cushions in both control (left) and mutant embryos. Mutant embryos demonstrate loss of Hdac3 expression in GFP-positive neural crest derivatives (arrowheads). **C.** Sagital sections of E14.5 adrenal glands. The adrenal medulla of control (left) and mutant embryos is populated by neural crest derivatives. Mutants demonstrate loss of Hdac3 expression specifically in GFP-positive cells (arrows), which represent chromaffin cells. Scale bars: **D.** Quantification of cells in the pharyngeal mesenchyme of aortic arches III-VI from serial sections of E11.5 control and mutant embryos. **A & B.** 100μm, **C.** 400μm

Figure 3.2

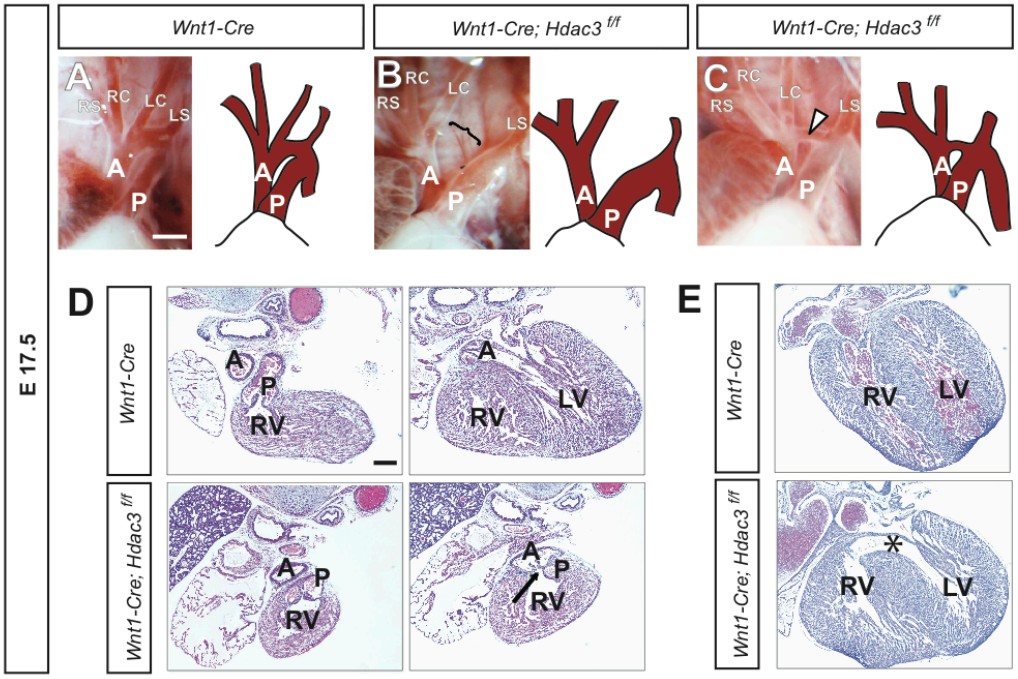
E 17.5
Wnt1-Cre
Wnt1-Cre; Hdac3 f/f
Wnt1-Cre; Hdac3 f/f
A
RC
RS
LC
LS
A
P
B
RC
RS
LC
LS
A
P
C
RC
RS
LC
LS
A
P
D
Wnt1-Cre
Wnt1-Cre; Hdac3 f/f
A
P
RV
A
RV
LV
A
P
RV
A
P
RV
E
Wnt1-Cre
Wnt1-Cre; Hdac3 f/f
RV
LV
RV
LV

Figure 3.2. Late gestation *Hdac3*^{Wnt1NCKO} embryos exhibit severe cardiovascular abnormalities. A-C. Gross images and drawings of E17.5 aortic arches. **A.** A control embryo, showing normal patterning of the great vessels in late gestation. **B.** A mutant embryo demonstrating a complete discontinuity of the aortic arch (open bracket), similar to interrupted aortic arch type B in humans. **C.** A mutant embryo showing hypoplasia of the aortic arch (arrowhead). A, aorta; P, pulmonary trunk; RS, right subclavian artery; RC, right common carotid artery; LC, left common carotid artery; LS, left subclavian artery. **D.** Sequential H&E-stained slides from the same control (top) and mutant hearts. In the control heart, the pulmonary trunk arises from the right ventricle (RV) while the aorta arises from the left ventricle (LV). In this mutant, both the pulmonary trunk and the aorta (arrow) arise from the right ventricle, indicating a double outlet right ventricle. **E.** A control embryo (top) with an intact ventricular septum and a littermate mutant with a large ventricular septal defect (*). The ventricular septal defect is the only cardiac abnormality in this mutant. Scale bars: **A-C.** 1mm, **D,E.** 300μm.

Figure 3.3

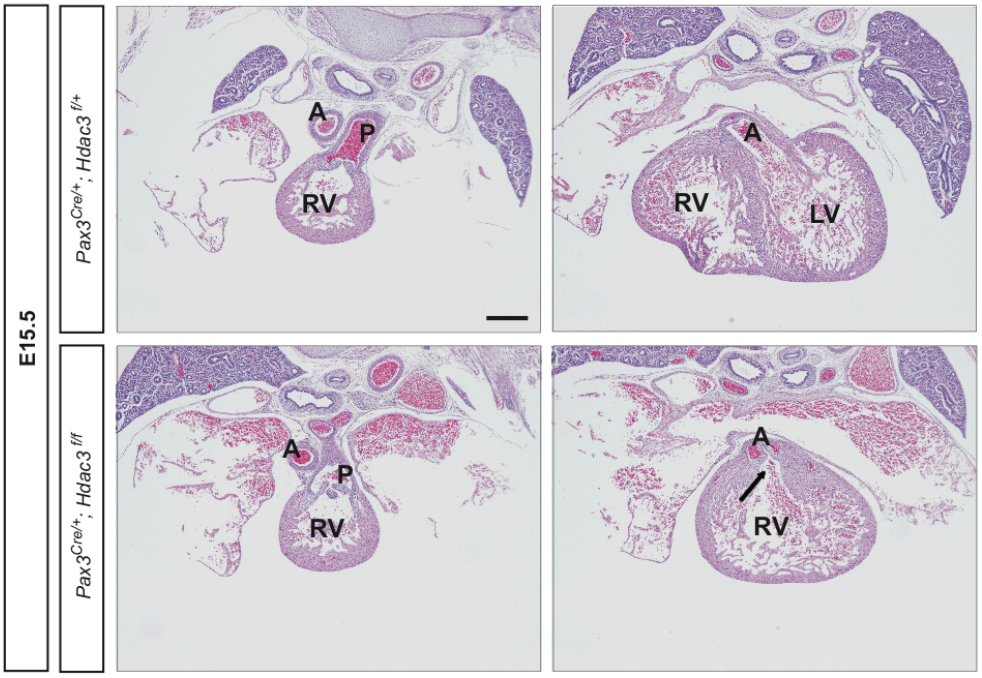

Figure 3.3. Cardiac abnormalities in late gestation *Hdac3*^{Pax3NCKO} embryos. Sequential H&E- stained slides from the same control (top) and mutant hearts. In control hearts, the pulmonary trunk arises from the right ventricle (RV) while the aorta arises from the left ventricle (LV). In this mutant, both the pulmonary trunk and the aorta (arrow) arise from the right ventricle, indicating a double outlet right ventricle. Scale bar: 300μm.

Figure 3.4

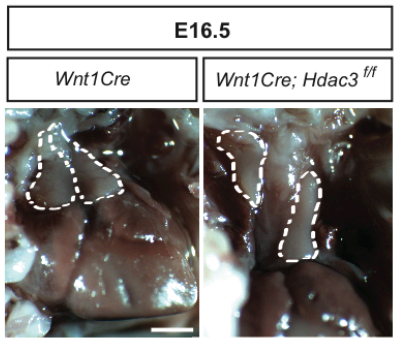

Figure 3.4. *Hdac3*^{Wnt1NCKO} embryos exhibit thymic abnormalities. Gross pictures of the mediastinum of control and mutant embryos at E16.5. By E16.5 the thymus (outlined in broken white line) normally sits ventral to the atria, as shown in the control (left). The mutant thymus is irregularly-shaped and has failed to descend correctly. Scale bar: 1mm.

Figure 3.5

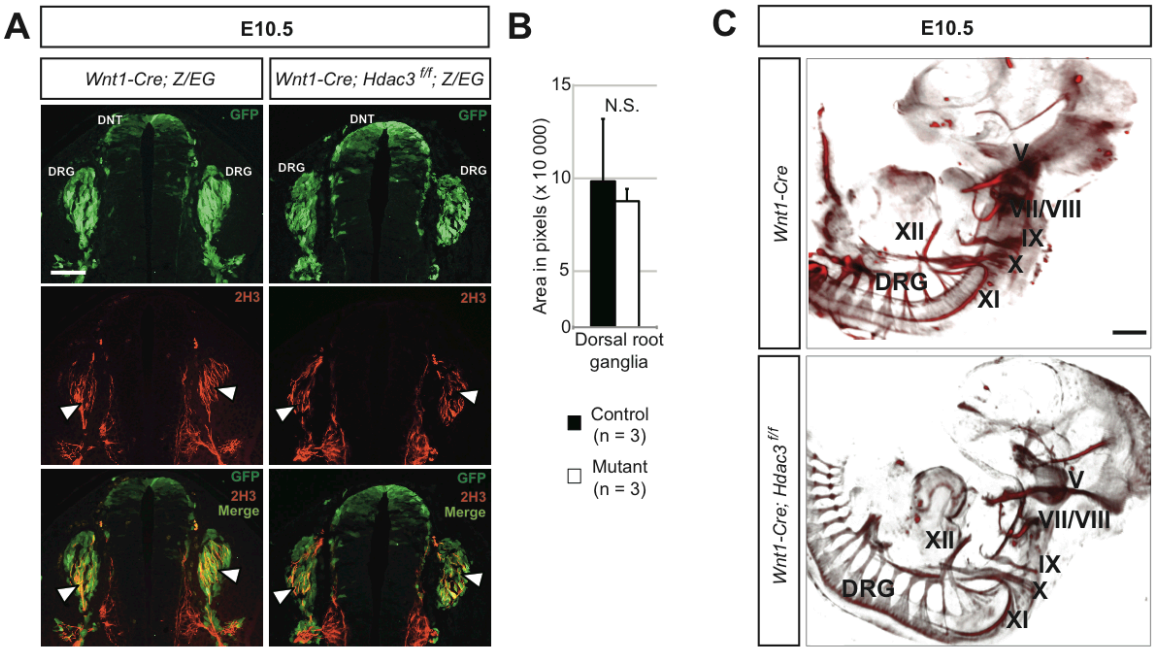
A
E10.5
Wnt1-Cre; Z/EG
Wnt1-Cre; Hdac3 f/f; Z/EG
DNT
GFP
DRG
DRG
2H3
GFP
2H3
Merge
B
15
10
5
0
N.S.
Area in pixels (x 10 000)
Dorsal root ganglia
Control (n = 3)
Mutant (n = 3)
C
E10.5
Wnt1-Cre
Wnt1-Cre; Hdac3 f/f
V
VII/VIII
XII
IX
X
DRG
XI

Figure 3.5. Peripheral neurogenesis occurs normally in the absence of neural crest expression of Hdac3. A. Immunohistochemistry for GFP and neurofilament (2H3), a marker of differentiated neurons, in frontal sections of the dorsal neural tube (DNT) and dorsal root ganglia (DRG). Both control and Mutant DRG feature differentiated, 2H3-positive neurons at E10.5 (arrowheads). **B.** Total neuronal area was calculated from anatomically matched sections from control and mutant embryos. Error bars represent SEM. N.S., not significantly different. **C.** Optical projection tomography renderings of whole mount 2H3-stained E10.5 embryos. Cranial nerves V, VII-XII (labeled) and DRG are present and patterned appropriately in mutant embryos. Scale bars: **A.** 100µm, **B.** 400µm.

Figure 3.6

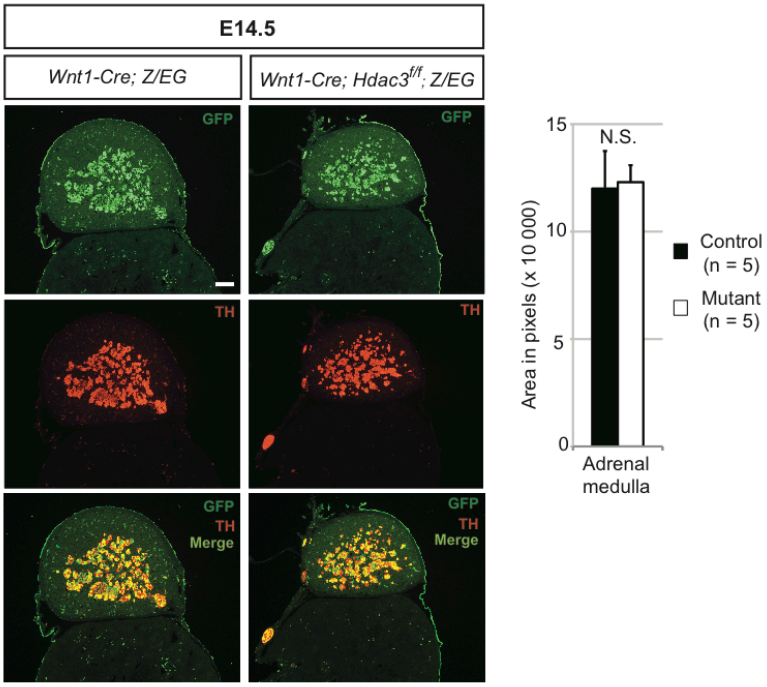
E14.5
Wnt1-Cre; Z/EG
Wnt1-Cre; Hdac3f/f; Z/EG
GFP
TH
GFP
TH
Merge
15
10
5
0
Area in pixels (x 10 000)
N.S.
Adrenal medulla
Control (n = 5)
Mutant (n = 5)

Figure 3.6. Chromaffin cells of the adrenal medulla develop normally in the absence of Hdac3. Immunohistochemistry for GFP and tyrosine hydroxylase (TH), a marker of neuroendocrine cells, in sagital sections of adrenal glands. Control (left) and mutant adrenal medulla are populated by TH-positive, neural crest-derived chromaffin cells. Quantification of TH- positive area was obtained from two serial sections of five control and five mutant adrenal glands. Scale bar: 100µm.

Figure 3.7

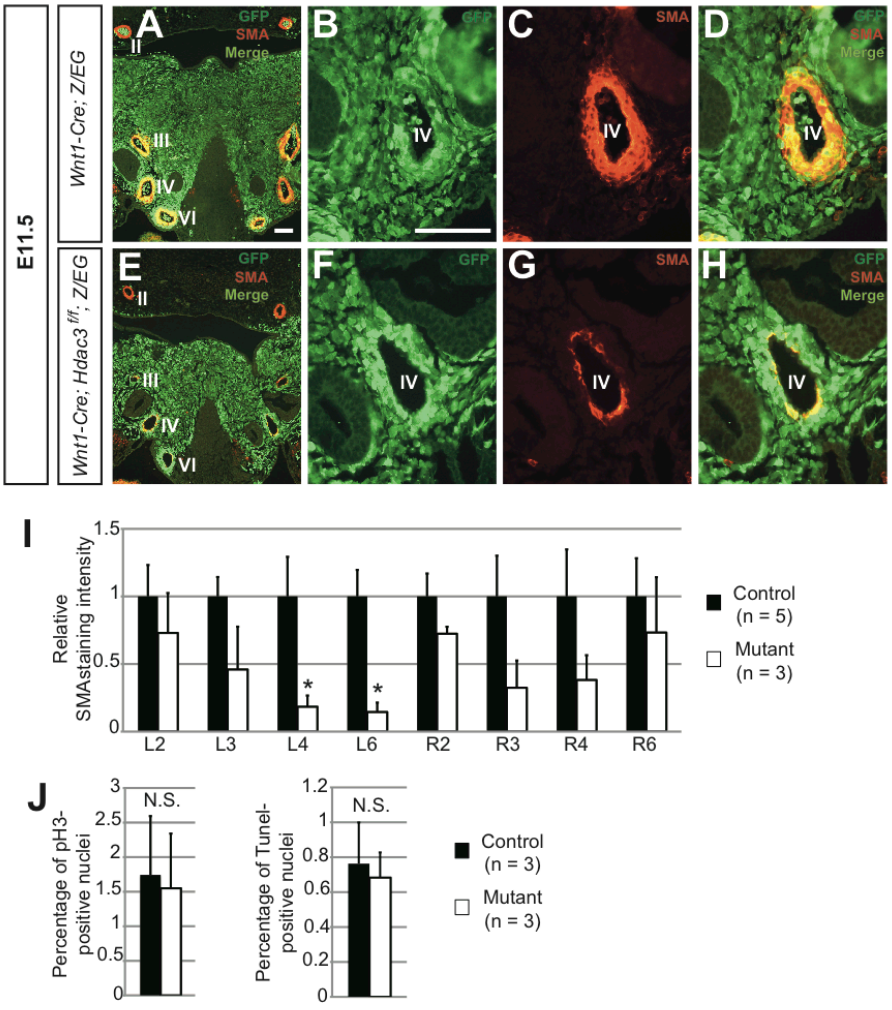
E11.5
Wnt1-Cre; Z/EG
Wnt1-Cre; Hdac3 f/f; Z/EG
A
B
C
D
E
F
G
H
GFP
SMA
Merge
II
III
IV
VI
I
Relative SMAstaining intensity
1.5
1
0.5
0
*
L2
L3
L4
L6
R2
R3
R4
R6
Control (n = 5)
Mutant (n = 3)
J
Percentage of pH3-positive nuclei
3
2.5
2
1.5
1
0.5
0
N.S.
Percentage of Tunel-positive nuclei
1.2
1
0.8
0.6
0.4
0.2
0
N.S.
Control (n = 3)
Mutant (n = 3)

Figure 3.7. *Hdac3*^{Wnt1NCKO} embryos display deficiencies in aortic arch artery smooth muscle at E11.5. A-H. Immunohistochemistry for GFP and α-smooth muscle actin (SMA) in frontal sections of E11.5 pharyngeal arches. **A.** Representative image of a control pharyngeal arch at low magnification, showing robust layers of smooth muscle surrounding aortic arch arteries II, III, IV and VI (labeled), bilaterally. Note that the bulk of pharyngeal mesenchyme is comprised of GFP-positive neural crest derivatives. **B-D.** High magnification images of the left fourth arch artery in the control embryo. **B.** Neural crest cells populate the region directly surrounding the artery. **C,D.** A layer of neural crest-derived, SMA-positive smooth muscle surrounds the control artery. **E.** Low magnification image of a mutant pharyngeal arch, showing neural crest derivatives populating the mesenchyme. Note the decreased smooth muscle in the regions surrounding the third, fourth and sixth arteries, particularly on the left side, while a thick layer of non-neural crest-derived smooth muscle surrounds the second arteries, as in the control **F-H.** High magnification images of the mutant left fourth artery. **F.** Neural crest cells appropriately populate the region surrounding the artery. **G,H.** In affected mutants, few neural crest-derived cells surrounding the fourth arch artery are SMA-positive smooth muscle cells. Three of four mutant and zero of four control embryos analyzed at this time point showed a similar pattern of staining. Roman numerals denote aortic arch artery number. **I.** Quantification of SMA staining intensity of each aortic arch artery, from serial sections in control and mutant embryos. Asterisks denote $p < 0.05$. **J.** Quantification of phospho-histone

H3 (pH3)- and Tunel-positive in serial sections of the pharyngeal arch mesenchyme. Scale bars: 100μm.

Figure 3.8

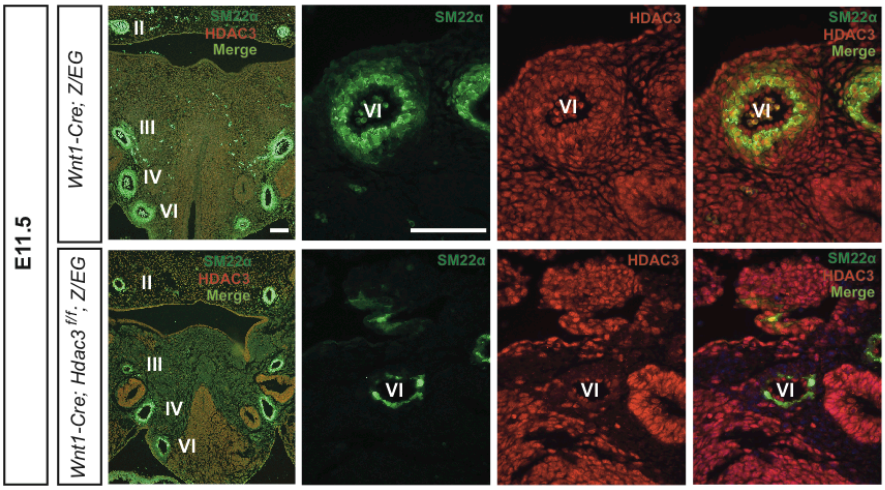
E11.5
Wnt1-Cre; Z/EG
Wnt1-Cre; Hdac3 f/f; Z/EG
SM22α
HDAC3
Merge
II
III
IV
VI

Figure 3.8. *Hdac3*^{Wnt1NCKO} pharyngeal arches display decreased expression of the smooth muscle marker Sm22*α* in the aortic arch arteries at E11.5. Immunohistochemistry for Sm22*α* and Hdac3 in frontal sections from E11.5 pharyngeal arches. Hdac3 is deleted in the neural crest-derived cells surrounding the nascent pharyngeal arches in mutant embryos. These embryos are also characterized by decreased expression of Sm22*α*. High magnification images show the left sixth artery. Scale bars: 100μm.

Figure 3.9

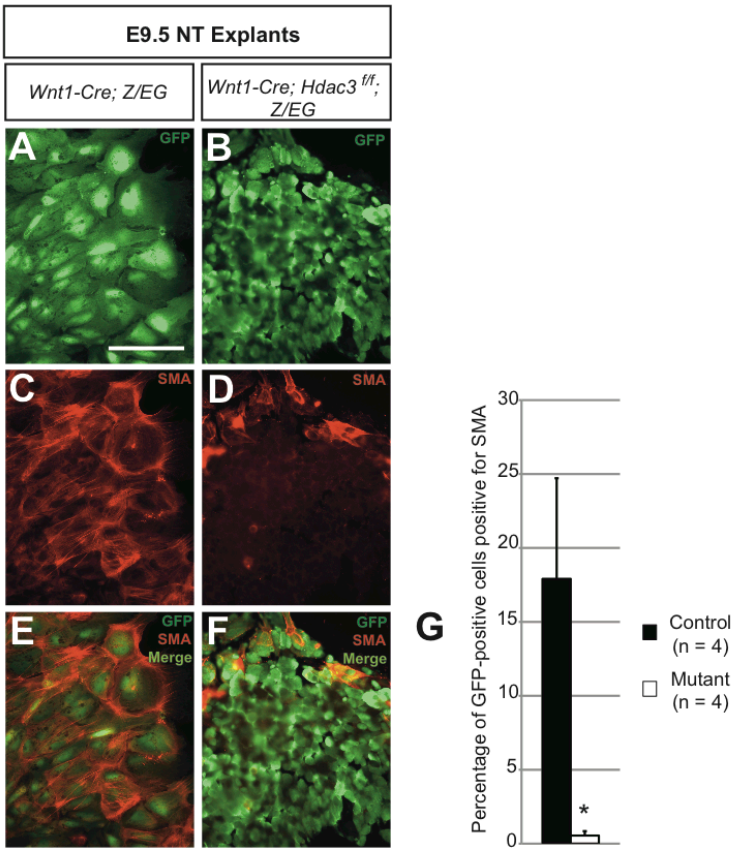
E9.5 NT Explants
Wnt1-Cre; Z/EG
Wnt1-Cre; Hdac3 f/f; Z/EG
A
GFP
B
GFP
C
SMA
D
SMA
E
GFP
SMA
Merge
F
GFP
SMA
Merge
G
Percentage of GFP-positive cells positive for SMA
30
25
20
15
10
5
0
*
Control (n = 4)
Mutant (n = 4)

Figure 3.9. Hdac3-deficient neural crest cells demonstrate a cell autonomous defect in smooth muscle differentiation. A-F. Immunocytochemistry for GFP and α-smooth muscle actin (SMA) in neural tube explant cultures. **A,B.** Representative images of control and mutant neural crest cells following two days of migration and growth. Note that mutant neural crest cells (**B**) are small and blastic compared to control cells (**A**). **C-F.** Significant numbers of control cells stain positive for SMA (**C,E**) while mutant cells are rarely SMA-positive (**D,F**). **G.** Each GFP-positive cell derived from four control and four mutant embryos was scored as SMA-positive or -negative. Scale bar: 100μm.

Figure 3.10

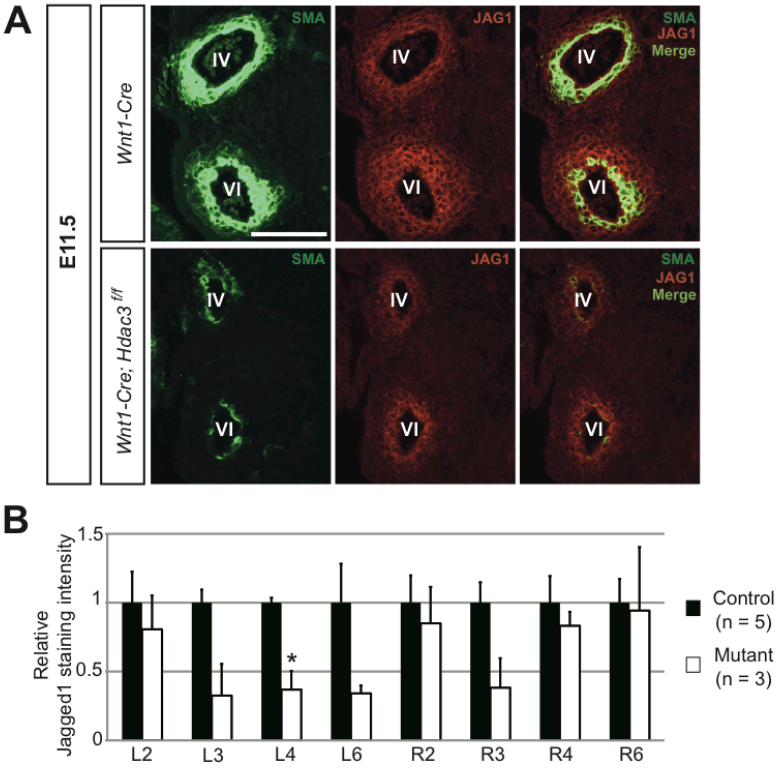
A
E11.5
Wnt1-Cre
Wnt1-Cre; Hdac3 f/f
SMA
JAG1
SMA
JAG1
Merge
IV
VI
B
Relative
Jagged1 staining intensity
1.5
1
0.5
0
*
L2
L3
L4
L6
R2
R3
R4
R6
Control
(n = 5)
Mutant
(n = 3)

Figure 3.10. Expression of the Notch ligand Jagged1, a critical regulator of smooth muscle differentiation in the aortic arch arteries, is dysregulated in *Hdac3*^{Wnt1NCKO} arches at E11.5. A. Representative immunohistochemistry for SMA and Jagged1 from frontal sections of mutant versus control left fourth and sixth arch arteries. **B.** Quantification of Jagged1 staining intensity in serial sections from three severely affected mutants relative to controls. Scale bar: 100µm.

Figure 3.11

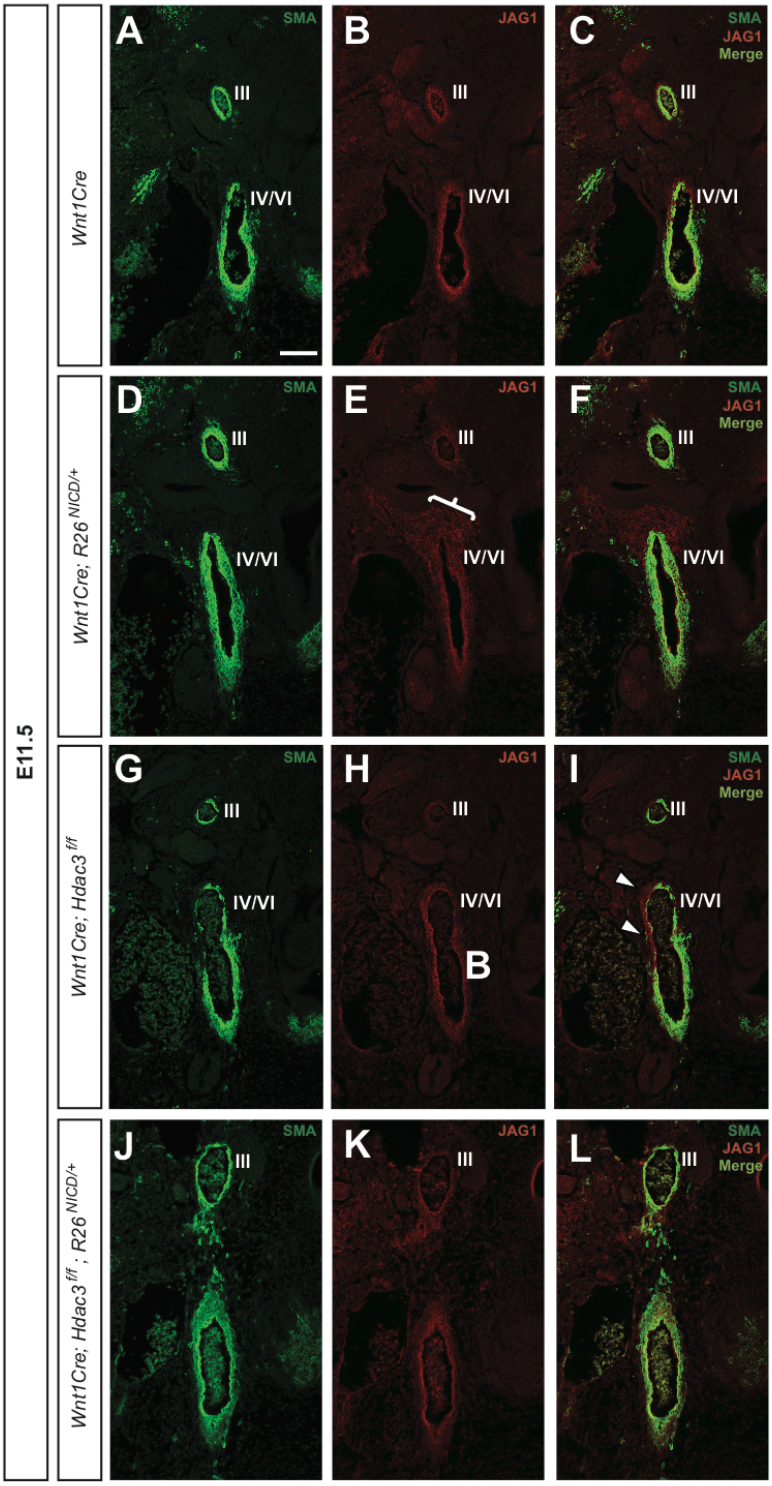
E11.5
Wnt1Cre
Wnt1Cre; R26 NICD/+
Wnt1Cre; Hdac3 f/f
Wnt1Cre; Hdac3 f/f ; R26 NICD/+
A
B
C
D
E
F
G
H
I
J
K
L
SMA
JAG1
Merge
III
IV/VI
B

Figure 3.11. Overexpression of the notch intracellular domain partially restores smooth muscle in developing aortic arch arteries. A-L. Immunohistochemistry for SMA and Jagged1 in frontal sections from E11.5 embryos at the confluence of the right fourth and sixth aortic arch arteries. **A-C.** A Control embryo showing the normal morphology at E11.5. Note the discontinuities in SMA staining in the region surroundind the fourth and sixth arch ateries. **D.** SMA staining in the setting of Notch overexpression in neural crest. Note the robust layer of smooth muscle surrounding the confluence, which is more robust than in the littermate control embryo. **E-F.** With overexpression of Notch, areas of ectopic Jagged1 expression are observed (open bracket), consistent with the existence of a Notch-Jagged1 positive feedback loop. **G-I.** In a litermate *Hdac3*^{Wnt1NCKO} mutant, there are large areas of discontinuous SMA staining and decreased expression of Jagged1. **J.** Overexpression of NICD in the *Hdac3*^{Wnt1NCKO} background in a littermate embryo results in robust SMA staining in the confluence. **K-L.** Ectopic Jagged1 expression is not observed in this embryo. Roman numerals delineate arch arteries. Scale bar: 50μm.

Chapter 4. Conclusions and future directions

Summary

The development of complex organisms is driven by the genesis of multiple distinct cell types from common progenitor cells. Given that each differentiated cell possesses the same genome as its progenitor cell precursor but exhibits a unique transcriptional and phenotypic profile, development is an inherently epigenetic process. The epigenetic regulation of progenitor cell biology has become an area of increasing investigation. Chromatin remodeling enzymes, including class I Hdacs, have proven to be important regulators of many aspects of progenitor cell behavior, including their differentiation. Furthermore, class I Hdacs have now been implicated in the converse process – the de-differentiation of committed cells into induced pluripotent progenitor cells (Anokye-Danso et al., 2011).

In this dissertation, I have used mouse genetics to explore the role of the chromatin remodeling enzyme Hdac3 in regulating distinct aspects of neural crest progenitor cell biology. In Chapter 2, I discuss the role of Hdac3 in neural crest-mediated craniofacial development. I have suggested that Hdac3 is required for the repression of the signaling molecule Bmp4 in neural crest cells, and that in the absence of Hdac3, excessive Bmp4 signaling results in aberrant cell cycle regulation and craniofacial abnormalities (Figure 4.1). Additionally, Hdac3 plays

an important role in osteogenesis, in part, through regulation of the important regulatory factor Runx2. In Chapter 3, I discuss the role of Hdac3 in cardiac outflow tract formation. Hdac3 is required for neural crest-mediated smooth muscle differentiation via the Notch signaling pathway (Figure 4.2). However, with regard to the role of Hdac3 in each of these distinct aspects of neural crest development, interesting questions, further discussed below, remain.

Discussion and Future Directions

Is there a single, parsimonious explanation for the cardiac and craniofacial abnormalities in Hdac3^{Wnt1NCKO} *embryos?*

Craniofacial and cardiac abnormalities often segregate together, both in human congenital abnormalities, and in mouse models in which various aspects of neural crest development have been genetically perturbed (Benish, 1975, Huh and Ornitz, 2010, Guo et al., 2011, Zhang et al., 2010b, Newbern et al., 2008, Vallejo-Illarramendi et al., 2009). Deletion of Hdac3 in neural crest yields an array of abnormalities reminiscent of those found both in patients with DiGeorge syndrome and in numerous murine models of neural crest abnormalities in which a single process has been disrupted. Therefore we have asked whether there exists a single, parsimonious explanation for the spectrum of abnormalities described in *Hdac3*^{Wnt1NCKO} mice. The mechanistic analysis of the craniofacial and cardiovascular phenotypes, presented in Chapters 2 and 3, however, suggests that dysregulation of a single gene or pathway is unlikely to account for the phenotype of *Hdac3*^{Wnt1NCKO} mice.

In cardiac outflow tract (OFT) development, we found that loss of Hdac3 results in decreased smooth muscle differentiation. We have implicated decreased Notch signaling via the Jagged1 ligand as one mechanism through which this smooth muscle differentiation defect occurs. Notch signaling is not involved in most aspects of craniofacial morphogenesis, including palatogenesis,

suggesting that the majority of craniofacial abnormalities in *Hdac3*^{Wnt1NCKO} pups do not occur due to Notch inhibition. However, Notch inhibition in neural crest – either by genetic deletion of Jagged1 or by expression of a dominant negative form of the transcription factor MAML - results in ossification abnormalities of the frontal bone (Frances High, unpublished). These abnormalities are similar to frontal bone abnormalities observed in *Hdac3*^{Wnt1NCKO} pups. Therefore the Hdac3-mediated regulation of Jagged1 expression may, in part, contribute to the ossification defects observed in *Hdac3*^{Wnt1NCKO} embryos. However, Notch inhibition is unlikely to contribute to additional craniofacial abnormalities.

In Chapter 1, I describe that the survival of cranial neural crest derivatives is significantly decreased in the absence of Hdac3, while in Chapter 2 I show that proliferation and apoptosis in cardiac neural crest are unaffected. The decrease in survival in craniofacial crest – mediated by dysregulation of a Bmp4-Msx2 pathway, is consistent with many of the craniofacial abnormalities identified in *Hdac3*^{Wnt1NCKO} mutants. In OFT development, Bmp4 and Msx genes are actually required for smooth muscle differentiation, cardiac crest survival and OFT remodeling, suggesting that their upregulation would not portend the OFT defects observed in *Hdac3*^{Wnt1NCKO} embryos (Stottmann et al., 2004, Chen et al., 2007, Nie et al., 2011, Zhang et al., 2010a). Indeed, ectopic activation of Bmp or Msx activity *in vivo* in the neural crest does not produce OFT defects (Winograd et al., 1997, He et al., 2010).

Our results therefore suggest that Hdac3 mediates distinct processes in craniofacial and cardiovascular development, and that dysregulation of a single gene or pathway is unlikely to account for the full spectrum of abnormalities described in this dissertation.

What is the nature of Hdac3-mediated repression of Bmp4?

Bmp signaling – particularly from ectodermal structures to neural crest cells - is important in multiple stages of craniofacial development (He et al., 2010, Zhang et al., 2000, Nie et al., 2006, Zhang et al., 2002). Bmp4 is expressed in the dorsal neural tube prior to neural crest cell delamination, and in the chick this signal has been shown to mediate apoptosis in a subset of neural crest cells (Graham et al., 1994). Later, as neural crest cells populate the face, Bmp signals from the epithelium regulate the survival and expansion of those cells, particularly in palatogenesis and tooth formation (Zhang et al., 2000, Zhang et al., 2002). We have proposed a model in which Hdac3 restricts *Bmp4* transcription in cranial neural crest, in order to regulate the growth and survival of these cells. We have demonstrated that loss of Hdac3 leads to upregulation of Bmp4, upregulation of targets of Bmp4 signaling, and craniofacial abnormalities. However, some craniofacial abnormalities described in this study, including ossification defects, have not previously been associated with increased Bmp4 activity. While ectodermal expression of Bmp4 is required for craniofacial morphogenesis, studies using a floxed allele of *Bmp4* have revealed that deletion of Bmp4 in

neural crest tissue itself does not affect craniofacial morphogenesis (Neves et al., 2011). A useful experiment for discerning which abnormalities in *Hdac3*^{Wnt1NCKO} embryos are mediated by cell autonomous upregulation of Bmp4 in neural crest cells would involve rescuing the defects on a *Bmp4*$^{flox/flox}$ background. Our model would predict that craniofacial hypoplasia, cleft palate and dental abnormalities would be rescued by deletion of Bmp4, while ossification abnormalities would persist.

The transcriptional regulation of *Bmp4* expression is a complex area of investigation. LacZ reporters spanning a 180kb region flanking the *Bmp4* coding sequence recapitulate only a small fraction of the normal Bmp4 expression pattern during embryogenesis (Chandler et al., 2009). The *Bmp4* gene exists in a highly conserved gene desert of over 1MB (Pregizer and Mortlock, 2009). This region is believed to contain multiple enhancer elements that drive Bmp4 expression, although the locations of these enhancers remain largely unknown (Pregizer and Mortlock, 2009). In light of the role of Hdac3 as a transcriptional repressor, we have hypothesized that Hdac3 directly represses *Bmp4* expression in neural crest by deacetylating histones at one or more of these *Bmp4* enhancer element. While relevant enhancers driving neural crest expression of *Bmp4* remain undescribed, ChIP-Seq for Hdac3 in cranial crest would identify potential sites of Hdac3 regulation in neural crest. Putative sites could then be cloned upstream of reporters in order to determine whether they direct neural crest transcription in the presence or absence of Hdac3. This approach could address

the question of whether Hdac3-mediated inhibition of *Bmp4* transcription is direct or indirect, and could also contribute to our understanding of how *Bmp4* transcription is regulated by distant-acting enhancers.

What is the nature of the genetic interaction between Hdac3 and Notch signaling in OFT development?

In Chapter 3 I describe a genetic interaction between Hdac3 and the Notch-Jagged1 positive feedback loop in smooth muscle differentiation. Notch signaling activates smooth muscle differentiation in a cell autonomous manner (High et al., 2007). As well, smooth muscle differentiation in the aortic arch arteries relies on this feedback loop to propagate the differentiation signal from the endothelium into the surrounding neural crest-derived mesenchyme (High et al., 2008, Feng et al., 2010). The evidence presented in Chapter 3 suggests that Hdac3 is required for Notch-mediated upregulation of Jagged1 expression, but not for cell autonomous NICD-mediated smooth muscle differentiation. However the nature of this requirement is unclear.

A plausible model to explain the interaction between Hdac3 and Notch signaling is one in which Hdac3 is responsible for repressing the expression of an inhibitor of the positive feedback loop via its role as a chromatin remodeling enzyme. Thus, in the absence of Hdac3, the positive feedback loop would be broken, with resulting deficiencies in smooth muscle differentiation. Smooth

muscle differentiation involves complex interactions between multiple signaling pathways, and it has been hypothesized that there is extensive positive and negative cross-regulation between these pathways (Owens et al., 2004). Therefore a screen among pathway components of these signaling pathways as well as additional known Notch inhibitors could prove fruitful for identifying potential inhibitors of Notch-mediated Jagged1 expression that are derepressed in the absence of Hdac3.

Is Hdac3 required for differentiation and/or survival of additional smooth muscle populations?

As discussed in Chapter 3, determining the mechanism of smooth muscle differentiation is relevant not only to developmental and regenerative biology, but to the study of adult disease processes (Yoshida and Owens, 2005). In Chapter 3 I discuss a novel and important pathway that regulates neural crest-derived smooth muscle differentiation, and we are interested in the applicability of this mechanism to additional developmental processes. One useful strategy for determining whether Hdac3 is required for differentiation of other smooth muscle populations, or for the survival of differentiated smooth muscle cells, is to cross the *Hdac3*^{f} allele to existing Cre lines and analyze smooth muscle derivatives in late gestation.

The smooth muscle of the descending aorta and much of the body vasculature is derived from the lateral plate mesoderm. Mice in which *Hdac3* is

deleted with the mesoderm-specific *Mesp1-Cre* die at E9.5, and preliminary analysis reveals evidence of circulatory collapse consistent with a failure of the vasculature to be formed correctly. However, preliminary analysis of *Sema3D-Cre; Hdac3*$^{f/f}$ embryos, in which Hdac3 is deleted in precursors of the smooth muscle of the coronary vasculature, suggests that these mice develop normally. Detailed analysis of these mice will reveal whether the requirement for Hdac3 in smooth muscle differentiation applies only to specific smooth muscle lineages.

Based on the normal rates of proliferation and apoptosis observed in *Hdac3*^{Wnt1NCKO} E11.5 aortic arch arteries, we hypothesized that deletion of Hdac3 does not affect the survival of differentiated smooth muscle cells. *Sm22*α*-Cre* is expressed in committed, early stage smooth muscle cells. Preliminary analysis of *Sm22α-Cre; Hdac3*$^{f/f}$ embryos suggests that deletion of Hdac3 using *Sm22*α*-Cre* does not affect patterning of the OFT and aortic arch, supporting our hypothesis that Hdac3 is required for smooth muscle differentiation, but ultimately not for the survival of differentiated cells.

How is Hdac3 targeted to genomic loci in different neural crest lineages?

As discussed in Chapter 2, the Hdac3-NCoR/Smrt corepressor complex does not possess intrinsic DNA binding ability. Rather, it is targeted to specific genomic loci by transcription factor and nuclear receptor binding partners. We have hypothesized that the preponderance of abnormalities resulting from the loss of Hdac3 in neural crest occurs due to the loss of Hdac3-mediated

transcriptional repression at specific loci. Therefore an exciting area of research will involve determining the binding partners of the Hdac3 coreprssor complex that lead to its genomic localization in neural crest.

Interesting candidate transcription factors include Hox family members, including Msx proteins. Hox proteins are differentially expressed along the rostro-caudal axis of neural crest and bind DNA in a sequence-specific manner (Marshall et al., 1992). In many developmental contexts, they have been shown to act both as transcriptional activators and transcriptional repressors - the latter activity occurring through direct interaction with chromatin remodeling complexes, incuding Hdac3-NCoR/SMRT (Saleh et al., 2000). Interestingly, abnormalities in Hox gene expression can cause a number of the defects observed with Hdac3 deletion (Makki and Capecchi, 2011).

Hdac3 ChIP-Seq studies described above would be useful for determining whether Hox proteins or additional classes of transcription factors dictate the genomic localization of Hdac3 in neural crest. Bioinformatic analysis of neural crest Hdac3 enrichment sites determined by ChIP-Seq could reveal putative binding sites for known transcription factors, including Hox proteins. Predicted interacting partners could then be validated by Co-IP and sequential ChIP experiments.

Given that work in the liver has suggested that a single factor may influence global Hdac3 localization within a given tissue (Feng et al., 2011), an unbiased screen for Hdac3 protein interacting partners in neural crest cells could

also identify the mediators of Hdac3 genomic targeting. In such a screen, Hdac3 would be precipitated from neural crest cells and its interacting partners identified by mass spectrometry. To this end, we have designed and are cloning a construct in which Hdac3 is tagged with an AviTag that leads to its biotinylation (Wang et al., 2006). This strategy has previously been used to identify interaction networks between transcription factors and chromatin remodeling enzymes in early developmental processes (Wang et al., 2006). Biotin-tagged Hdac3 could be expressed in cultured neural crest cells and precipitated with high affinity by streptavadin; such a strategy would maximize the signal to noise ratio in a proteomic screen for Hdac3 interacting partners, and identify candidate interactions that could be further explored.

Are the functions of Hdac3 in neural crest mediated by interactions with non-histone proteins?

Classically, Hdacs act as transcriptional repressors by directly deacetylating histone tails. However, class I Hdacs can also regulate transcription by directly deacetylating non-histone targets (LeBoeuf et al., 2010). Hdac3 has been proposed to directly deacetylate Mef2d and p53 to regulate their activity (Gregoire et al., 2007, Zeng et al., 2006). It is possible that the phenotypes elicited by deletion of Hdac3 in neural crest arise due to hyperacetylation of transcription factors in the absence of this important regulatory enzyme.

Interestingly, the class III Hdac Sirt1 has been shown to directly deacetylate the Notch effector molecule NICD, suggesting the intriguing possibility that Hdac3 could deacetylate NICD to regulate OFT development (Guarani et al., 2011). However, this study identified the hyperacetylated form of NICD as the active form, which is not consistent with a model in which Notch activity is decreased in the absence of direct deacetylation from Hdac3.

One strategy to identify candidate transcription factors that may be direct targets of Hdac3 deacetylation is to analyze microarray data from Hdac3-deficient versus control tissue, in order to identify patterns of dysregulation among the known targets of individual transcription factors. An additional strategy to identify potential non-histone targets of Hdac3 deacetylation involves the use of the unbiased proteomics screen described above. For candidates identified through these strategies, interactions could subsequently be explored in the *in vitro* model systems employed in Chapters 2 and 3.

Concluding Remarks

The work described in this dissertation has identified downstream targets and processes in neural crest development that are regulated by Hdac3. We have shown that Hdac3 is essential for neural crest-mediated craniofacial and cardiovascular development, while it is not required for neuroendocrine development. An exciting area of future research will involve indentifying the upstream pathways and stimuli that regulate Hdac3 function in neural crest cells. These studies will shed further light on the molecular regulation of neural crest development, and provide a more complete understanding of how external stimuli are linked to heritable changes in progenitor cell gene expression.

Figure 4.1

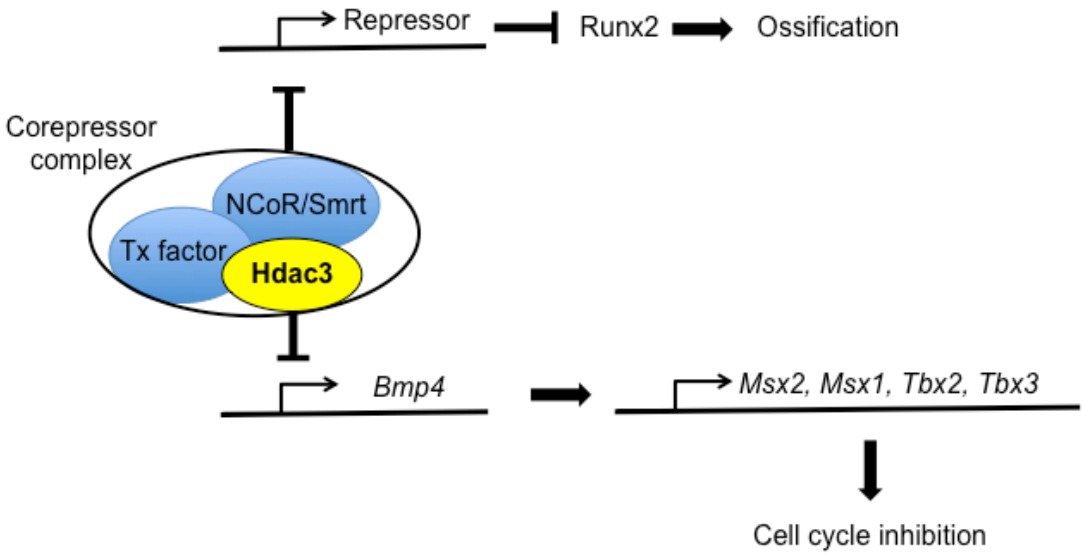
Repressor
Runx2
Ossification
Corepressor complex
NCoR/Smrt
Tx factor
Hdac3
Bmp4
Msx2, Msx1, Tbx2, Tbx3
Cell cycle inhibition

Figure 4.1. Model of Hdac3 regulation of craniofacial development. Hdac3 regulates both neural crest cell survival as well as ossification during craniofacial development. Regulation of ossification occurs through a Runx2-mediated pathway. We propose that Hdac3 is responsible for repressing a repressor of ossification, through histone deacetylation. Hdac3-mediated regulation of the cell cycle occurs through transcriptional silencing of *Bmp4*, which we hypothesize is also mediated by the transcriptional repressive functions of the Hdac3 complex. The histone deacetylase activity of Hdac3 requires its association with NCoR and/or Smrt in a corepressor complex.

Figure 4.2

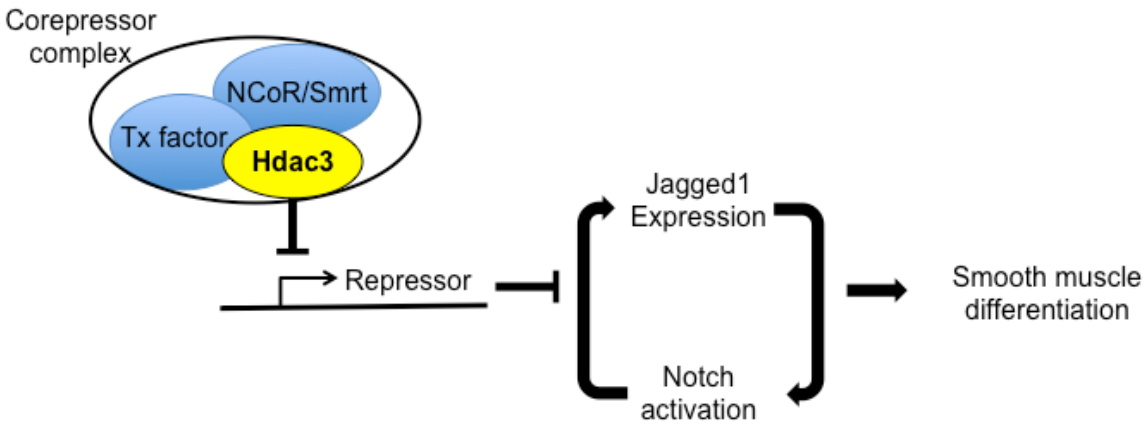
Corepressor complex
NCoR/Smrt
Tx factor
Hdac3
Repressor
Jagged1 Expression
Notch activation
Smooth muscle differentiation

Figure 4.2. Model of Hdac3 regulation of cardiac outflow tract development. Smooth muscle differentiation in the aortic arch arteries relies on a Notch-Jagged1 positive feedback loop. Hdac3 is required for propagation of this feedback loop in neural crest cells. We hypothesize that Hdac3, through its activity as a transcriptional repressor, inhibits the expression of an inhibitor of this process.

Appendix. Diet induced lethality due to deletion of the *Hdac3* gene in heart and skeletal muscle

This appendix contains data that has been published in the Journal of Biological Chemistry in a collaborative project with the Zheng Sun of the Lazar lab (Sun et al., 2011). In addition to experimental design and data analysis, I directly contributed data in figures 1A, 2B,D, 3A,C,D.

Summary

In chapter 1, I discussed phenotypes arising from cardiac deletion of Hdac3 in different stages of cardiac development. Briefly, deletion of Hdac3 in bipotent progenitor cells results in premature cardiomyocyte differentiation and proliferation defects; deletion of Hdac3 in ventricular cardiomyocytes results in inefficient lipid metabolism, leading to oxidative damage, progressive heart failure and death.

In this appendix, I describe the results of Hdac3 deletion in differentiated cardiomyocytes. In the context of the aforementioned studies of Hdac3 in cardiac development, this work provides an example of the differential roles played by Hdac3 within a single cell lineage at different developmental time points.

Results and Discussion

Excising *Hdac3* with Cre recombinase under the control of the muscle creatine kinase promoter (*Mck-Cre*) results in progressive deletion of Hdac3 in cardiomyocytes and skeletal muscle during the perinatal period (Appendix, Figure 1). *Mck-Cre; Hdac3$^{f/f}$* mice fed a normal diet (11% kcalories from fat) are viable, with no reduction in survival (Appendix, Figure 2A). At 4 months of age, they show mild cardiac hypertrophy, but no upregulation of markers of heart failure (Appendix, Figure 2B,C). Echocardiography reveals increases in ejection fraction and fractional shortening, consistent with mild, early stage cardiac disease, and histological analysis of 8 month old hearts shows mild infiltrate at 8 months of age (Appendix, Figure 2D-F).

Expression profiling of 4-month-old *Mck-Cre; Hdac3$^{f/f}$* hearts reveals that a different subset of metabolic genes is dysregulated, compared to in *αMHC-Cre; Hdac3$^{f/f}$* hearts (Appendix, Table 1). Genes found to be downregulated in *Mck-Cre; Hdac3$^{f/f}$* hearts include important regulators of the mitochondrial response to lipid overload (Appendix, Table 1). Therefore when placed on a high fat diet (60% fat by kilocalorie), these mice exhibit profound cardiac defects. Four-month-old *Mck-Cre; Hdac3$^{f/f}$* mice treated for three months on a high fat diet demonstrate pronounced cardiac hypertrophy, as measured by heart weight: tibial length ratio, expression of markers of heart failure, and increased myocyte diameter (Appendix, Figure 3A-D). These hypertrophic hearts are functionally

compromised, with significant decreases in contractility and ejection fraction, as well as wall motion abnormalities consistent with destruction of normal myocardial architecture (Appendix, Figure 3E,F). Histological analysis confirms this disruption of normal myocardial architecture, revealing significant fibrosis and a mononuclear cell infiltrate in *Mck-Cre; Hdac3*$^{f/f}$ hearts (Appendix, Figure 3D). These cardiac abnormalities lead to lethality between 4-6 months (Appendix, Figure 3G). The severity of the cardiac abnormalities in *Mck-Cre; Hdac3*$^{f/f}$ mice on a high fat diet lies in stark contrast to the subtle abnormalities of littermate controls fed normal chow, demonstrating an important interaction between environmental stimuli – in this case the nutritional environment – and the function of Hdac3 as a modulator of gene expression.

Table A.1. Genes differentially expressed in 6 week old (normal diet) *Mck-Cre; Hdac3$^{f/f}$* versus *Hdac3$^{f/f}$* hearts

Process	Gene	Gene name	Fold-change KO vs WT	q-value
Electron Transport Chain & ATP synthesis	Atp5g1	ATP synthase, H+ transporting, mitochondrial F0 complex, subunit C1	-1.55	0.022
	Atp5g2	ATP synthase, H+ transporting, mitochondrial F0 complex, subunit C2	-1.31	0.036
	Atp5l	ATP synthase, H+ transporting, mitochondrial F0 complex, subunit g	-1.28	0.025
	Atp5s	ATP synthase, H+ transporting, mitochondrial F0 complex, subunit s	-1.21	0.044
	Cox15	COX15 homolog, cytochrome c oxidase assembly protein (yeast)	-1.30	0.024
	Cox19	COX19 cytochrome c oxidase assembly homolog (S. cerevisiae)	-1.25	0.030
	Ndufs1	NADH dehydrogenase (ubiquinone) Fe-S protein 1	-1.30	0.021
	Ndufaf4	NADH dehydrogenase (ubiquinone) 1 alpha subcomplex, af 4	-1.26	0.027
	Ndufs2	NADH dehydrogenase (ubiquinone) Fe-S protein 2	-1.24	0.025
	Ndufs8	NADH dehydrogenase (ubiquinone) Fe-S protein 8	-1.23	0.029
	Ndufv1	NADH dehydrogenase (ubiquinone) flavoprotein 1	-1.20	0.040
TCA cycles	Aco1	aconitase 1	-1.31	0.022
	Fh1	fumarate hydratase 1	-1.31	0.021
	Idh1	isocitrate dehydrogenase 1 (NADP+), soluble	-1.21	0.042
	Mdh2	malate dehydrogenase 2, NAD (mitochondrial)	-1.29	0.024
	Ogdhl	oxoglutarate dehydrogenase-like	-3.67	0.019
	Pdha1	pyruvate dehydrogenase E1 alpha 1	-1.21	0.027
	Sdhb	succinate dehydrogenase complex, subunit B, iron sulfur (Ip)	-1.20	0.027
	Sdha	succinate dehydrogenase complex, subunit A, flavoprotein (Fp)	-1.19	0.029
Fatty acid metabolism	Cpt1b	carnitine palmitoyltransferase 1b, muscle	-1.49	0.020
	Ehhadh	enoyl-Coenzyme A, hydratase	-1.26	0.039
	Acads	acyl-Coenzyme A dehydrogenase, short chain	-1.55	0.020
	Acad8	acyl-Coenzyme A dehydrogenase family, member 8	-1.36	0.021
	Crot	carnitine O-octanoyltransferase	-1.33	0.023
	Peci	peroxisomal delta3, delta2-enoyl-Coenzyme A isomerase	-1.27	0.026
	Acss1	acyl-CoA synthetase short-chain family member 1	-1.38	0.021
	Acsl5	acyl-CoA synthetase long-chain family member 5	+1.34	0.026
	Acot2	acyl-CoA thioesterase 2	-1.55	0.020
Glycerolipid metabolism	Agpat9	1-acylglycerol-3-phosphate O-acyltransferase 9	-1.34	0.022
	Akr1b10	aldo-keto reductase family 1, member B10 (aldose reductase)	-2.20	0.019
	Dgat1	diacylglycerol O-acyltransferase 1	-1.58	0.020
	Gyk	glycerol kinase	-1.39	0.020
Other metabolic process	Ucp2	uncoupling protein 2 (mitochondrial, proton carrier)	+2.06	0.019
	Ucp3	uncoupling protein 3 (mitochondrial, proton carrier)	+1.96	0.020
	G6pdx	glucose-6-phosphate dehydrogenase X-linked	+1.41	0.022
	Me3	malic enzyme 3, NADP(+)-dependent, mitochondrial	-1.19	0.033
	Pdk1	pyruvate dehydrogenase kinase, isoenzyme 1	-1.26	0.027
	Pfkfb1	6-phosphofructo-2-kinase	-2.06	0.019
Transcription regulation	Ppargc1b	peroxisome proliferative activated receptor, gamma, coactivator 1 beta	-1.26	0.044
	Mlxipl	MLX interacting protein-like	-1.53	0.020
	Ireb2	iron responsive element binding protein 2	-1.21	0.029

Figure A.1

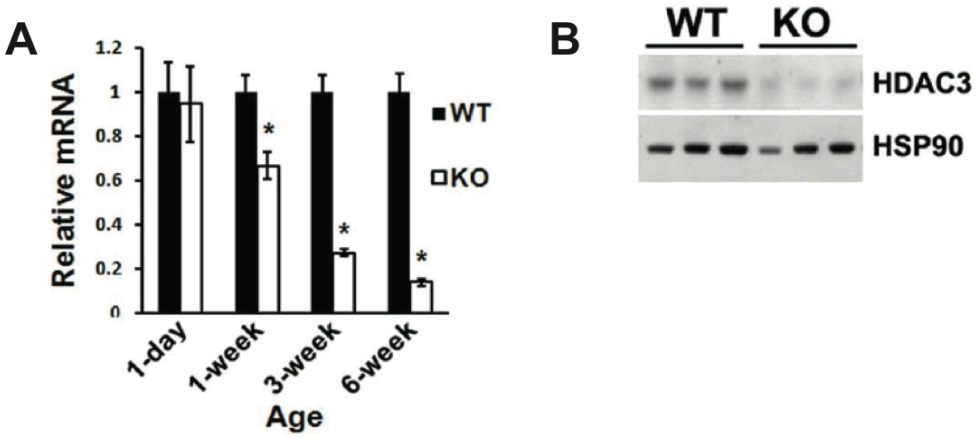
A
Relative mRNA
1.2
1
0.8
0.6
0.4
0.2
0
WT
KO
*
*
*
1-day
1-week
3-week
6-week
Age
B
WT
KO
HDAC3
HSP90

Figure A.1. Efficient postnatal deletion of Hdac3 In *Mck-Cre; Hdac3$^{f/f}$* hearts. A. qPCR analysis of *Hdac3* transcript in mice at the age of 1-day, 1-week, 3-week, and 6-week. n=4. *Arbp* was used as a reference control. Error bar = S.E.M. Asterisks indicate $p < 0.05$ by two-sided student's t-test. **B,** Western blot analysis of 4-month-old mice. KO: Mck-Cre; Hdac3$^{f/f}$. WT: littermate Hdac3$^{f/f}$.

Figure A.2

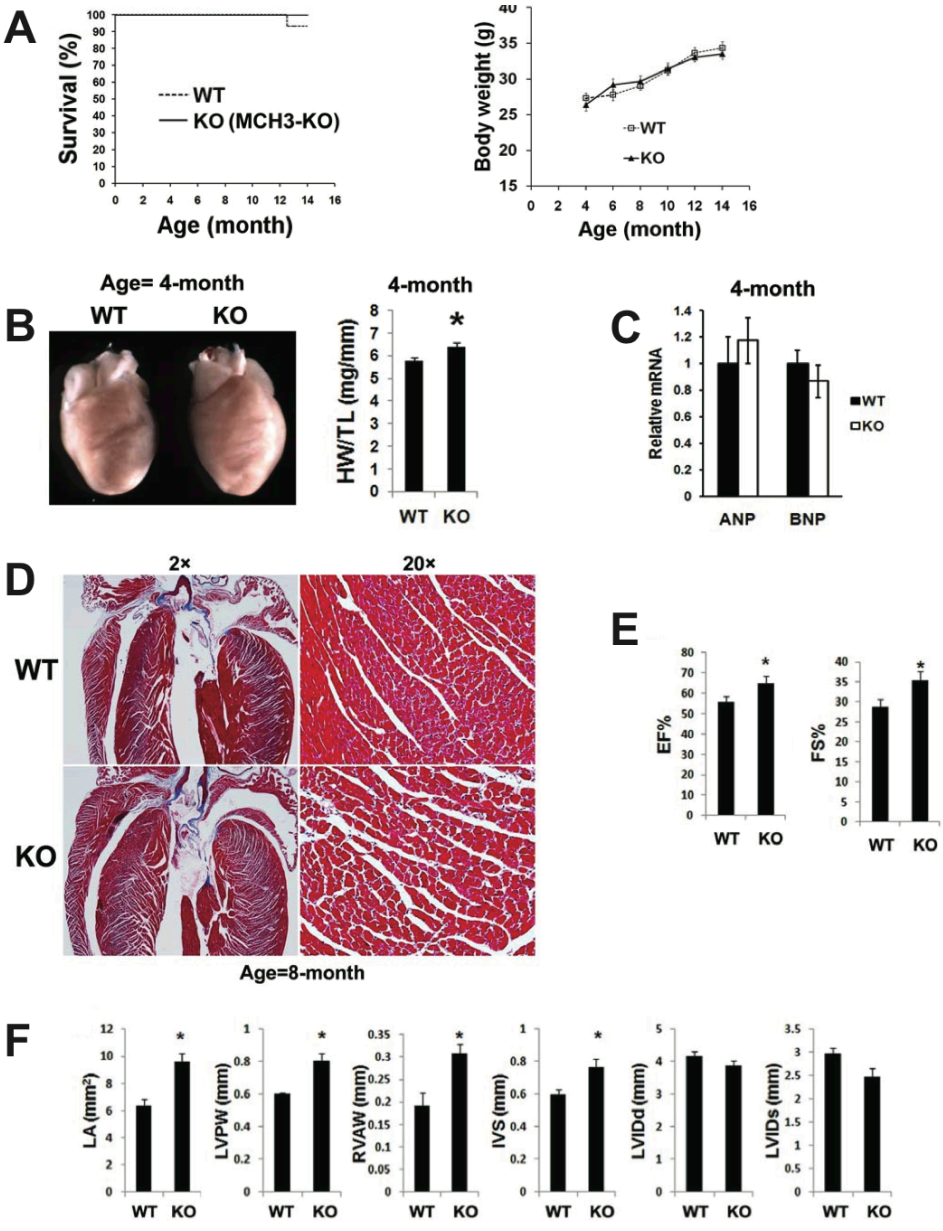
A
Survival (%)
WT
KO (MCH3-KO)
Age (month)
Body weight (g)
WT
KO
Age (month)
B
Age= 4-month
WT
KO
4-month
HW/TL (mg/mm)
WT KO
C
4-month
Relative mRNA
WT
KO
ANP
BNP
D
2×
20×
WT
KO
Age=8-month
E
EF%
WT KO
FS%
WT KO
F
LA (mm²)
LVPW (mm)
RVAW (mm)
IVS (mm)
LVIDd (mm)
LVIDs (mm)
WT KO

Figure A.2. Mild alterations in Hdac3-deficient hearts on normal chow. A. Kaplan-Meier survival curves and body weight are unchanged on normal chow. n=12-15. **B.** Gross picture of hearts at the age of 4-months, and heart weight (HW) to tibia length (TL) ratio of 4-month-old mice on normal chow. n=7-8. **C.** qPCR analysis of 4-month-old mice for cardiac atrial natriuretic peptide (ANP) and brain natriuretic peptide (BNP), markers for heart failure. n=3. **D.** Trichrome stain of hearts from 8-month-old mice, revealing normal myocardial architecture. **E-F**. Echocardiography analysis of cardiac structure and function on 4-month-old mice on normal chow. . n=4-5. **E.** Parameters measuring cardiac function reveal subtle abnormalities in Hdac3-deficient hearts, representing increased cardiac function. EF: left ventricular ejection fraction FS: left ventricular fractional shortening. **F.** Parameters measuring cardiac structure reveal subtle abnormalities in Hdac3-deficient hearts. IVRT: isovolumic relaxation time; LVIDd: left ventricular diameter during diastole; LVIDs: Left ventricular diameter during systole; LA: left atrium area; LVPW: LV posterior wall thickness during diastole; RVAW: right ventricular anterior wall thickness; IVS: interventricular septal thickness during diastole.

Figure A.3

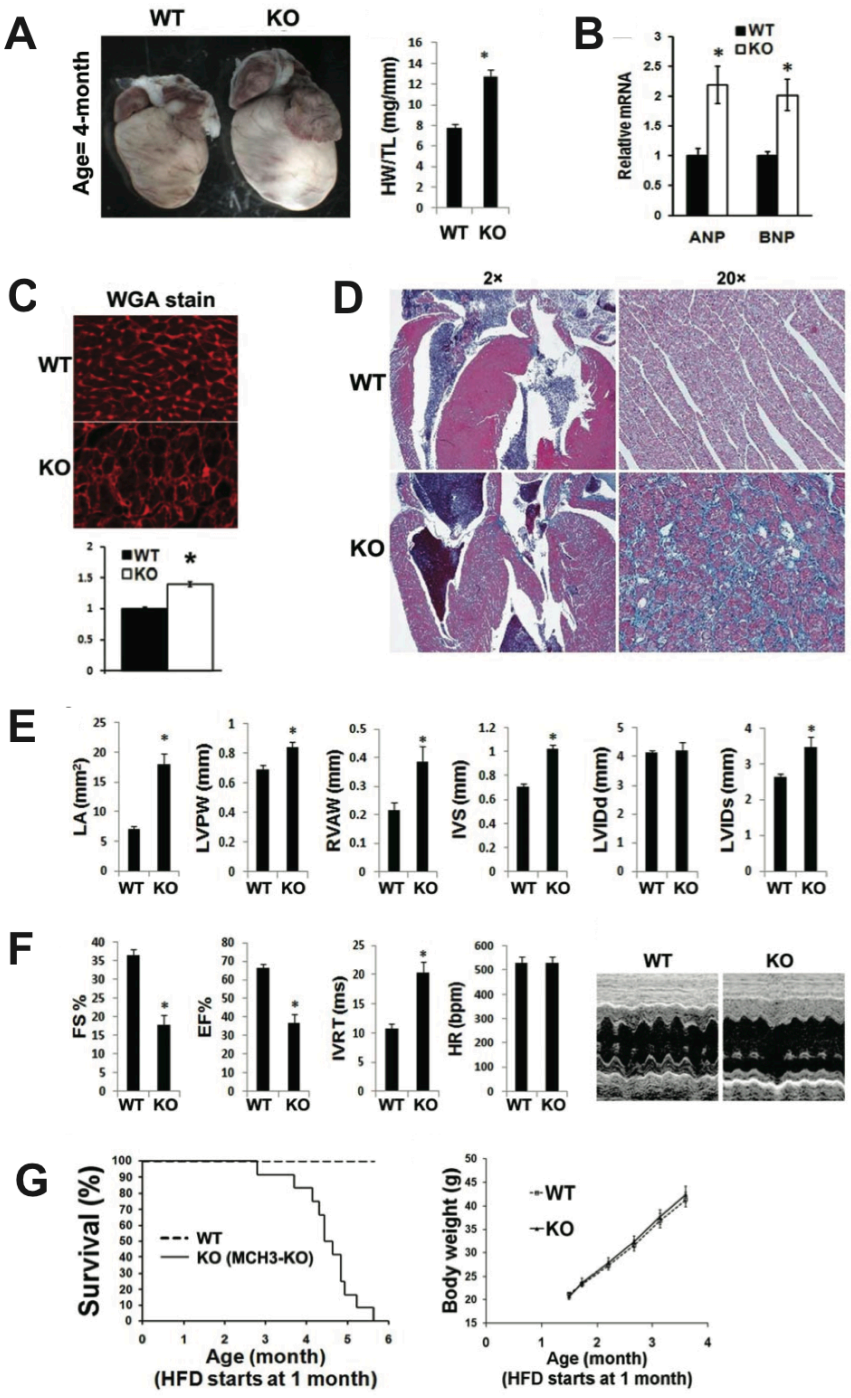
A
WT
KO
Age= 4-month
HW/TL (mg/mm)
WT KO
B
WT
KO
Relative mRNA
ANP
BNP
C
WGA stain
WT
KO
WT
KO
D
2×
20×
WT
KO
E
LA (mm²)
LVPW (mm)
RVAW (mm)
IVS (mm)
LVIDd (mm)
LVIDs (mm)
WT KO
F
FS %
EF%
IVRT (ms)
HR (bpm)
WT KO
WT
KO
G
Survival (%)
WT
KO (MCH3-KO)
Age (month)
(HFD starts at 1 month)
Body weight (g)
WT
KO
Age (month)
(HFD starts at 1 month)

Figure A.3. Dietary lipid overload induced severe cardiac defects in mice lacking cardiac Hdac3. A. Gross picture and heart weight (HW) to tibia length (TL) ratio of hearts from 4-month-old mice after 3 months on a high fat diet (HFD). n=4-5. **B.** qPCR analysis of myocardial ANP and BNP from 4-month-old mice. n=4-5. **C.** Wheat germ agglutinin (WGA) staining of cross sections of ventricles from 4-month-old mice on HFD. Myocyte diameter was quantified using 6 random 20x fields of view from 3 WT and 5 KO hearts. **D.** Trichrome stain of hearts from 4-month-old mice on HFD shows extensive areas of fibrosis (blue) and destruction of normal myocardial architecture. **E-F.** Echocardiography analysis of cardiac structure and function on 4-month-old mice on high fat diet. n=4-5. **E.** Cardiac structure data. **F.** Contractile function data and representative short-axis M-mode images from echocardiography. **G.** Kaplan-Meier survival curves on high fat diet (HFD). n=10 for WT, n=12 for KO. KO mice have normal weight gain on HFD.

Bibliography

ALAPPAT, S., ZHANG, Z. Y. & CHEN, Y. P. 2003. Msx homeobox gene family and craniofacial development. *Cell Res,* 13**,** 429-42.

ALENGHAT, T., MEYERS, K., MULLICAN, S. E., LEITNER, K., ADENIJI-ADELE, A., AVILA, J., BUCAN, M., AHIMA, R. S., KAESTNER, K. H. & LAZAR, M. A. 2008. Nuclear receptor corepressor and histone deacetylase 3 govern circadian metabolic physiology. *Nature,* 456**,** 997-1000.

ANDERSSON, E. R., SANDBERG, R. & LENDAHL, U. 2011. Notch signaling: simplicity in design, versatility in function. *Development,* 138**,** 3593-612.

ANOKYE-DANSO, F., TRIVEDI, C. M., JUHR, D., GUPTA, M., CUI, Z., TIAN, Y., ZHANG, Y., YANG, W., GRUBER, P. J., EPSTEIN, J. A. & MORRISEY, E. E. 2011. Highly efficient miRNA-mediated reprogramming of mouse and human somatic cells to pluripotency. *Cell Stem Cell,* 8**,** 376-88.

BAEK, J. A., LAN, Y., LIU, H., MALTBY, K. M., MISHINA, Y. & JIANG, R. 2011. Bmpr1a signaling plays critical roles in palatal shelf growth and palatal bone formation. *Dev Biol,* 350**,** 520-31.

BAJPAI, R., CHEN, D. A., RADA-IGLESIAS, A., ZHANG, J., XIONG, Y., HELMS, J., CHANG, C. P., ZHAO, Y., SWIGUT, T. & WYSOCKA, J. 2010. CHD7 cooperates with PBAF to control multipotent neural crest formation. *Nature,* 463**,** 958-62.

BEI, M. & MAAS, R. 1998. FGFs and BMP4 induce both Msx1-independent and Msx1-dependent signaling pathways in early tooth development. *Development,* 125**,** 4325-33.

BENISH, B. M. 1975. Letter: "The neurocristopathies: a unifying concept of disease arising in neural crest development". *Hum Pathol,* 6**,** 128.

BERGER, S. L., KOUZARIDES, T., SHIEKHATTAR, R. & SHILATIFARD, A. 2009. An operational definition of epigenetics. *Genes Dev,* 23**,** 781-3.

BHASKARA, S., CHYLA, B. J., AMANN, J. M., KNUTSON, S. K., CORTEZ, D., SUN, Z. W. & HIEBERT, S. W. 2008. Deletion of histone deacetylase 3 reveals critical roles in S phase progression and DNA damage control. *Mol Cell,* 30**,** 61-72.

CHANDLER, K. J., CHANDLER, R. L. & MORTLOCK, D. P. 2009. Identification of an ancient Bmp4 mesoderm enhancer located 46 kb from the promoter. *Dev Biol,* 327**,** 590-602.

CHANG, C. P. & BRUNEAU, B. 2011. Epigenetics and Cardiovascular Development. *Annu Rev Physiol*.

CHEN, Y., ZHANG, Y., JIANG, T. X., BARLOW, A. J., ST AMAND, T. R., HU, Y., HEANEY, S., FRANCIS-WEST, P., CHUONG, C. M. & MAAS, R. 2000. Conservation of early odontogenic signaling pathways in Aves. *Proc Natl Acad Sci U S A,* 97**,** 10044-9.

CHEN, Y. H., ISHII, M., SUN, J., SUCOV, H. M. & MAXSON, R. E., JR. 2007. Msx1 and Msx2 regulate survival of secondary heart field precursors and

post-migratory proliferation of cardiac neural crest in the outflow tract. *Dev Biol,* 308**,** 421-37.

CONDIE, B. G., BAIN, G., GOTTLIEB, D. I. & CAPECCHI, M. R. 1997. Cleft palate in mice with a targeted mutation in the gamma-aminobutyric acid-producing enzyme glutamic acid decarboxylase 67. *Proc Natl Acad Sci U S A,* 94**,** 11451-5.

COULY, G. F., COLTEY, P. M. & LE DOUARIN, N. M. 1993. The triple origin of skull in higher vertebrates: a study in quail-chick chimeras. *Development,* 117**,** 409-29.

DAVY, A., AUBIN, J. & SORIANO, P. 2004. Ephrin-B1 forward and reverse signaling are required during mouse development. *Genes Dev,* 18**,** 572-83.

DENG, C., ZHANG, P., HARPER, J. W., ELLEDGE, S. J. & LEDER, P. 1995. Mice lacking p21CIP1/WAF1 undergo normal development, but are defective in G1 checkpoint control. *Cell,* 82**,** 675-84.

ENGLEKA, K. A., GITLER, A. D., ZHANG, M., ZHOU, D. D., HIGH, F. A. & EPSTEIN, J. A. 2005. Insertion of Cre into the Pax3 locus creates a new allele of Splotch and identifies unexpected Pax3 derivatives. *Dev Biol,* 280**,** 396-406.

EPSTEIN, J. A. 2010. Franklin H. Epstein Lecture. Cardiac development and implications for heart disease. *N Engl J Med,* 363**,** 1638-47.

FENG, D., LIU, T., SUN, Z., BUGGE, A., MULLICAN, S. E., ALENGHAT, T., LIU, X. S. & LAZAR, M. A. 2011. A circadian rhythm orchestrated by histone deacetylase 3 controls hepatic lipid metabolism. *Science,* 331**,** 1315-9.

FENG, X., KREBS, L. T. & GRIDLEY, T. 2010. Patent ductus arteriosus in mice with smooth muscle-specific Jag1 deletion. *Development,* 137**,** 4191-9.

FOSTER, K., SHERIDAN, J., VEIGA-FERNANDES, H., RODERICK, K., PACHNIS, V., ADAMS, R., BLACKBURN, C., KIOUSSIS, D. & COLES, M. 2008. Contribution of neural crest-derived cells in the embryonic and adult thymus. *J Immunol,* 180**,** 3183-9.

FOSTER, K. E., GORDON, J., CARDENAS, K., VEIGA-FERNANDES, H., MAKINEN, T., GRIGORIEVA, E., WILKINSON, D. G., BLACKBURN, C. C., RICHIE, E., MANLEY, N. R., ADAMS, R. H., KIOUSSIS, D. & COLES, M. C. 2010. EphB-ephrin-B2 interactions are required for thymus migration during organogenesis. *Proc Natl Acad Sci U S A,* 107**,** 13414-9.

GAMMILL, L. S., GONZALEZ, C. & BRONNER-FRASER, M. 2007. Neuropilin 2/semaphorin 3F signaling is essential for cranial neural crest migration and trigeminal ganglion condensation. *Dev Neurobiol,* 67**,** 47-56.

GANS, C. & NORTHCUTT, R. G. 1983. Neural crest and the origin of vertebrates: a new head. *Science,* 220**,** 268-73.

GRAHAM, A., FRANCIS-WEST, P., BRICKELL, P. & LUMSDEN, A. 1994. The signalling molecule BMP4 mediates apoptosis in the rhombencephalic neural crest. *Nature,* 372**,** 684-6.

GREGOIRE, S., XIAO, L., NIE, J., ZHANG, X., XU, M., LI, J., WONG, J., SETO, E. & YANG, X. J. 2007. Histone deacetylase 3 interacts with and deacetylates myocyte enhancer factor 2. *Mol Cell Biol,* 27**,** 1280-95.

GUARANI, V., DEFLORIAN, G., FRANCO, C. A., KRUGER, M., PHNG, L. K., BENTLEY, K., TOUSSAINT, L., DEQUIEDT, F., MOSTOSLAVSKY, R., SCHMIDT, M. H., ZIMMERMANN, B., BRANDES, R. P., MIONE, M., WESTPHAL, C. H., BRAUN, T., ZEIHER, A. M., GERHARDT, H., DIMMELER, S. & POTENTE, M. 2011. Acetylation-dependent regulation of endothelial Notch signalling by the SIRT1 deacetylase. *Nature,* 473**,** 234-8.

GUENTHER, M. G., BARAK, O. & LAZAR, M. A. 2001. The SMRT and N-CoR corepressors are activating cofactors for histone deacetylase 3. *Mol Cell Biol,* 21**,** 6091-101.

GUO, C., SUN, Y., ZHOU, B., ADAM, R. M., LI, X., PU, W. T., MORROW, B. E. & MOON, A. 2011. A Tbx1-Six1/Eya1-Fgf8 genetic pathway controls mammalian cardiovascular and craniofacial morphogenesis. *J Clin Invest,* 121**,** 1585-95.

HABERLAND, M., MOKALLED, M. H., MONTGOMERY, R. L. & OLSON, E. N. 2009a. Epigenetic control of skull morphogenesis by histone deacetylase 8. *Genes Dev,* 23**,** 1625-30.

HABERLAND, M., MONTGOMERY, R. L. & OLSON, E. N. 2009b. The many roles of histone deacetylases in development and physiology: implications for disease and therapy. *Nat Rev Genet,* 10**,** 32-42.

HANG, C. T., YANG, J., HAN, P., CHENG, H. L., SHANG, C., ASHLEY, E., ZHOU, B. & CHANG, C. P. 2010. Chromatin regulation by Brg1 underlies heart muscle development and disease. *Nature,* 466**,** 62-7.

HE, F., XIONG, W., WANG, Y., LI, L., LIU, C., YAMAGAMI, T., TAKETO, M. M., ZHOU, C. & CHEN, Y. 2011. Epithelial Wnt/beta-catenin signaling regulates palatal shelf fusion through regulation of Tgfbeta3 expression. *Dev Biol,* 350**,** 511-9.

HE, F., XIONG, W., WANG, Y., MATSUI, M., YU, X., CHAI, Y., KLINGENSMITH, J. & CHEN, Y. 2010. Modulation of BMP signaling by Noggin is required for the maintenance of palatal epithelial integrity during palatogenesis. *Dev Biol,* 347**,** 109-21.

HEGNER, B., LANGE, M., KUSCH, A., ESSIN, K., SEZER, O., SCHULZE-LOHOFF, E., LUFT, F. C., GOLLASCH, M. & DRAGUN, D. 2009. mTOR regulates vascular smooth muscle cell differentiation from human bone marrow-derived mesenchymal progenitors. *Arterioscler Thromb Vasc Biol,* 29**,** 232-8.

HEIDT, A. B. & BLACK, B. L. 2005. Transgenic mice that express Cre recombinase under control of a skeletal muscle-specific promoter from mef2c. *Genesis,* 42**,** 28-32.

HESSE, E., SAITO, H., KIVIRANTA, R., CORREA, D., YAMANA, K., NEFF, L., TOBEN, D., DUDA, G., ATFI, A., GEOFFROY, V., HORNE, W. C. & BARON, R. 2010. Zfp521 controls bone mass by HDAC3-dependent attenuation of Runx2 activity. *J Cell Biol,* 191**,** 1271-83.

HIGH, F. A., JAIN, R., STOLLER, J. Z., ANTONUCCI, N. B., LU, M. M., LOOMES, K. M., KAESTNER, K. H., PEAR, W. S. & EPSTEIN, J. A. 2009. Murine Jagged1/Notch signaling in the second heart field orchestrates Fgf8 expression and tissue-tissue interactions during outflow tract development. *J Clin Invest,* 119**,** 1986-96.

HIGH, F. A., LU, M. M., PEAR, W. S., LOOMES, K. M., KAESTNER, K. H. & EPSTEIN, J. A. 2008. Endothelial expression of the Notch ligand Jagged1 is required for vascular smooth muscle development. *Proc Natl Acad Sci U S A,* 105**,** 1955-9.

HIGH, F. A., ZHANG, M., PROWELLER, A., TU, L., PARMACEK, M. S., PEAR, W. S. & EPSTEIN, J. A. 2007. An essential role for Notch in neural crest during cardiovascular development and smooth muscle differentiation. *J Clin Invest,* 117**,** 353-63.

HUH, S. H. & ORNITZ, D. M. 2010. Beta-catenin deficiency causes DiGeorge syndrome-like phenotypes through regulation of Tbx1. *Development,* 137**,** 1137-47.

HUNT, P., GULISANO, M., COOK, M., SHAM, M. H., FAIELLA, A., WILKINSON, D., BONCINELLI, E. & KRUMLAUF, R. 1991. A distinct Hox code for the branchial region of the vertebrate head. *Nature,* 353**,** 861-4.

ITO, Y., YEO, J. Y., CHYTIL, A., HAN, J., BRINGAS, P., JR., NAKAJIMA, A., SHULER, C. F., MOSES, H. L. & CHAI, Y. 2003. Conditional inactivation of Tgfbr2 in cranial neural crest causes cleft palate and calvaria defects. *Development,* 130**,** 5269-80.

JACOB, C., CHRISTEN, C. N., PEREIRA, J. A., SOMANDIN, C., BAGGIOLINI, A., LOTSCHER, P., OZCELIK, M., TRICAUD, N., MEIJER, D., YAMAGUCHI, T., MATTHIAS, P. & SUTER, U. 2011. HDAC1 and HDAC2 control the transcriptional program of myelination and the survival of Schwann cells. *Nat Neurosci,* 14**,** 429-36.

JAIN, R., RENTSCHLER, S. & EPSTEIN, J. A. 2010. Notch and cardiac outflow tract development. *Ann N Y Acad Sci,* 1188**,** 184-90.

JIANG, X., ROWITCH, D. H., SORIANO, P., MCMAHON, A. P. & SUCOV, H. M. 2000. Fate of the mammalian cardiac neural crest. *Development,* 127**,** 1607-16.

KIM, H., KANG, K., EKRAM, M. B., ROH, T. Y. & KIM, J. 2011. Aebp2 as an epigenetic regulator for neural crest cells. *PLoS One,* 6**,** e25174.

KLAUS, A. & BIRCHMEIER, W. 2008. Wnt signalling and its impact on development and cancer. *Nat Rev Cancer,* 8**,** 387-98.

KNUTSON, S. K., CHYLA, B. J., AMANN, J. M., BHASKARA, S., HUPPERT, S. S. & HIEBERT, S. W. 2008. Liver-specific deletion of histone deacetylase 3 disrupts metabolic transcriptional networks. *EMBO J,* 27**,** 1017-28.

LALANI, S. R., SAFIULLAH, A. M., FERNBACH, S. D., HARUTYUNYAN, K. G., THALLER, C., PETERSON, L. E., MCPHERSON, J. D., GIBBS, R. A., WHITE, L. D., HEFNER, M., DAVENPORT, S. L., GRAHAM, J. M., BACINO, C. A., GLASS, N. L., TOWBIN, J. A., CRAIGEN, W. J., NEISH, S. R., LIN, A. E. & BELMONT, J. W. 2006. Spectrum of CHD7 mutations in 110 individuals with CHARGE syndrome and genotype-phenotype correlation. *Am J Hum Genet,* 78**,** 303-14.

LAN, Y. & JIANG, R. 2009. Sonic hedgehog signaling regulates reciprocal epithelial-mesenchymal interactions controlling palatal outgrowth. *Development,* 136**,** 1387-96.

LE DOUARIN, N. M., CREUZET, S., COULY, G. & DUPIN, E. 2004. Neural crest cell plasticity and its limits. *Development,* 131**,** 4637-50.

LE DOUARIN, N. M., RENAUD, D., TEILLET, M. A. & LE DOUARIN, G. H. 1975. Cholinergic differentiation of presumptive adrenergic neuroblasts in interspecific chimeras after heterotopic transplantations. *Proc Natl Acad Sci U S A,* 72**,** 728-32.

LEBOEUF, M., TERRELL, A., TRIVEDI, S., SINHA, S., EPSTEIN, J. A., OLSON, E. N., MORRISEY, E. E. & MILLAR, S. E. 2010. Hdac1 and Hdac2 act

redundantly to control p63 and p53 functions in epidermal progenitor cells. *Dev Cell,* 19**,** 807-18.

LEE, J. M., KIM, J. Y., CHO, K. W., LEE, M. J., CHO, S. W., ZHANG, Y., BYUN, S. K., YI, C. K. & JUNG, H. S. 2007. Modulation of cell proliferation during palatogenesis by the interplay between Tbx3 and Bmp4. *Cell Tissue Res,* 327**,** 285-92.

LEROY, G., RICKARDS, B. & FLINT, S. J. 2008. The double bromodomain proteins Brd2 and Brd3 couple histone acetylation to transcription. *Mol Cell,* 30**,** 51-60.

LI, Y., KAO, G. D., GARCIA, B. A., SHABANOWITZ, J., HUNT, D. F., QIN, J., PHELAN, C. & LAZAR, M. A. 2006. A novel histone deacetylase pathway regulates mitosis by modulating Aurora B kinase activity. *Genes Dev,* 20**,** 2566-79.

LIU, Y. H., KUNDU, R., WU, L., LUO, W., IGNELZI, M. A., JR., SNEAD, M. L. & MAXSON, R. E., JR. 1995. Premature suture closure and ectopic cranial bone in mice expressing Msx2 transgenes in the developing skull. *Proc Natl Acad Sci U S A,* 92**,** 6137-41.

MAKKI, N. & CAPECCHI, M. R. 2011. Cardiovascular defects in a mouse model of HOXA1 syndrome. *Hum Mol Genet*.

MARSHALL, H., NONCHEV, S., SHAM, M. H., MUCHAMORE, I., LUMSDEN, A. & KRUMLAUF, R. 1992. Retinoic acid alters hindbrain Hox code and

induces transformation of rhombomeres 2/3 into a 4/5 identity. *Nature,* 360**,** 737-41.

MARTIN, K. A., RZUCIDLO, E. M., MERENICK, B. L., FINGAR, D. C., BROWN, D. J., WAGNER, R. J. & POWELL, R. J. 2004. The mTOR/p70 S6K1 pathway regulates vascular smooth muscle cell differentiation. *Am J Physiol Cell Physiol,* 286**,** C507-17.

MITSIADIS, T. A., GRAF, D., LUDER, H., GRIDLEY, T. & BLUTEAU, G. 2010. BMPs and FGFs target Notch signalling via jagged 2 to regulate tooth morphogenesis and cytodifferentiation. *Development,* 137**,** 3025-35.

MONTGOMERY, R. L., DAVIS, C. A., POTTHOFF, M. J., HABERLAND, M., FIELITZ, J., QI, X., HILL, J. A., RICHARDSON, J. A. & OLSON, E. N. 2007. Histone deacetylases 1 and 2 redundantly regulate cardiac morphogenesis, growth, and contractility. *Genes Dev,* 21**,** 1790-802.

MONTGOMERY, R. L., HSIEH, J., BARBOSA, A. C., RICHARDSON, J. A. & OLSON, E. N. 2009. Histone deacetylases 1 and 2 control the progression of neural precursors to neurons during brain development. *Proc Natl Acad Sci U S A,* 106**,** 7876-81.

MONTGOMERY, R. L., POTTHOFF, M. J., HABERLAND, M., QI, X., MATSUZAKI, S., HUMPHRIES, K. M., RICHARDSON, J. A., BASSEL-DUBY, R. & OLSON, E. N. 2008. Maintenance of cardiac energy metabolism by histone deacetylase 3 in mice. *J Clin Invest,* 118**,** 3588-97.

MORINI, F., COZZI, D. A., ILARI, M., CASATI, A. & COZZI, F. 2001. Pattern of cardiovascular anomalies associated with esophageal atresia: support for a caudal pharyngeal arch neurocristopathy. *Pediatr Res,* 50**,** 565-8.

MUKHOPADHYAY, P., SINGH, S., GREENE, R. M. & PISANO, M. M. 2006. Molecular fingerprinting of BMP2- and BMP4-treated embryonic maxillary mesenchymal cells. *Orthod Craniofac Res,* 9**,** 93-110.

MYSLIWIEC, M. R., BRESNICK, E. H. & LEE, Y. 2011. Endothelial Jarid2/Jumonji is required for normal cardiac development and proper Notch1 expression. *J Biol Chem,* 286**,** 17193-204.

NEVES, H., DUPIN, E., PARREIRA, L. & LE DOUARIN, N. M. 2011. Modulation of Bmp4 signalling in the epithelial-mesenchymal interactions that take place in early thymus and parathyroid development in avian embryos. *Dev Biol*.

NEWBERN, J., ZHONG, J., WICKRAMASINGHE, R. S., LI, X., WU, Y., SAMUELS, I., CHEROSKY, N., KARLO, J. C., O'LOUGHLIN, B., WIKENHEISER, J., GARGESHA, M., DOUGHMAN, Y. Q., CHARRON, J., GINTY, D. D., WATANABE, M., SAITTA, S. C., SNIDER, W. D. & LANDRETH, G. E. 2008. Mouse and human phenotypes indicate a critical conserved role for ERK2 signaling in neural crest development. *Proc Natl Acad Sci U S A,* 105**,** 17115-20.

NIE, X., BROWN, C. B., WANG, Q. & JIAO, K. 2011. Inactivation of Bmp4 from the Tbx1 expression domain causes abnormal pharyngeal arch artery and cardiac outflow tract remodeling. *Cells Tissues Organs,* 193**,** 393-403.

NIE, X., LUUKKO, K. & KETTUNEN, P. 2006. BMP signalling in craniofacial development. *Int J Dev Biol,* 50**,** 511-21.

NOVAK, A., GUO, C., YANG, W., NAGY, A. & LOBE, C. G. 2000. Z/EG, a double reporter mouse line that expresses enhanced green fluorescent protein upon Cre-mediated excision. *Genesis,* 28**,** 147-55.

OWENS, G. K., KUMAR, M. S. & WAMHOFF, B. R. 2004. Molecular regulation of vascular smooth muscle cell differentiation in development and disease. *Physiol Rev,* 84**,** 767-801.

PARK, E. J., WATANABE, Y., SMYTH, G., MIYAGAWA-TOMITA, S., MEYERS, E., KLINGENSMITH, J., CAMENISCH, T., BUCKINGHAM, M. & MOON, A. M. 2008. An FGF autocrine loop initiated in second heart field mesoderm regulates morphogenesis at the arterial pole of the heart. *Development,* 135**,** 3599-610.

PORRELLO, E. R., MAHMOUD, A. I., SIMPSON, E., HILL, J. A., RICHARDSON, J. A., OLSON, E. N. & SADEK, H. A. 2011. Transient regenerative potential of the neonatal mouse heart. *Science,* 331**,** 1078-80.

PREGIZER, S. & MORTLOCK, D. P. 2009. Control of BMP gene expression by long-range regulatory elements. *Cytokine Growth Factor Rev,* 20**,** 509-15.

QIU, M., BULFONE, A., MARTINEZ, S., MENESES, J. J., SHIMAMURA, K., PEDERSEN, R. A. & RUBENSTEIN, J. L. 1995. Null mutation of Dlx-2 results in abnormal morphogenesis of proximal first and second branchial arch derivatives and abnormal differentiation in the forebrain. *Genes Dev,* 9**,** 2523-38.

RANDALL, V., MCCUE, K., ROBERTS, C., KYRIAKOPOULOU, V., BEDDOW, S., BARRETT, A. N., VITELLI, F., PRESCOTT, K., SHAW-SMITH, C., DEVRIENDT, K., BOSMAN, E., STEFFES, G., STEEL, K. P., SIMRICK, S., BASSON, M. A., ILLINGWORTH, E. & SCAMBLER, P. J. 2009. Great vessel development requires biallelic expression of Chd7 and Tbx1 in pharyngeal ectoderm in mice. *J Clin Invest,* 119**,** 3301-10.

RAZIDLO, D. F., WHITNEY, T. J., CASPER, M. E., MCGEE-LAWRENCE, M. E., STENSGARD, B. A., LI, X., SECRETO, F. J., KNUTSON, S. K., HIEBERT, S. W. & WESTENDORF, J. J. 2010. Histone deacetylase 3 depletion in osteo/chondroprogenitor cells decreases bone density and increases marrow fat. *PLoS One,* 5**,** e11492.

RICHARTE, A. M., MEAD, H. B. & TALLQUIST, M. D. 2007. Cooperation between the PDGF receptors in cardiac neural crest cell migration. *Dev Biol,* 306**,** 785-96.

ROYBAL, P. G., WU, N. L., SUN, J., TING, M. C., SCHAFER, C. A. & MAXSON, R. E. 2010. Inactivation of Msx1 and Msx2 in neural crest reveals an

unexpected role in suppressing heterotopic bone formation in the head. *Dev Biol,* 343**,** 28-39.

SALEH, M., RAMBALDI, I., YANG, X. J. & FEATHERSTONE, M. S. 2000. Cell signaling switches HOX-PBX complexes from repressors to activators of transcription mediated by histone deacetylases and histone acetyltransferases. *Mol Cell Biol,* 20**,** 8623-33.

SANTAGATI, F. & RIJLI, F. M. 2003. Cranial neural crest and the building of the vertebrate head. *Nat Rev Neurosci,* 4**,** 806-18.

SAUKA-SPENGLER, T. & BRONNER-FRASER, M. 2008. A gene regulatory network orchestrates neural crest formation. *Nat Rev Mol Cell Biol,* 9**,** 557-68.

SCHROEDER, T. M., KAHLER, R. A., LI, X. & WESTENDORF, J. J. 2004. Histone deacetylase 3 interacts with runx2 to repress the osteocalcin promoter and regulate osteoblast differentiation. *J Biol Chem,* 279**,** 41998-2007.

SHARPE, J., AHLGREN, U., PERRY, P., HILL, B., ROSS, A., HECKSHER-SORENSEN, J., BALDOCK, R. & DAVIDSON, D. 2002. Optical projection tomography as a tool for 3D microscopy and gene expression studies. *Science,* 296**,** 541-5.

SHIRAI, M., OSUGI, T., KOGA, H., KAJI, Y., TAKIMOTO, E., KOMURO, I., HARA, J., MIWA, T., YAMAUCHI-TAKIHARA, K. & TAKIHARA, Y. 2002.

The Polycomb-group gene Rae28 sustains Nkx2.5/Csx expression and is essential for cardiac morphogenesis. *J Clin Invest,* 110**,** 177-84.

SINGH, N., TRIVEDI, C. M., LU, M., MULLICAN, S. E., LAZAR, M. A. & EPSTEIN, J. A. 2011. Histone deacetylase 3 regulates smooth muscle differentiation in neural crest cells and development of the cardiac outflow tract. *Circ Res,* 109**,** 1240-9.

STANGER, B. Z., DATAR, R., MURTAUGH, L. C. & MELTON, D. A. 2005. Direct regulation of intestinal fate by Notch. *Proc Natl Acad Sci U S A,* 102**,** 12443-8.

STOLLER, J. Z. & EPSTEIN, J. A. 2005. Cardiac neural crest. *Semin Cell Dev Biol,* 16**,** 704-15.

STOTTMANN, R. W., CHOI, M., MISHINA, Y., MEYERS, E. N. & KLINGENSMITH, J. 2004. BMP receptor IA is required in mammalian neural crest cells for development of the cardiac outflow tract and ventricular myocardium. *Development,* 131**,** 2205-18.

SUN, Z., SINGH, N., MULLICAN, S. E., EVERETT, L. J., LI, L., YUAN, L., LIU, X., EPSTEIN, J. A. & LAZAR, M. A. 2011. Diet-induced Lethality Due to Deletion of the Hdac3 Gene in Heart and Skeletal Muscle. *J Biol Chem,* 286**,** 33301-9.

TRIVEDI, C. M., LU, M. M., WANG, Q. & EPSTEIN, J. A. 2008. Transgenic overexpression of Hdac3 in the heart produces increased postnatal

cardiac myocyte proliferation but does not induce hypertrophy. *J Biol Chem,* 283**,** 26484-9.

TRIVEDI, C. M., LUO, Y., YIN, Z., ZHANG, M., ZHU, W., WANG, T., FLOSS, T., GOETTLICHER, M., NOPPINGER, P. R., WURST, W., FERRARI, V. A., ABRAMS, C. S., GRUBER, P. J. & EPSTEIN, J. A. 2007. Hdac2 regulates the cardiac hypertrophic response by modulating Gsk3 beta activity. *Nat Med,* 13**,** 324-31.

VALLEJO-ILLARRAMENDI, A., ZANG, K. & REICHARDT, L. F. 2009. Focal adhesion kinase is required for neural crest cell morphogenesis during mouse cardiovascular development. *J Clin Invest,* 119**,** 2218-30.

VINCENT, S. D. & BUCKINGHAM, M. E. 2010. How to make a heart: the origin and regulation of cardiac progenitor cells. *Curr Top Dev Biol,* 90**,** 1-41.

WADE, P. A., PRUSS, D. & WOLFFE, A. P. 1997. Histone acetylation: chromatin in action. *Trends Biochem Sci,* 22**,** 128-32.

WANG, J., RAO, S., CHU, J., SHEN, X., LEVASSEUR, D. N., THEUNISSEN, T. W. & ORKIN, S. H. 2006. A protein interaction network for pluripotency of embryonic stem cells. *Nature,* 444**,** 364-8.

WANG, Z., ZANG, C., CUI, K., SCHONES, D. E., BARSKI, A., PENG, W. & ZHAO, K. 2009. Genome-wide mapping of HATs and HDACs reveals distinct functions in active and inactive genes. *Cell,* 138**,** 1019-31.

WANG, Z., ZANG, C., ROSENFELD, J. A., SCHONES, D. E., BARSKI, A., CUDDAPAH, S., CUI, K., ROH, T. Y., PENG, W., ZHANG, M. Q. & ZHAO,

K. 2008. Combinatorial patterns of histone acetylations and methylations in the human genome. *Nat Genet,* 40**,** 897-903.

WILSON, A. J., BYUN, D. S., NASSER, S., MURRAY, L. B., AYYANAR, K., ARANGO, D., FIGUEROA, M., MELNICK, A., KAO, G. D., AUGENLICHT, L. H. & MARIADASON, J. M. 2008. HDAC4 promotes growth of colon cancer cells via repression of p21. *Mol Biol Cell,* 19**,** 4062-75.

WINOGRAD, J., REILLY, M. P., ROE, R., LUTZ, J., LAUGHNER, E., XU, X., HU, L., ASAKURA, T., VANDER KOLK, C., STRANDBERG, J. D. & SEMENZA, G. L. 1997. Perinatal lethality and multiple craniofacial malformations in MSX2 transgenic mice. *Hum Mol Genet,* 6**,** 369-79.

WU, M., LI, J., ENGLEKA, K. A., ZHOU, B., LU, M. M., PLOTKIN, J. B. & EPSTEIN, J. A. 2008. Persistent expression of Pax3 in the neural crest causes cleft palate and defective osteogenesis in mice. *J Clin Invest,* 118**,** 2076-87.

YANG, X. J. & SETO, E. 2003. Collaborative spirit of histone deacetylases in regulating chromatin structure and gene expression. *Curr Opin Genet Dev,* 13**,** 143-53.

YANG, X. J. & SETO, E. 2008. The Rpd3/Hda1 family of lysine deacetylases: from bacteria and yeast to mice and men. *Nat Rev Mol Cell Biol,* 9**,** 206-18.

YE, F., CHEN, Y., HOANG, T., MONTGOMERY, R. L., ZHAO, X. H., BU, H., HU, T., TAKETO, M. M., VAN ES, J. H., CLEVERS, H., HSIEH, J., BASSEL-

DUBY, R., OLSON, E. N. & LU, Q. R. 2009. HDAC1 and HDAC2 regulate oligodendrocyte differentiation by disrupting the beta-catenin-TCF interaction. *Nat Neurosci,* 12**,** 829-38.

YOSHIDA, T. & OWENS, G. K. 2005. Molecular determinants of vascular smooth muscle cell diversity. *Circ Res,* 96**,** 280-91.

ZACHARIAH, M. A. & CYSTER, J. G. 2010. Neural crest-derived pericytes promote egress of mature thymocytes at the corticomedullary junction. *Science,* 328**,** 1129-35.

ZENG, L., XIAO, Q., MARGARITI, A., ZHANG, Z., ZAMPETAKI, A., PATEL, S., CAPOGROSSI, M. C., HU, Y. & XU, Q. 2006. HDAC3 is crucial in shear- and VEGF-induced stem cell differentiation toward endothelial cells. *J Cell Biol,* 174**,** 1059-69.

ZHANG, J., CHANG, J. Y., HUANG, Y., LIN, X., LUO, Y., SCHWARTZ, R. J., MARTIN, J. F. & WANG, F. 2010a. The FGF-BMP signaling axis regulates outflow tract valve primordium formation by promoting cushion neural crest cell differentiation. *Circ Res,* 107**,** 1209-19.

ZHANG, J., CHANG, J. Y., HUANG, Y., LIN, X., LUO, Y., SCHWARTZ, R. J., MARTIN, J. F. & WANG, F. 2010b. The FGF-BMP Signaling Axis Regulates Outflow Tract Valve Primordium Formation by Promoting Cushion Neural Crest Cell Differentiation. *Circ Res*.

ZHANG, M., CHEN, M., KIM, J. R., ZHOU, J., JONES, R. E., TUNE, J. D., KASSAB, G. S., METZGER, D., AHLFELD, S., CONWAY, S. J. &

HERRING, B. P. 2011. SWI/SNF complexes containing Brahma or Brahma-related gene 1 play distinct roles in smooth muscle development. *Mol Cell Biol,* 31**,** 2618-31.

ZHANG, Y., ZHANG, Z., ZHAO, X., YU, X., HU, Y., GERONIMO, B., FROMM, S. H. & CHEN, Y. P. 2000. A new function of BMP4: dual role for BMP4 in regulation of Sonic hedgehog expression in the mouse tooth germ. *Development,* 127**,** 1431-43.

ZHANG, Z., SONG, Y., ZHAO, X., ZHANG, X., FERMIN, C. & CHEN, Y. 2002. Rescue of cleft palate in Msx1-deficient mice by transgenic Bmp4 reveals a network of BMP and Shh signaling in the regulation of mammalian palatogenesis. *Development,* 129**,** 4135-46.

ZHU, W., TRIVEDI, C. M., ZHOU, D., YUAN, L., LU, M. M. & EPSTEIN, J. A. 2009. Inpp5f is a polyphosphoinositide phosphatase that regulates cardiac hypertrophic responsiveness. *Circ Res,* 105**,** 1240-7.

ZIRZOW, S., LUDTKE, T. H., BRONS, J. F., PETRY, M., CHRISTOFFELS, V. M. & KISPERT, A. 2009. Expression and requirement of T-box transcription factors Tbx2 and Tbx3 during secondary palate development in the mouse. *Dev Biol,* 336**,** 145-55.